

University of Alberta

Characterization of Oil Sands Fly Ash

by

Heemun Jang



A thesis submitted to the Faculty of Graduate Studies and Research in partial fulfillment
of the requirements for the degree of Master of Science

in

Materials Engineering

Department of Chemical and Materials Engineering

Edmonton, Alberta

Fall 2004



Library and
Archives Canada

Bibliothèque et
Archives Canada

Published Heritage
Branch

Direction du
Patrimoine de l'édition

395 Wellington Street
Ottawa ON K1A 0N4
Canada

395, rue Wellington
Ottawa ON K1A 0N4
Canada

Your file *Votre référence*
ISBN: 0-612-95778-0
Our file *Notre référence*
ISBN: 0-612-95778-0

The author has granted a non-exclusive license allowing the Library and Archives Canada to reproduce, loan, distribute or sell copies of this thesis in microform, paper or electronic formats.

L'auteur a accordé une licence non exclusive permettant à la Bibliothèque et Archives Canada de reproduire, prêter, distribuer ou vendre des copies de cette thèse sous la forme de microfiche/film, de reproduction sur papier ou sur format électronique.

The author retains ownership of the copyright in this thesis. Neither the thesis nor substantial extracts from it may be printed or otherwise reproduced without the author's permission.

L'auteur conserve la propriété du droit d'auteur qui protège cette thèse. Ni la thèse ni des extraits substantiels de celle-ci ne doivent être imprimés ou autrement reproduits sans son autorisation.

In compliance with the Canadian Privacy Act some supporting forms may have been removed from this thesis.

Conformément à la loi canadienne sur la protection de la vie privée, quelques formulaires secondaires ont été enlevés de cette thèse.

While these forms may be included in the document page count, their removal does not represent any loss of content from the thesis.

Bien que ces formulaires aient inclus dans la pagination, il n'y aura aucun contenu manquant.

Canada

Acknowledgements

The author wishes to express his appreciation to the staff of the Department of Chemical and Materials Engineering for their assistance, in particular Tina Barker with the scanning electron microscopy work for this project and Shiraz Merali for the x-ray diffraction analysis. Special thanks to Preston Holloway, a fellow graduate student, for his interest and criticism of the work, and for generous assistance on atomic absorption spectroscopy work.

The author would also like to thank Syncrude Canada Limited and Suncor Inc. for providing the coke samples used in this testwork.

Finally, many thanks to my supervisor, Dr. Thomas Etsell for his guidance and assistance in this research.

TABLE OF CONTENTS

1.0	Introduction.....	1
2.0	Literature Survey	4
2.1	Characterization of Coal Fly Ash	4
2.1.1	Mineralogy of Coal Fly Ash	5
2.1.1.1	Equilibrium Phase Diagrams	5
2.1.1.2	Mineral Phases and Their Thermal Transitions	9
2.1.2	Ash Formation Mechanisms	16
2.1.3	Particle Size and Morphology.....	20
2.2	Characterization of Oil Sands Fly Ash	25
2.2.1	Crude Bitumen Production in Alberta	25
2.2.2	Fly Ash Production in Alberta Oil Sands	25
2.2.3	Particle Size and Morphology.....	26
2.2.4	Chemical Composition of Oil Sands Fly Ash.....	29
2.2.5	Mineralogy of Oil Sands Fly Ash	32
3.0	Analysis Methods and Procedure.....	33
3.1	Sample Preparation	33
3.2	Analytical Methods.....	34
4.0	Metal Value Beneficiation	38
4.1	High Intensity Magnetic Separation	38
4.2	Centrifuge	40
4.3	Other Separation Methods	42
4.4	Discussion.....	43
5.0	Characterization of Suncor Fly Ash.....	44
5.1	Chemical Composition.....	44
5.2	Morphology of Suncor Ash	45
5.3	Mineralogy of Suncor Ash.....	61
5.3.1	Amorphocity of Suncor Ash	61
5.3.2	Qualitative Analysis.....	62
5.3.3	Quantitative Analysis.....	68
5.4	Discussion and Conclusions	75
5.4.1	Mineral Phase Transition on Combustion.....	75
5.4.2	Ash Formation and Morphology.....	79
5.4.3	Comparison with As-Received Ash.....	80

6.0	Characterization of Syncrude Fly Ash.....	83
6.1	Chemical Composition.....	83
6.2	Morphology of Syncrude Ash.....	84
6.3	Mineralogy of Syncrude Ash.....	95
6.3.1	Amorphocity of Syncrude Ash	95
6.3.2	Qualitative Analysis.....	97
6.3.3	Quantitative Analysis.....	100
6.4	Discussion and Conclusions	104
6.4.1	Mineral Phase Transitions on Combustion.....	104
6.4.2	Ash Formation and Morphology.....	106
6.4.3	Comparison with As-Received Ash.....	108
7.0	Comparison between Suncor Ash and Syncrude Ash.....	110
7.1	Mineralogy of Oil Sands Fly Ash	110
7.2	Ash Formation and Morphology of Oil Sands Fly Ash.....	112
8.0	Future Work.....	114
9.0	Conclusions.....	116
	BIBLIOGRAPHY	118
	APPENDIX	124

List of Tables

Table 2.1	Trace Elements Present in Coal Ashes (ppm)	6
Table 2.1	Mineral Pairs and Heating Products	9
Table 2.2	Some Common Minerals in Coal [24]	10
Table 2.3	Chemical Composition of Some Coals and Cokes	31
Table 2.4	Chemical Composition of Some Coal and Coke Ashes	31
Table 3.1	Ash Content of Oil Sands Coke	33
Table 4.1	Chemical Composition of Magnetic and Non-magnetic Fractions of Suncor Ash	39
Table 4.2	Recovery from Centrifuge Tests on As-received Syncrude Ash	40
Table 4.3	Recovery from Centrifuge Tests on As-received Suncor Ash	41
Table 5.1	Elemental Analyses of Suncor Coke Ash (wt%)	45
Table 5.2	Chemical Composition of a Microcrystal Found in a 900°C Sample (wt%)	59
Table 5.3	Chemical Composition of Microcrystals Found in an 1100°C Sample	60
Table 5.4	Quantitative Analysis of Mineral Phases in Suncor Ash (wt%)	71
Table 5.5	Chemical Composition of Phases in Suncor Ash for Different Time Periods (700°C, wt%)	74
Table 6.1	Elemental Analyses of Syncrude Coke Ash (wt%)	83
Table 6.2	Quantitative Analysis of Mineral Phases in Syncrude Ash (wt%)	103

List of Figures

Figure 2.1	Phase Equilibrium Diagram of the CaO-Al ₂ O ₃ -SiO ₂ System	7
Figure 2.2	Phase Equilibrium Diagram of the FeO-Al ₂ O ₃ -SiO ₂ System	7
Figure 2.3	General Mechanism of Ash Formation [43]	18
Figure 2.4	Spheres Found in Coal Fly Ash from a Kentucky Power Plant	22
Figure 2.5	Morphology of Some Spanish Coal Ashes	23
Figure 2.6	Minerals Found in some Spanish Coal Ashes	24
Figure 2.7	Simplified Suncor Process Flowsheet [5]	27
Figure 2.8	Simplified Syncrude Process Flowsheet	27
Figure 2.9	Micrographs of Suncor Fly Ash Samples [5]	28
Figure 2.10	Micrographs of Syncrude Fly Ash Samples [5]	29
Figure 4.1	Micrographs of Magnetic Fraction (left) and Non-magnetic Fraction (right) of Suncor Fly Ash (×5000, bar: 6μm)	39
Figure 5.1	Micrographs of Suncor Fly Ash with Increasing Temperature (×1500)	51
Figure 5.2	Micrographs of Suncor Fly Ash (× 5000)	56
Figure 5.3	Pleurosphere-like Particle (left) and Cenosphere-like Particle (right) from 1100°C Sample (× 500, bar: 60μm)	58
Figure 5.4	Point Analysis on Needles and Matrix of 1100°C Suncor Ash Sample	60
Figure 5.5	Suncor Ash Amorphocity Determination	62
Figure 5.6	XRD Raw Patterns of Suncor Ash	63
Figure 5.7	XRD Patterns of Suncor Ash Mixed with 10 wt% ZnO	70
Figure 5.8	Mineral Phases Identified at Low Temperature	72
Figure 5.9	Mineral Phases Identified at High Temperature	72
Figure 5.10	Mineral Phase Transitions of Suncor Fly Ash	77
Figure 5.11	XRD pattern of As-Received Suncor Ash	81
Figure 5.12	SEM Micrograph of As-Received Suncor Ash [5]	81
Figure 6.1	Micrographs of Syncrude Fly Ash (× 1500)	89
Figure 6.2	Micrographs of Syncrude Fly Ash (× 5000)	94
Figure 6.3	Syncrude Ash Amorphocity Determination	96

Figure 6.4	XRD Raw Patterns of Syncrude Ash	98
Figure 6.5	XRD Patterns of Syncrude Ash Mixed with 10 wt% ZnO	102
Figure 6.6	Mineral Phases Identified in Syncrude Ash	103
Figure 6.7	Mineral Phase Transitions of Syncrude Fly Ash	105
Figure 6.8	XRD pattern of As-Received Syncrude Ash	108
Figure 6.9	SEM Micrograph of As-Received Suncor Ash [5]	109

List of Minerals and Chemical Formulae

Minerals	Chemical Formulae	Others
Andalusite	Al_2SiO_5	
Anhydrite	CaSO_4	
Anorthite	$\text{CaAl}_2\text{Si}_2\text{O}_8$	
Albite	$\text{NaAlSi}_3\text{O}_8$	
Bassanite	$\text{CaSO}_4 \cdot 1/2\text{H}_2\text{O}$	
Coquimbite	$\text{Fe}_2(\text{SO}_4)_3 \cdot 9\text{H}_2\text{O}$	
Corundum	Al_2O_3	
Cristobalite	SiO_2	
Dolomite	$\text{CaMg}(\text{CO}_3)_2$	
Fayalite	Fe_2SiO_4	
Gehlenite	$\text{Ca}_2\text{Al}_2\text{SiO}_7$	
Gypsum	$\text{CaSO}_4 \cdot 2\text{H}_2\text{O}$	
Hematite	Fe_2O_3	
Hercynite	FeAl_2O_4	
Illite	$\text{K}_{0.7}\text{Al}_2(\text{Si},\text{Al})_4\text{O}_{10}(\text{OH})_2$	Illite-1M
Kaolinite	$\text{Al}_2\text{Si}_2\text{O}_5(\text{OH})_4$	Kaolinite-1Md
Kyanite	Al_2SiO_5	
Lawsonite	$\text{CaAl}_2\text{Si}_2\text{O}_7(\text{OH})_2 \cdot \text{H}_2\text{O}$	
Leucite	KAlSi_2O_6	
Lime	CaO	
Magnetite	Fe_3O_4	
Mayenite	$\text{Ca}_{12}\text{Al}_{14}\text{O}_{33}$	
Microcline	KAlSi_3O_8	
Montmorillonite	$\text{Na}_{0.3}(\text{Al},\text{Mg})_2\text{Si}_4\text{O}_{10}(\text{OH})_2 \cdot n\text{H}_2\text{O}$	Montmorillonite-14A
Mullite	$3\text{Al}_2\text{O}_3 \cdot 2\text{SiO}_2$	
Muscovite	$\text{KAl}_2\text{Si}_3\text{AlO}_{10}(\text{OH})_2$	Muscovite-1M ₁
Oldhamite	$(\text{Ca},\text{Mg},\text{Fe})\text{S}$	
Pseudobrookite	Fe_2TiO_5	
Pseudowollastonite	CaSiO_3	
Pyrite	FeS_2	
Pyrrhotite	Fe_{1-x}S	
Quartz	SiO_2	
Rutile	TiO_2	
Siderite	FeCO_3	
Sillimanite	Al_2SiO_5	

1.0 Introduction

Oil sands are also known as tar sands and bituminous sands. They are found throughout the world, but the largest deposit in the world is in the Athabasca area in northern Alberta, Canada [1]. Suncor Energy Inc. and Syncrude Canada Ltd. operate commercial mining plants in this area for bitumen recovery from the oil sands. Oil sands are composed of bitumen (10-11 wt% of oil sands), water and sand grains [2]. Bitumen, in its raw state, is black, asphalt-like oil, which is not suitable for commercial usage. It requires separation and upgrading processes to make it transportable by pipeline and usable by conventional refineries. A substantial amount of oil sands coke is produced from this upgrading process of bitumen. Currently, the combined daily production of oil sands coke by Suncor and Syncrude exceeds 6000 tonnes [3].

Even though the proximity of the production mines of the Suncor and Syncrude operations would suggest a similar composition of the mineral matter, Suncor fly ash and Syncrude fly ash are quite different in nature, mainly due to the difference in the pretreatment of bitumen and in ash formation temperature. First, Suncor uses centrifuging after flotation to increase the purity of bitumen by removing more sand grains, whereas Syncrude uses flotation as a primary separation process. This difference in pretreatment results in a higher content of silica in Syncrude ash so that a mineralogical difference in the ash is also expected. Second, the difference in ashing temperature significantly affects mineralogy, chemistry and morphology of fly ash. Suncor fly ash is produced when the coke left in the coking reactor as a solid residue is burned in the boilers that generate electricity. The temperature of the boilers is assumed to be around 1200°C. On the other

hand, Syncrude fly ash is produced when the coke obtained from its fluid cokers is burned in the cokers to maintain the coker temperature, which is normally held at around 630°C [2]. Approximately 22% of the bitumen is converted into coke in eight Suncor delayed cokers, whereas around 15% of the bitumen is converted into coke in two fluid cokers at Syncrude with two-thirds of the coke being stockpiled [4]. Currently, approximately 250 and 50 tonnes of fly ash are produced by Suncor and Syncrude per day, respectively [5].

Mineral constituents of oil sands fly ash and the phase changes of these minerals on combustion are of scientific and commercial interest since a significant amount of metal values and other mineral matter originating in the oil sands are concentrated in the fly ash when bitumen undergoes upgrading processes, especially coking processes. Mineral composition of the oil sands is over 90% quartz with minor amounts of potash feldspar, chert and muscovite. Clay minerals include kaolinite ($\text{Al}_2\text{Si}_2\text{O}_5(\text{OH})_4$), illite and a small amount of montmorillonite [6]. Metal values found in oil sands residues include appreciable amounts of vanadium, titanium and nickel. Vanadium is concentrated to between 2.0 and 3.5 wt% (3.6 to 6.2% V_2O_5) in the fly ash when the coke is burned [5, 7]. Extensive research has been conducted on oil sands fly ash to leach out these metal values for over the last two decades. These work have enhanced the processability by developing hydrometallurgical processes including salt roasting in some cases. However, very little work has been completed on the mineral phases and their behavior on heating so that characteristics of oil sands fly ash have not been, so far, well understood.

This thesis focuses on the characterization of oil sands fly ash produced by Suncor and Syncrude Canada in northern Alberta. Characterization studies mainly include chemical and physical properties of fly ash: their chemistry, mineralogy and ash formation mechanisms. In this study, a series of ash samples was produced by ashing both Suncor and Syncrude coke at different temperatures. These coke ash samples were, then, characterized and compared to as-received oil sands fly ash. By using oil sands coke, not fly ash directly received from producers, good evidence of ash formation mechanisms as well as transformation behavior of mineral phases were revealed. Moreover, upon using a low temperature asher (LTA), which can sufficiently remove carbon without changing any mineralogy of the original coke, the nature of coke was also uncovered for the first time. The results from this study will give a better understanding of fly ash to optimize the roasting and leaching conditions to, ultimately, determine the feasibility of producing high purity vanadium and byproduct metals and chemicals from oil sands fly ash.

2.0 Literature Survey

Articles on the following topics were reviewed to provide a comprehensive background for the characterization studies on oil sands fly ash:

- (1) Chemistry, Mineralogy, Morphology, Size Distribution and Ash Formation Models for Coal Fly Ash
- (2) Occurrence, Chemistry, Mineralogy and Morphology of Oil Sands Fly Ash

2.1 Characterization of Coal Fly Ash

The ASTM classification of coals which is commonly used is primarily based on the percent volatile matter and calorific value, ranging in the order of anthracite, bituminous, subbituminous and lignite [8]. Anthracite normally contains a high content of carbon and a low content of volatile matter which result in higher calorific value, whereas lignite contains low carbon and high volatiles. Another classification normally used in the U.S. is based on the amount of Al_2O_3 , SiO_2 and Fe_2O_3 in the ash. When the sum of these three oxides is higher than 50 wt% and lower than 70 wt% of total weight, the fly ash is called “class C”, or “cementitious”, whereas when the amount of these oxides is higher than 70 wt%, the fly ash is called “class F”, or “pozzolanic” [9]. Higher $\text{Al}_2\text{O}_3+\text{SiO}_2+\text{Fe}_2\text{O}_3$ means lower contents of CaO and other constituents, such as MgO, Na_2O and K_2O . All bituminous coal falls into class F coals, though class F coals come not only from bituminous but also from subbituminous and lignite coals.

Coal combustion results in a residue which is composed of inorganic minerals in the coal and the organic char particles. Inorganic minerals normally make up from 3 to 30% of the coal residue [8]. Petrographic analysis has shown that glass is the primary component of ash, constituting 50-90% of the total weight [8]. It is also known that finer particles generally contain a higher portion of glass than coarser ones. The major constituents of ash, which make up 95 to 99% of the total composition, are silicon, aluminum, iron and calcium. Minor constituents, such as Mg, Ti, Na, K, S and P comprise 0.5 to 3.5%. Fly ash also contains 20 to 50 trace elements [10-16]. Table 2.1 shows the amount of trace elements present in coal ashes [17]. More details on chemical compositions of coal fly ashes, their mineralogy and their morphology have been studied and are described in this chapter.

2.1.1 Mineralogy of Coal Fly Ash

2.1.1.1 Equilibrium Phase Diagrams

In order to understand the crystallization behavior of coal ash on heating, equilibrium phase diagrams of the $\text{SiO}_2\text{-Al}_2\text{O}_3\text{-CaO}$ system, the $\text{SiO}_2\text{-Al}_2\text{O}_3\text{-FeO}$ system and the $\text{SiO}_2\text{-Al}_2\text{O}_3\text{-K}_2\text{O}$ system along with those of minor phases were studied (Figures 2.1 and 2.2) [18]. All primary phases obtained from these phase diagrams provide useful information to further predict the secondary or ternary phases. Since coal ash is a complex mixture of mineral components, many researchers have tried to combine some of phase equilibrium diagrams.

Table 2.1 Trace Elements Present in Coal Ashes (ppm)

Elements	Anthracites	High Volatile	Low Volatile	Medium Volatile	Subbituminous
		Bituminous	Bituminous	Bituminous	& Lignite
Ag	1	1~3	1~1.4	1	1~50
B	90	770	123	218	1020
Ba	866	1253	740	896	5027
Be	9	17	16	13	6
Co	81	64	172	105	45
Cr	304	193	221	169	54
Cu	405	293	379	313	655
Ga	42	40	41	10~52	23
Ge	20	20~285	20	20	20~100
La	142	111	110	83	62
Mn	270	170	280	1432	688
Ni	220	154	141	263	129
Pb	81	183	89	96	60
Sc	61	32	50	56	18
Sn	962	171	92	75	156
Sr	177	1987	818	668	4660
V	248	249	278	390	125
Y	106	102	152	151	51
Yb	8	10	10	9	4
Zn	155~350	310	231	195	50~320
Zr	688	411	458	326	245

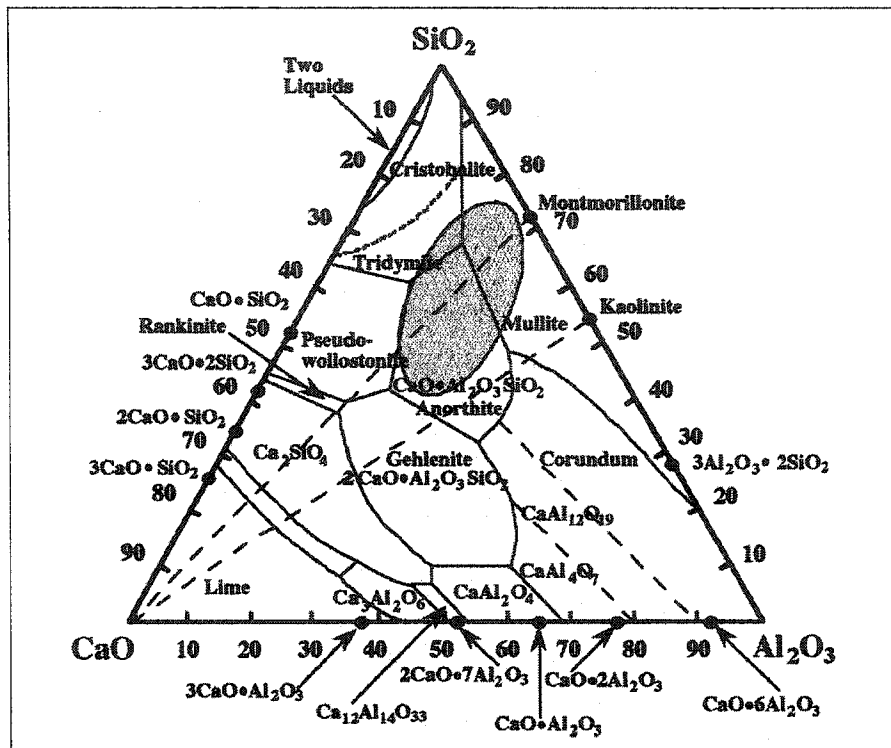


Figure 2.1 Phase Equilibrium Diagram of the $\text{CaO-Al}_2\text{O}_3\text{-SiO}_2$ System
 Shaded area represents the composition of Texas lignite coal ash [19]

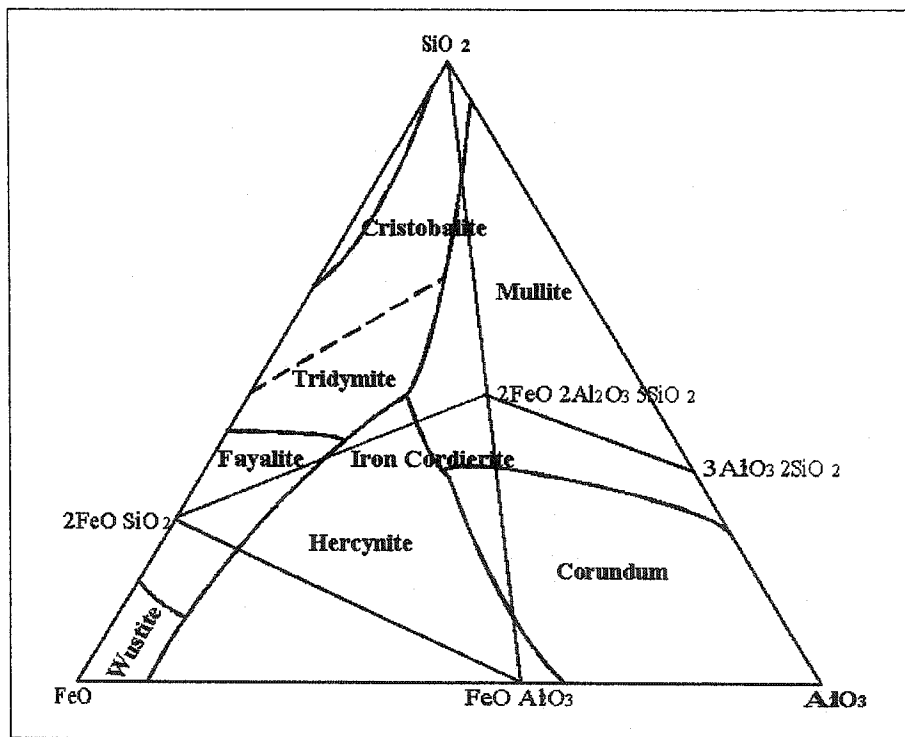


Figure 2.2 Phase Equilibrium Diagram of the $\text{FeO-Al}_2\text{O}_3\text{-SiO}_2$ System

Kalmanovitch and Williamson [20] studied the systems of $\text{SiO}_2\text{-Al}_2\text{O}_3\text{-CaO-MgO}$ and $\text{SiO}_2\text{-Al}_2\text{O}_3\text{-CaO-FeO}$, based on the $\text{SiO}_2\text{-Al}_2\text{O}_3\text{-CaO}$ equilibrium diagram. Using ashes which contained anorthite ($\text{CaAl}_2\text{Si}_2\text{O}_8$) and/or mullite ($3\text{Al}_2\text{O}_3\cdot 2\text{SiO}_2$) as a primary phase, they reported that FeO was relatively inactive with other phases, while the addition of MgO significantly changed the phase equilibria.

Falcon and Schobert [21] used synthetic compound mixtures to predict high temperature phase minerals and their transformations on heating. They stated that a big difference occurring at high temperature was a reflection of differences not so much in the original mineral matter but in the total inorganic composition of the coal. The presence of exchangeable alkali cations (specifically, sodium and calcium) was the most important constituent in determining the mineral phases formed at high temperature.

Biggs and Lindsay [22] prepared known mineral pairs and observed their thermal behavior at high temperature. Table 2.1 shows the results of their experiments. They found that calcite and quartz were quite inert at all temperatures, while pyrite was so active that iron enrichment in clay mineral residues was commonly identified.

Table 2.1 Mineral Pairs and Heating Products

Mineral Pair	T _{max} (°C)	Products Identified
Calcite - Illite	1310	Lime
Calcite - Kaolinite	1322	Lime
Calcite - Pyrite	1253	Lime, pyrrhotite, oldhamite (CaS)
Calcite - Quartz	1467	Quartz, lime
Illite - Kaolinite	1410	Mullite
Illite - Pyrite	1519	Pyrrhotite, troilite (FeS)
Illite - Quartz	1450	Quartz
Kaolinite - Pyrite	1445	Mullite
Kaolinite - Quartz	1220	Quartz
Pyrite - Quartz	1571	Quartz

2.1.1.2 Mineral Phases and Their Thermal Transitions

The majority of minerals found in coal ash are generally classified into one of four groups: aluminosilicates, carbonates, sulfides and sulfates. Among those, aluminosilicates are the most abundant mineral group found in coal ash. During combustion, some minerals are altered thermally, while other minerals such as silica may remain unaltered. Thermally treated coal impurities along with unburned carbon make up the fly ash. The major constituents of fly ash are silica (SiO₂), mullite, hematite (Fe₂O₃), lime (CaO) and gypsum (CaSO₄·2H₂O). Sarofim et al. [23] studied both lignite and bituminous coals and identified kaolinite, bassanite, lawsonite, quartz, dolomite and rutile in lignite samples, and kaolinite, illite, quartz, pyrite, coquimbite, calcite and anhydrite (CaSO₄) in bituminous samples. Some coal minerals described by Renton [24] are shown in Table 2.2.

Aluminosilicates

Aluminosilicates are the most abundant constituent of fly ash, which are aluminum-silicon-oxygen compounds, mixed with smaller amounts of sodium, calcium, titanium, vanadium, potassium and numerous trace elements. Clays such as kaolinite and illite, sillimanite (Al_2SiO_5), feldspars such as albite ($\text{NaAlSi}_3\text{O}_8$), microcline (KAlSi_3O_8) and anorthite, and quartz group minerals (quartz, cristobalite and tridymite) are all included in these aluminosilicates.

Table 2.2 Some Common Minerals in Coal [24]

Major	Silicates	Clay Minerals	Kaolinite	$\text{Al}_2\text{Si}_2\text{O}_5(\text{OH})_4$
			Illite	$\text{KAl}_2(\text{Si}_3\text{Al})\text{O}_{10}(\text{OH})_2$
			Mixed layer	Illite + Montmorillonite
			Chlorite	$(\text{MgFeAl})_6(\text{SiAl})_4\text{O}_{10}(\text{OH})_8$
			Quartz	SiO_2
Minor		Carbonate	Calcite	CaCO_3
			Dolomite	$(\text{Ca},\text{Mg})(\text{CO}_3)_2$
			Ankerite	$\text{Ca}(\text{Fe},\text{Mg})(\text{CO}_3)_2$
			Siderite	FeCO_3
		Disulfides	Pyrite	FeS_2
			Marcasite	FeS_2
		Sulfates	Coquimbite	$\text{Fe}_2(\text{SO}_4)_3 \cdot 9\text{H}_2\text{O}$
			Gypsum	$\text{CaSO}_4 \cdot 2\text{H}_2\text{O}$
			Bassanite	$\text{CaSO}_4 \cdot 1/2\text{H}_2\text{O}$
			Anhydrite	CaSO_4
		Feldspar	Plagioclase	$(\text{NaCa})\text{Al}(\text{AlSi})\text{Si}_2\text{O}_8$

Hulett and Weinberger [25] suggested that these aluminosilicates be separated into three categories; glass, aluminum-rich mullite structures and silicon-rich quartz structures. They also reported that the amount of crystalline mullite and quartz was as much as 30-40% and the rest of the aluminosilicates was glass.

Clays and Mullite

Mullite has been reported as a major component in many coal fly ashes. It does not occur naturally in coal; thus it is assumed to form during combustion by the thermal decomposition of naturally occurring clay minerals, such as kaolinite. Clay minerals undergo dehydration when they are heated to relatively high temperatures. This reaction involves the loss of water and significant changes in structure. Mullite formation from kaolinite is well known: at relatively low temperatures (between 400-525°C) the loss of water is expected followed by formation of metakaolinite. At higher temperatures (above 950°C), metakaolinite decomposes into mullite and silica. Several ceramists indicate the formation of $\gamma\text{-Al}_2\text{O}_3$ and cristobalite is also easily identified along with mullite since significant structural deformation is expected as kaolinite decomposes [26]. While some ceramic chemists such as Spears [27] mention that mullite crystals are largely attributed to kaolinite, whereas illite contributes towards the glass, dehydrated illite and some dehydrated montmorillonite are also a source of mullite formation. Illite originated mullite may accompany the formation of corundum ($\alpha\text{-Al}_2\text{O}_3$), $\gamma\text{-Al}_2\text{O}_3$, cristobalite and leucite, whereas montmorillonite originated mullite may be found along with anorthite, quartz, corundum and cristobalite.

Mullite is believed to accommodate some transition metals, such as Fe and Ti. Hulett and Weinberger [25] investigated mullite structures and concluded that Fe and Ti could be kept in the mullite structure interstitially on combustion, while Na, Mg, K, Ca and other alkali components might be frozen out of mullite and quartz phases and concentrated into the glass. Since V and Cr, along with Fe and Ti, are also reported to possibly substitute in the aluminum sites of kyanite and of all polymorphs of Al_2SiO_5 , it is possible that mullite has vanadium interstitially in its structure [28]. Bruhns and Fischer [29] found that the mullite structure could accommodate 3.2 mole % vanadium and 3.8 mole % iron when illite clays were mixed with 5 wt% of V_2O_5 and heated up to 1000°C .

Mullite formation from kaolinite can be significantly enhanced by the presence of Zn, Li, Mg, Fe, Mn, Ce and Mo, slightly enhanced by Ca and B, and retarded by Na, K, Ti and Sn [26]. Mullite formation is not likely in the coal fly ash when $\text{Al}_2\text{O}_3 + \text{SiO}_2$ contents are less than 60% and the mole fraction of Al_2O_3 is less than 17% [27].

Kyanite, andalusite and sillimanite are anhydrous aluminosilicate minerals that have the same chemical formula, Al_2SiO_5 , but differ in crystal structure and physical properties. When calcined at high temperatures (around 1350 to 1380°C for kyanite and slightly higher for andalusite and sillimanite), these minerals are converted to mullite and silica [30, 31]. Sillimanite and mullite have similar crystal structures: both have chains of AlO_6 octahedra that are cross-linked by double chains of tetrahedrally coordinated Si and Al. However, in comparison with sillimanite, mullite has oxygen vacancies, and the

excess Al occupies a unique tetrahedral site. The transformation of sillimanite into mullite may be visualized by the replacement of Si^{+4} by Al^{+4} . [28]

Quartz group minerals (Quartz, Cristobalite, Tridymite)

Quartz is one of the most abundant minerals found in fly ash. It is normally found unchanged up to 1100°C. However, at 1200°C or higher, it forms amorphous phases by reactions with other compounds. Cristobalite and tridymite are the polymorphs of quartz and are normally referred to as higher temperature phases. Thermodynamically, cristobalite is not stable at the relatively low temperatures of 900-1200°C. Even though tridymite is more thermodynamically stable in this temperature range than cristobalite, it is not commonly found in fly ash. Instead, cristobalite formed from the decomposition of kaolinite is kinetically stable in the fly ash. On the other hand, Mollah et al. [19] suggest that cristobalite forms by amorphous to crystalline transitions. They mentioned that the presence of alkali and alkaline earth elements accelerated this transition reaction.

Iron Oxides (Hematite, Magnetite)

Pyrite is a common iron mineral at lower temperature (< 500°C) but it is oxidized to form hematite or magnetite, depending on the oxidation conditions and the residence time in the combustion system. Hatt and Bull [32] reported that rapid quenching of iron promoted the formation of hematite while exposure of iron to hot flue gas for an extended period of time could promote the formation of magnetite. At elevated temperatures (>1650°C), both hematite and magnetite melt and recrystallize upon cooling. During recrystallization, excess Fe oxides could be incorporated into glass [33]. This finding

indicates that hematite and magnetite partly transform into glass at high temperature. McCarthy et al. [34] stated in their research that iron-rich grains observed in the SEM often had magnetite (partially oxidized iron) cores and hematite (fully oxidized iron) rims due to the difference in cooling rate. When pyrite is oxidized, the formation of anhydrite is also predictable since pyritic sulphur may react with calcite. Mitchell and Gluskoter [35] found the evidence of anhydrite formation in heat treatment of mixtures of pyrite and calcite. They said that hematite and anhydrite began to form at 500°C and were major phases to 800°C.

Ca-Bearing Minerals

Anhydrite is a common mineral phase formed during combustion and is stable up to 1000°C. The formation of anhydrite is explained by the decomposition of calcium carbonate. Akhtar and Schlorholtz [36] reported an abundance of limestone in ash produced by fluidized bed combustion, and suggested that limestone be first calcined to CaO, then react with SO₂ and oxygen during combustion to form anhydrite, thereby removing some of the CO₂ from the flue gases. However, a higher fraction of anhydrite could also possibly form directly from dehydration of the original gypsum in the ash. The dehydration temperature normally goes down to as low as 400°C. Gypsum has a transition sequence of gypsum-bassanite-anhydrite, and this transition which accompanies the loss of water by means of dehydration could begin at a temperature of above 60°C due to the presence of alkali elements [37]. Mitchell and Gluskoter [35] suggested in their low temperature ashing experiments that bassanite (CaSO₄ · ½H₂O) was

the major phase until it was dehydrated to form anhydrite. They found that dehydration of bassanite was completed at 400°C.

Some of montmorillonite group clay minerals are found to form anorthite along with mullite, quartz and spinel when the dehydration is completed, whereas no evidence of anorthite is found in illite or kaolinite clays when they are decomposed.

The presence of anhydrite in the ash is associated with the formation of anorthite at higher temperatures, while the presence of lime (CaO) is related to the formation of mayenite ($\text{Ca}_{12}\text{Al}_{14}\text{O}_{33}$). Many researchers have stated that anorthite forms when anhydrite reacts with alumina and silica derived from kaolinite. On the other hand, CaO reacts only with alumina components to form mayenite or other calcium aluminates such as tricalcium aluminate, $\text{Ca}_3\text{Al}_2\text{O}_6$. Akhtar and Schlorholtz [36] stated that, when the amount of limestone was in excess of that needed for the formation of anhydrite, it could be also combined with silica to form wollastonite (CaSiO_3). In some coal fly ashes, which are poor in Al_2O_3 and rich in CaO, gehlenite ($\text{Ca}_2\text{Al}_2\text{SiO}_7$) was found to be a major phase instead of anorthite. Mitchell and Gluskoter [35] said that anorthite was detected in the range from 800 through 1300°C and gehlenite found in a Wyoming fly ash sample was stable from 900 to 1200°C.

Feldspars

Anorthite and albite are the most abundant plagioclase feldspar structures present in coal fly ash. Potash feldspar, microcline, is also found in some coal ashes. Vassilev et al. [38]

found that the quantity of feldspars generally increased with increasing temperature. This can be related to solid-state formation of new feldspars, especially basic plagioclases (500-1000°C) as a result of reaction between liberated Ca, K, Na, Al-oxides and quartz, and the aluminosilicate matrix. It could also be related to an intensive crystallization from silicate melts enriched with Ca (>1000°C).

2.1.2 Ash Formation Mechanisms

During coal combustion, coal minerals undergo many transformations until they form ash. Formation reactions are very complicated, heterogeneous reactions so that it is not easy to explain the formation mechanisms. In addition, many conditions governing the combustion process should be considered to understand ash formation. Among many conditions that influence the ash formation processes are particle size, combustion conditions such as temperature, residence time and oxygen concentration, and mineral types or association of minerals.

It is generally believed that small ash particles, normally in sub-micron sizes, form by vaporization of volatile components in the coal followed by condensation and coagulation or form by fragmentation of minerals, whereas bigger particles (1-100µm) form directly by coagulation. Flagan and Friedlander [39] also proposed a simple mechanical break up mechanism for coarse ash particles and a vaporization-condensation mechanism for fine particles. They suggested the break-up model should explain 99% of the ash particles (0.1-50µm particles), while around 1% of particles be related to the sub-micron size (<0.1µm) ash formation model. They reported that these vaporized droplets

would undergo homogeneous nucleation to form extremely small particles (0.01-0.15 μm), and heterogeneous condensation to form slightly bigger particles (<0.1 μm). These small particles could deposit onto relatively bigger particles. Figure 2.3 illustrates the mechanisms of ash formation.

Couch [40] classified mineral matter found in the fly ash as either included or excluded depending on its association with organic coal. Excluded minerals, which are completely liberated during milling, are coarser than included minerals, and commonly become ash individually with or without extensive fragmentation. On the other hand, included minerals, which are embedded within the organic coal particles, are normally accompanied by coalescence of minerals [41]. McLennan et al. [42] found in their research that the included minerals were relatively small (typically 5-30 μm) than the excluded minerals whose sizes were normally 45-75 μm . They also stated that included minerals were subjected to chemical interaction between minerals resulting in reduced melting temperatures due to the burning of char which introduces localized reducing conditions, so that more volatiles were formed, followed by vaporization and coalescence, whereas excluded minerals were not so active in chemical interactions such that ash formed directly by coagulation. Yan et al. [41] developed a mathematical model to study ash formation using a high rank coal ash (e.g., bituminous coal), and confirmed that the ash typically formed by the combination of coalescence of included minerals and fragmentation of excluded minerals.

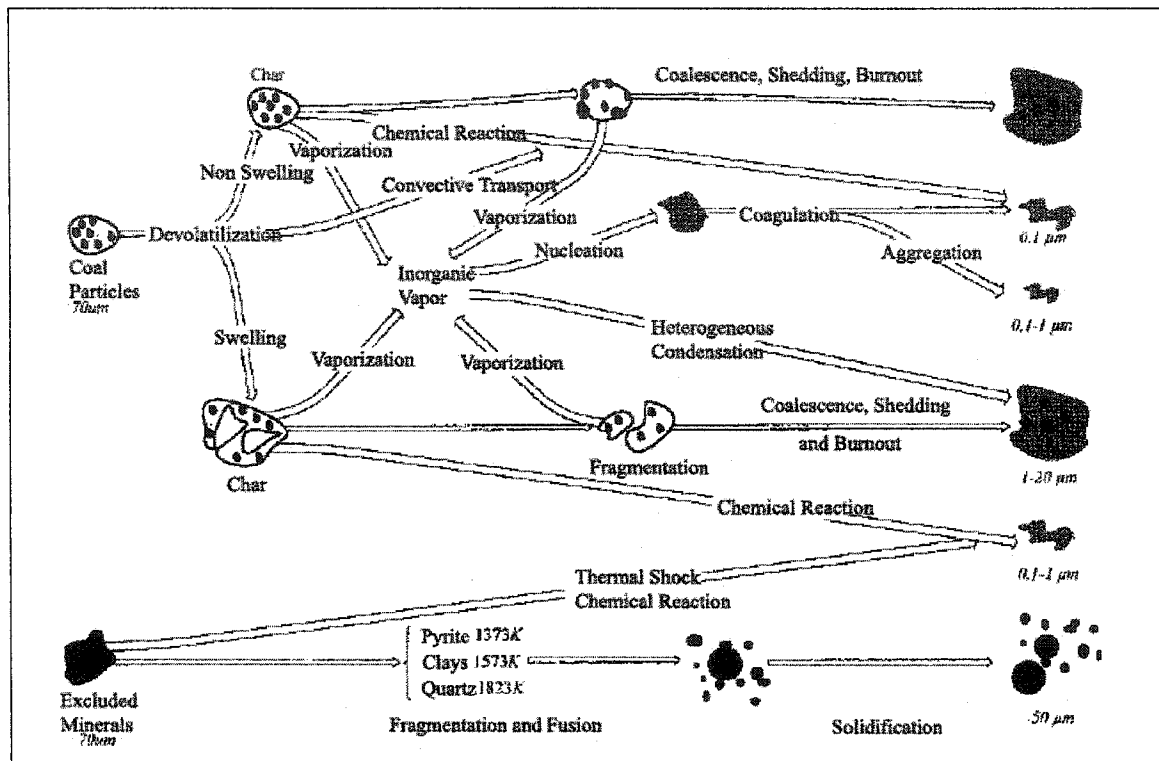


Figure 2.3 General Mechanism of Ash Formation [43]

Each coal particle can form an ash particle. However, it may disintegrate on combustion producing small particles, possibly sub-micron ash particles [27]. The interior part of each particle undergoes slower cooling to form crystallites and the outer part of the particle experiences rapid cooling to form more glassy phases [19]. If this mechanism is true, it is expected that smaller particles, which undergo rapid quenching, will have more amorphous phases, whereas bigger particles have more crystallites. However, many scientists argue that smaller particles are normally enriched with trace elements which may be related to the crystallites [23, 27, 39].

The role of char particles in ash formation is also very important since it affects the fragmentation of each coal particle. If a char particle does not fragment on combustion, only one ash particle is expected to form from one coal particle. When a char particle fragments, however, it produces more than one ash particle [43]. Sarofim et al. [23] reported that three ash particles per coal particle were formed for lignite and five ash particles per coal particle were formed for bituminous coal. It was concluded that high rank coals, such as bituminous coals fragmented more so that more ash particles formed. In addition, as the size and the porosity of the char particle increases, the amount of fragmentation increases [44]. Wu et al. [43] report that char fragmentation determines ash formation for early and middle combustion stages resulting in finer ash particles, while the coalescence of included minerals results in the coarser ash particles during later combustion stages.

It is commonly assumed that Na, Mg, K, Ca and many trace elements are enriched at the surface of the particle. This behavior is normally explained by the vaporization-condensation model [45, 46]. This is because they are the last elements to condense on the particle when cooling. Another model which explains this behavior is that these trace elements can diffuse out from the inside to the surface of the particle since the activation energy of inside components is higher than that of outside components due to the difference in cooling rate between them [25].

McLennan et al. [42] introduced the behavior of each individual mineral in their recent study. They found that excluded minerals such as calcite, quartz, kaolinite and other clays

were not affected on heating. Excluded pyrite decomposed to form pyrrhotite, and then oxidized to form magnetite and hematite while excluded siderite decomposed into wüstite, which oxidized to form magnetite later under oxidizing conditions. Included pyrite and siderite also decomposed directly to form magnetite and hematite. However, when they contacted aluminosilicates, they directly formed iron-aluminosilicate glass ash particles.

Evolution of CO₂ gas during coal combustion is believed to be responsible for cenospheres. When the ash droplets are cooled down, they solidify around entrapped CO₂ gas bubbles, resulting in hollow spheres. Spears [27] says that K₂O, which is normally found in illite, also affects the formation of cenospheres.

2.1.3 Particle Size and Morphology

Fly ash is mainly composed of aluminosilicate spheres. The morphology studies on coal fly ash using scanning electron microscopy (SEM) indicate that spherical shape particles generally account for about 80-90% of fly ash, and irregular shape particles and acicular shape microcrystals comprise the rest. For some high calcium coal samples, typical anhydrite grains have also been reported. The size of spherical particles usually varies from 0.5 μm to 100 μm.

Kaufherr and Lichtman [47] studied the size distribution of coal fly ash obtained from the power plant in Oak Ridge, and stated the majority of the particles were 2-5 μm, and the average of sub-micron size particles was 0.6 μm. They found that the major part of the

micron and sub-micron particles was spherical and only a small fraction of different shapes were found. These non-spherical particles were associated with high SiO₂ content. The surface of the spheres is not smooth and contains irregular shapes of mineral phases. It is normally assumed that Na, Mg, K, Ca and many trace elements are enriched in the surface of the particle [25]. Fishman et al. [48] also confirmed the presence of K, and they stated that these irregular shape minerals would be the S-bearing minerals when they compared the chemistry of fly ash samples before and after leaching tests. Figure 2.4 shows the difference in surface morphology before and after the leaching. The left side pictures show the irregular mass of surface coating before leaching, and the right side picture shows the smoothness of the surface after leaching. They suggested that the possible S-bearing minerals include Na₂SO₄ and CaSO₄. Other researchers such as Sarofim et al. [23] confirmed the presence of trace elements on the surface by means of vaporization, followed by condensation of these elements. They stated that the trace elements deposited on the surface were enriched in sub-micron silica particles.

Fly ash can also be characterized by the presence of cenospheres and pleuroospheres. Cenospheres refer to hollow spheres while pleuroospheres refer to spheres whose interior is filled with many small ash spheres. Ash droplets, which solidify on entrapped gases, may be responsible for the formation of these spheres. The formation temperature would be between 1200 and 1500°K, where the temperature is high enough for particles to be fluid, but low enough for the spheres not to burst [39]. Sarofim et al. [23] also state cenospheres form between 1200 and 1400°K below which the formation time is insufficient and above which the gases evolved during decomposition have ample time to

escape from the molten ash. These spheres are usually large (~50 μm), but, generally, account for less than 5% of the total mass of coal ash [39].

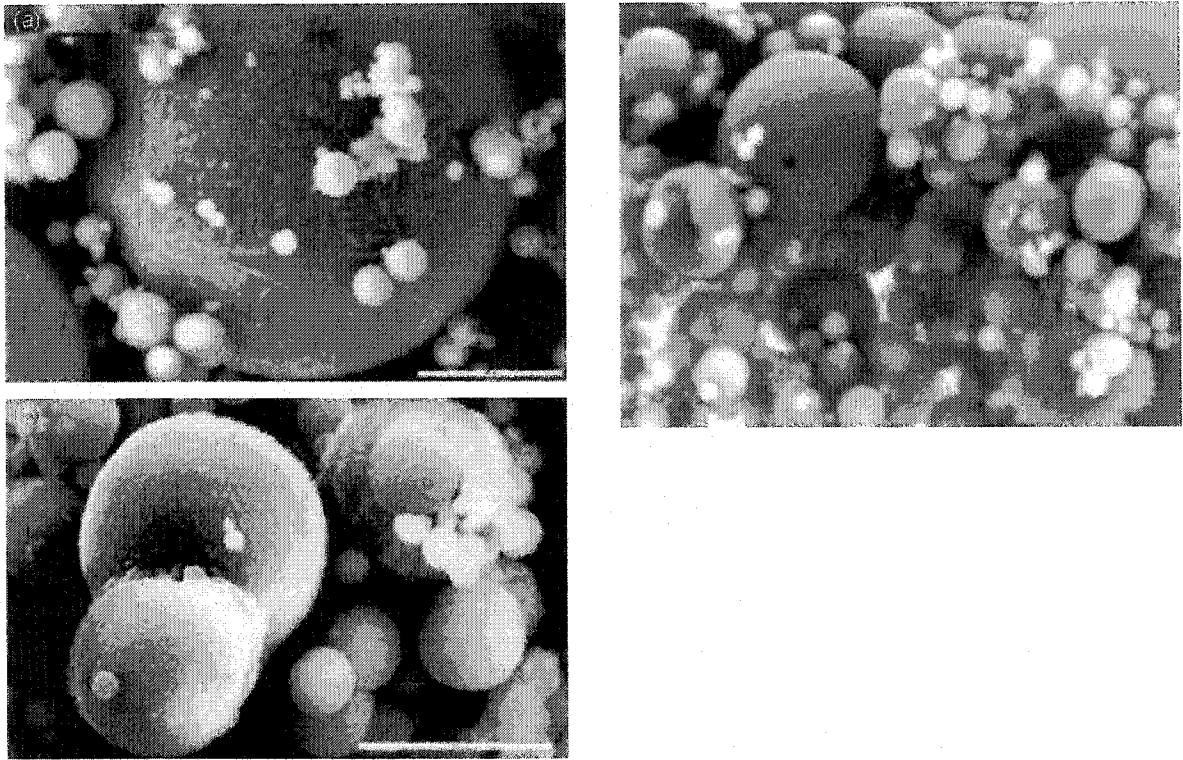
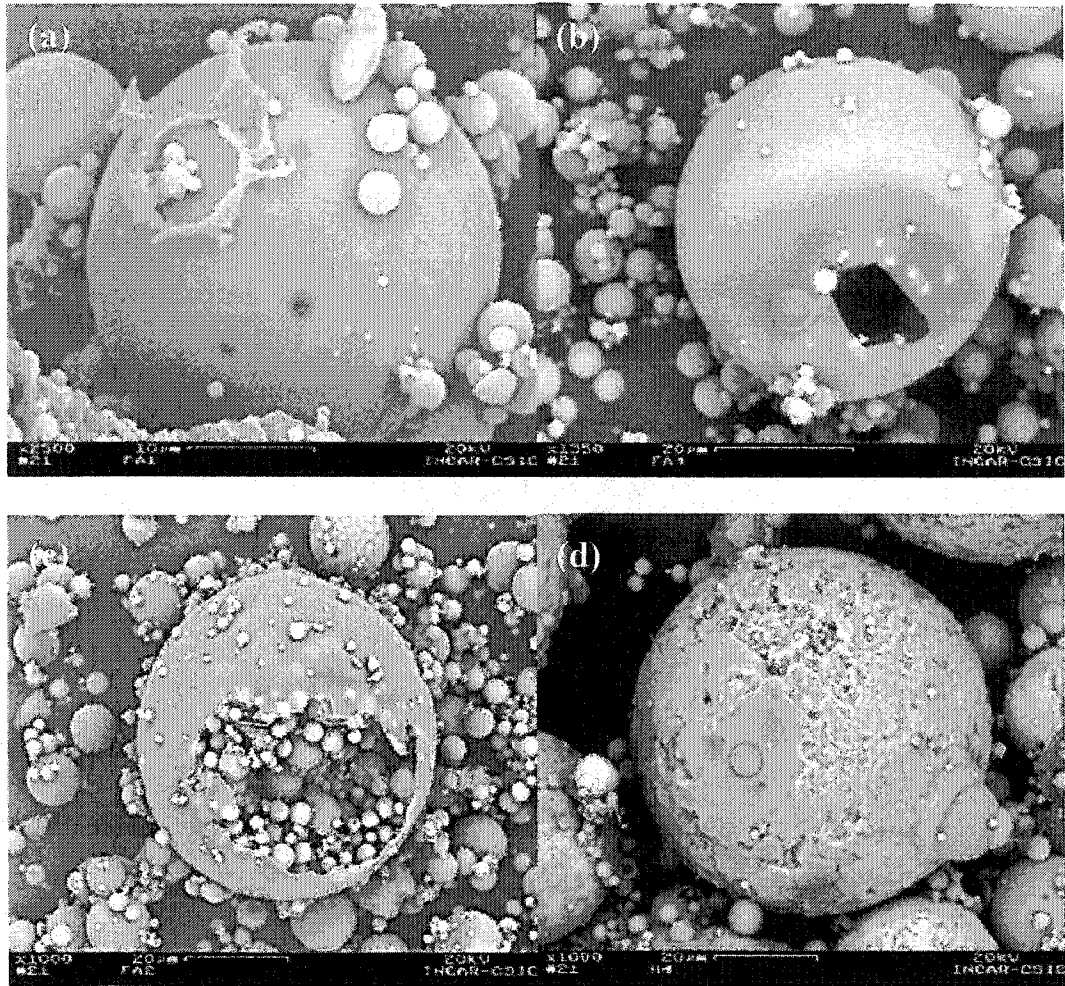


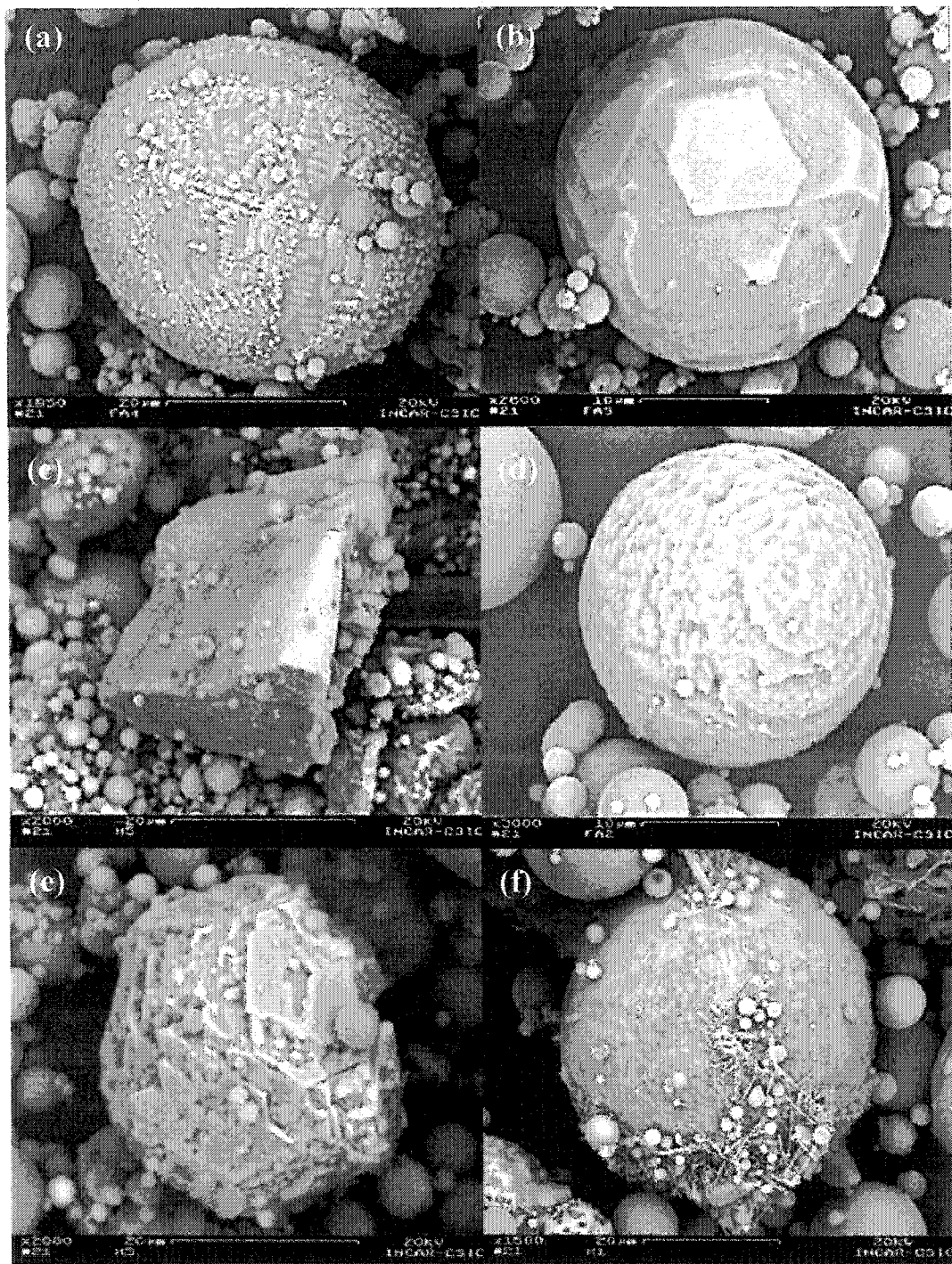
Figure 2.4 Spheres Found in Coal Fly Ash from a Kentucky Power Plant

Vassilev et al. [49] recently published more detailed mineralogy and morphology of ash using some Spanish coal ashes and some imported ashes. They confirmed the presence of many types of spheres including cenospheres, pleuroospheres and dermaspheres (Fig 2.5), and they also reported the presence of mineral phases found on the aluminosilicate spheres, which included dendritic and octahedral magnetite, hematite, wollastonite, gypsum, anhydrite and quartz (Fig 2.6).



- (a) aluminosilicate glass sphere
- (b) aluminosilicate glass cenosphere
- (c) dermasphere (larnite, Ca_2SiO_4 , covered by aluminosilicate glass skin)

Figure 2.5 Morphology of Some Spanish Coal Ashes



(a) dentritic magnetite (b) octahedral magnetite (c) semi-fused quartz
 (d) wollastonite (e) prismatic hematite
 (f) needle anhydrite-gypsum crystals

Figure 2.6 Minerals Found in some Spanish Coal Ashes

2.2 Characterization of Oil Sands Fly Ash

2.2.1 Crude Bitumen Production in Alberta

Alberta's oil sands, located in the north of Alberta, Canada, contain the largest crude bitumen resource in the world. In Alberta, conventional crude oil production is rapidly decreasing while crude bitumen production is drastically increasing with the development of bitumen upgrading techniques. The EUB (Alberta Energy and Utilities Board) [50] estimated that approximately 50 billion m³ (315 billion barrels) are considered potentially recoverable in this area. In 2002, Alberta produced 48.1 million m³ (303 million barrels) of crude bitumen. Bitumen produced from mining was upgraded, yielding 25.6 million m³ (161 million barrels) of synthetic crude oil (SCO) [50]. The two major tar sands oil producers, Suncor and Syncrude, produce more than 325,000 barrels of crude oil per day.

2.2.2 Fly Ash Production in Alberta Oil Sands

Oil sand is composed of sand, bitumen, mineral rich clays and water. Bitumen, in its raw state, is black, asphalt-like oil. It requires separation and upgrading processes to make it transportable by pipeline and usable by conventional refineries. The upgraded bitumen product consists of naphtha and light and heavy gas oils. A substantial amount of petroleum coke is produced from this upgrading process. Currently, the combined daily production of oil sands coke by Suncor and Syncrude Canada exceeds 6000 t [3]. Figure 2.7 [5] and Figure 2.8 show schematic flow sheets of petroleum coke and fly ash production.

Suncor fly ash is produced when the coke produced from the coker is burned in the boilers that generate electricity. The temperature of the boilers is assumed to be around 1200°C (Figure 2.7). On the other hand, Syncrude fly ash is produced when the coke obtained from fluid cokers is burned in the cokers to maintain the coker temperature, which is normally held at around 630°C (Figure 2.8).

Approximately 22% of the bitumen is converted into coke in eight Suncor cokers, whereas around 15% of the bitumen is converted into coke in two fluid cokers of Syncrude with two-thirds of the coke being stockpiled [51]. Currently, approximately 250 and 50 tonnes of fly ash are produced by Suncor and Syncrude per day, respectively [5].

2.2.3 Particle Size and Morphology

The size and shape of Suncor fly ash is quite similar to that of coal fly ash since both coke and coal undergo phase transformations to form fly ash at similar temperatures. Suncor fly ash basically consists of both ash spheres and irregular carbon particles, and the size is quite fine (80% < 45 µm).

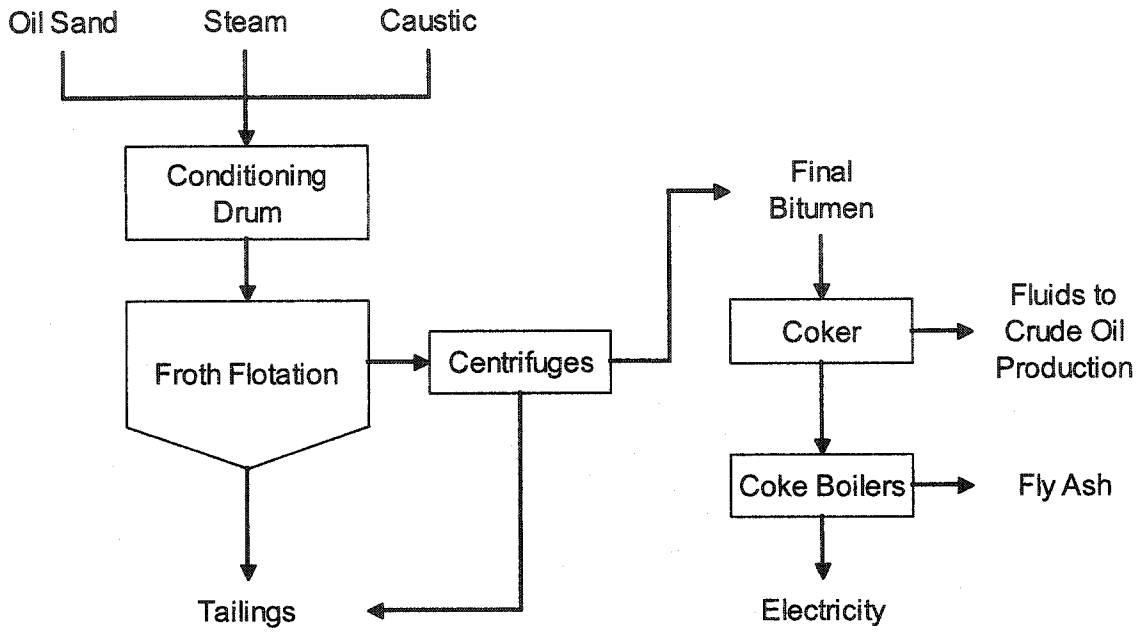


Figure 2.7 Simplified Suncor Process Flowsheet [5]

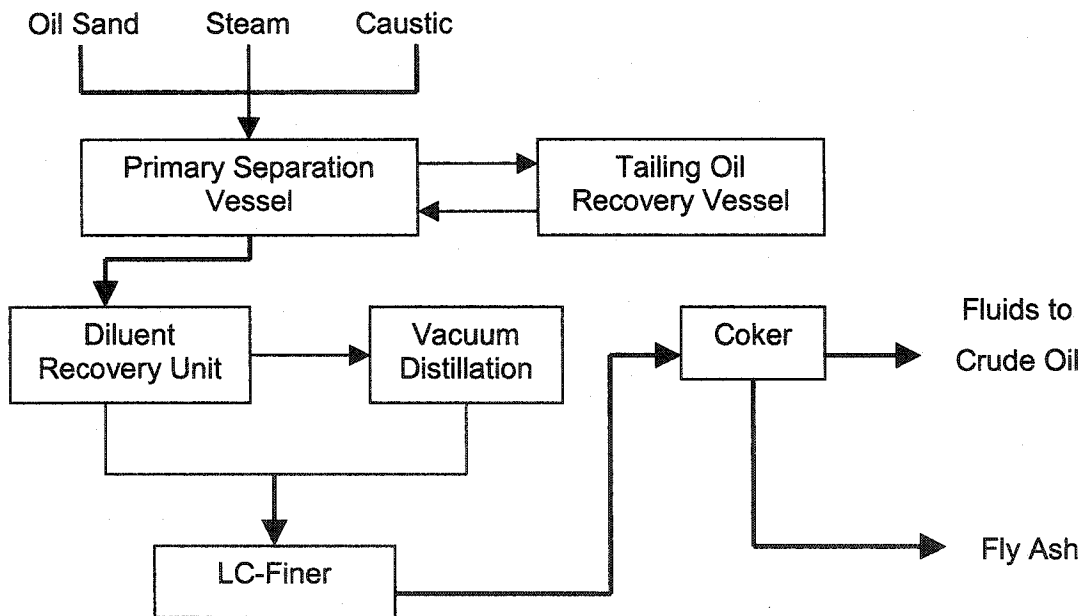


Figure 2.8 Simplified Syncrude Process Flowsheet

Holloway and Etsell [7] found that the size of spheres was around 2 to 30 μm . Cenospheres and pleuroospheres were also observed in Suncor fly ash (Figure 2.9). Microcrystals normally growing on the surface of spherical particles are found in some fly ash samples. Griffin and Etsell [4] also confirmed the presence of these microcrystals in finer spherical particles. They reported that the microcrystals were between 0.1 and 0.8 μm in width and 0.5 to 5 μm in length. In addition, the crystals were shown to contain much higher levels of V, Fe, Ti and Ni than the surrounding aluminosilicate spheres. Figure 2.9 shows micrographs of Suncor fly ash.

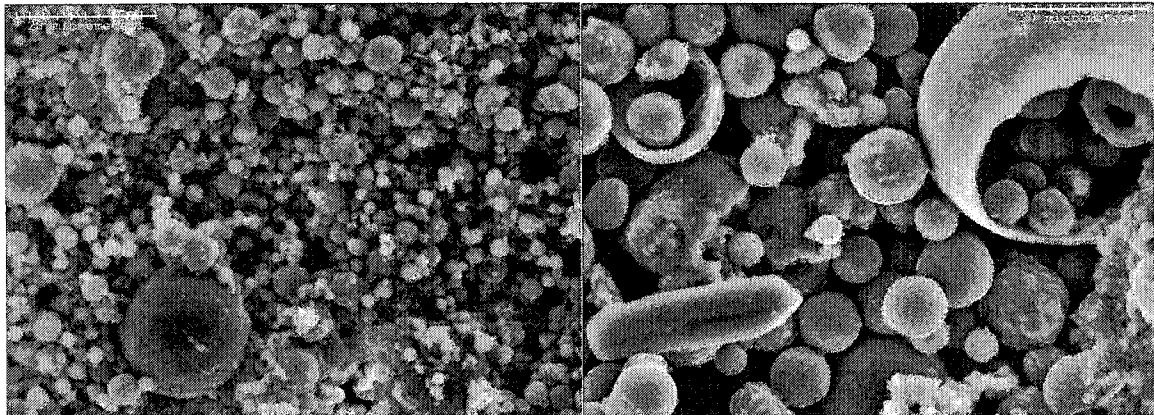


Figure 2.9 Micrographs of Suncor Fly Ash Samples [5]

Syncrude fly ash is somewhat different in particle morphology since ash is produced at relatively lower temperatures, as mentioned already. Almost all particles are flaky aluminosilicate particles with a few spheres and microcrystals (Figure 2.10). Free quartz particles are also reported in many Syncrude ash samples and their size range from 10 to 30 μm [7]. Figure 2.10 shows micrographs of Syncrude fly ash samples.

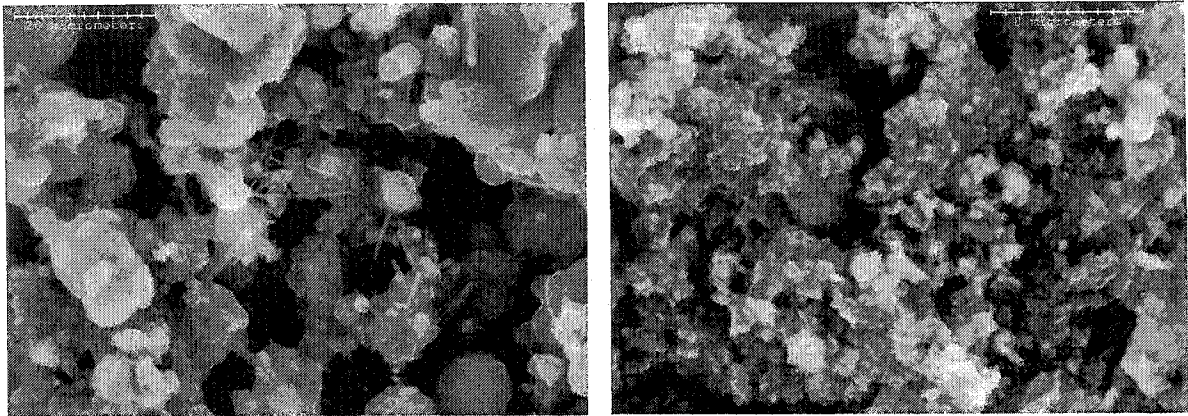


Figure 2.10 Micrographs of Syncrude Fly Ash Samples [5]

2.2.4 Chemical Composition of Oil Sands Fly Ash

Oil sands coke contains 79-84% C and 5-8% S as major components, and Al, Si and Fe as minor elements [51]. The quantity of carbon is high and comparable to that of bituminous coal. The amount of sulfur is significantly higher in oil sands coke than in coal. While sulfur is believed to occur mostly as pyritic sulfur in coal, Furimsky[3] suggested that more than 95% of the sulfur be of organic origin in bitumen and should be buried in the coke due to the prolonged heating in both Suncor and Syncrude coking processes. The structure of sulfur in petroleum has been well documented due to its environmental importance. Sulfur in oil sands is in two main forms. The most common type of sulfur is in aromatic rings which are difficult to remove. The other type is in thioethers which are much easier to remove [2]. In both cases, a significant amount of the total sulfur is kept in the residues, such as asphaltene and coke.

Structural information on vanadium and nickel occurring in petroleum or crude oil reveals that these metal components occur in the oil sands as either a porphyrin type or non-porphyrin type [52-54]. All the sites where metal components can be placed in these two common structures are extremely stable so that they are resistant to treatment and kept in the residues [55, 56]. Boduszynski [57] states in his research report that all metals, especially V, Ni and Fe, are found as organometallic compounds in petroleum, and also concludes that heteroatoms (S, N) and metals occur in the same molecular structure. Unfortunately, migration or transition of these metal values and heteroatoms to the coke and coke ash is not well understood.

Chemical compositions of Suncor and Syncrude fly ash after removing all carbon from the coke have been reported in detail [5]. It is obvious that, compared to coal fly ash, significant amounts of V, Ni and Ti are contained in oil sands fly ash. On the other hand, the amount of base elements such as Ca, Na and Mg is much lower in oil sands fly ash than in coal ash. Ash content of coal is normally around 10% but more than 20% ash content is found in some areas, whereas coke ash is normally lower than 6% (Tables 2.3 and 2.4).

Table 2.3 Chemical Composition of Some Coals and Cokes

Contents	Coal ^a				Coke	
	Iowa	Wyoming	Illinois	Kentucky	Syncrude ^b	Suncor ^c
Ash	11.7	6.8	9.6	10.38	5.9	3.99
Carbon	53.95	69.5	61.81	72.18	81.3	84.02
Hydrogen	3.98	4.9	4.19	4.99	1.9	3.67
Nitrogen	1.24	1.1	1.04	1.48	1.7	1.38
Sulfur	3.8	0.5	3.7	1.47	8.7	5.73
Oxygen	6.61	17.2	7.6	19.88	0.5	1.21

a) taken from Torrey [8]

b) taken from Har [58]

c) taken from Furimsky [3]

Table 2.4 Chemical Composition of Some Coal and Coke Ashes

Contents	Coal Ash ^a			Coke Ash ^b	
	Lignite	Subbituminous	Bituminous	Syncrude	Suncor
SiO ₂	19.7	27.4	42.0	37.64	42.18
Al ₂ O ₃	11.1	12.7	18.1	24.33	22.72
Fe ₂ O ₃	9.1	13.9	5.7	11.42	11.85
TiO ₂	0.4	0.6	0.8	4.63	3.28
P ₂ O ₅	0.3	0.5	0.6	0.40	0.29
CaO	24.6	16.6	17.8	2.94	3.45
MgO	6.9	5.5	2.4	1.46	1.59
SO ₃	19.5	17.0	8.2	2.88	2.53
Na ₂ O	6.5	2.2	1.4	1.67	0.75
K ₂ O	0.4	0.5	0.3	1.72	1.93
V ₂ O ₅	Tr.	Tr.	Tr.	4.94	4.40

a) taken from Torrey [8]

b) taken from Furimsky [3]

2.2.5 Mineralogy of Oil Sands Fly Ash

Very little work has been previously conducted on the mineral phases of oil sands fly ash and their transformation behavior on combustion. Recently, Holloway [5] revealed some detailed mineralogy on oil sands fly ash. He found that most of Suncor fly ash was made up of aluminosilicate glass, with small amounts of mullite and anhydrite as the secondary crystalline phases. Quartz, anhydrite, hematite, pseudobrookite (Fe_2TiO_5), nickel titanate (NiTiO_3) and cristobalite were identified in Syncrude fly ash. Even though oil sands ash is distinguished by a high portion of vanadium, no V-related minerals have been identified in either Suncor or Syncrude fly ashes. Gomez-Bueno et al. [59] speculated that all metal values were tied up in the aluminosilicate glass matrix so that it was difficult to identify the crystalline phases. Holloway and Etsell [7] proposed in their salt roasting tests with Suncor ash that vanadium be substituting in Al sites of aluminosilicate glass; thus vanadium-bearing minerals could hardly be identified. They also found that an addition of sodium could pull out vanadium from the aluminosilicate glass such that water-soluble sodium vanadium compounds could be formed.

3.0 Analysis Methods and Procedure

3.1 Sample Preparation

Cokes from Suncor and Syncrude were ashed at 100°C intervals from 400 to 1200°C before analysis. All the samples were combusted in a muffle furnace until constant weight was achieved. Except for LTA samples, 50 g of coke samples were ashed until they achieved constant weight, and ash contents were determined. Table 3.1 indicates the ash content of oil sands coke as temperature varies. It was expected that all early volatiles including carbon were completely removed by this method. It was also assumed that some minerals, especially sulfides, such as pyrite and pyrrhotite, which would possibly be present in the ash, underwent phase transformation so that the original mineralogy of the ash could not be revealed by this method.

Table 3.1 Ash Content of Oil Sands Coke

Temperature (°C)	Ash Contents (%)	
	Suncor coke	Syncrude coke
LTA	12.45	12.83
400	3.04	8.48
500	3.06	8.86
600	2.75	8.95
700	2.82	8.73
800	2.43	8.55
900	2.74	7.91
1000	2.25	7.48
1100	2.43	7.87
1200	2.13	4.82

In order to preserve the original mineral phases of the ash, a low temperature ashing (LTA) technique was used. Each coke sample was placed in two sample chambers of model LTA-302 purchased from LFE Corporation, Massachusetts, USA, which were held in an activated oxygen-plasma atmosphere generated by a radio-frequency field [60]. The main advantage of using the low temperature asher, or radio-frequency asher, is that the organically bonded minerals can be broken apart without mineral alterations as activated oxygen generated from a radio-frequency oscillator, reacts with organic substances of the coke. It usually took more than 15 days to ash a few grams of coke. This was because the presence of organically bonded inorganics drastically increased ashing time [21]. It was inevitably considered that it was also possible for organic sulfur and cations that were released from the organically bonded inorganics to contact other mineral matter during oxidation, thereby increasing the chance of mineral alteration. The temperature of LTA was reported to be typically 125 to 150°C, but the actual temperature of sample chambers in this LTA was 65°C so that this temperature was used throughout this thesis to represent the LTA temperature.

3.2 Analytical Methods

Samples obtained from mineral processing tests were analyzed using atomic absorption spectroscopy (AAS). A fraction of each sample was fused with lithium metaborate (LiBO_2) at 900 to 1000°C, with the fusate dissolved in dilute hydrochloric acid. The solution was then analyzed by AAS. The concentrations of Al, Fe, Mo, Ni, Si, Ti and V were analyzed using a single-element Perkin-Elmer 4000 atomic absorption spectrometer.

Standards were prepared to minimize matrix effects and interference by other elements in the analyte, based on recommendations given in an atomic absorption manual [61].

A combination of scanning electron microscopy (SEM) and x-ray diffraction analysis (XRD) was used to characterize the mineral phases in the sample. X-ray data were collected using CuK α radiation in the range between 10° and 90° and steps of 0.05° 2 θ with a count time of one second per step. These diffraction data obtained from the Rigaku-Denki generator were then used for both qualitative and quantitative analyses.

Quantitative analysis of fly ash is extremely challenging because of its high content of amorphous phases, resulting in weak peak intensities and overlaps of the peaks. As part of the XRD studies on oil sands fly ash, quantitative analyses have been performed with the Siroquant software package using the scale factors from the Rietveld refinements. The Rietveld method [62, 63] was originally developed to use the data in a neutron wavelength-dispersive powder diffraction trace to refine the crystal structure of a material. Currently this method has been expanded to x-ray powder diffraction and is widely used to obtain not only structural information, but also quantitative information about a material [64, 65].

The main disadvantage of the conventional XRD powder method is the peak overlaps, which prevent proper determination of the structure. The Rietveld method creates an effective separation of these overlapping data, thereby allowing an accurate determination of the structure. Refinement of Rietveld parameters leading to a successful

fit of the total calculated pattern to the observed pattern is usually done in a certain sequence. In the first stage, all mineral phases identified using a search and match program should be inputted into the software. The crystallographic data of each mineral phase should include the name of the phase, chemical formula, the name of the space group (lattice type), all six unit cell dimensions and x-ray data (2θ angle and radiation type). In the second step, a calculated pattern can be drawn based on the inputted data, and the difference between calculated and observed patterns can be also drawn. In the final stage, the refinement routine should be done until two patterns reach minimal difference. Background subtraction, instrumental error correction, preferred orientation, the shape correction, asymmetry correction, particle size and absorption correction, and other parameters are refined in this stage. The determination of the best fit is expressed as a figure of merit, Chi-squared (χ^2). The χ^2 value approaches 1 for the perfect fit, but in general, a value below 3.0 indicates a well refined pattern. The Rietveld scale factor is, then, used to quantify the weight % of a mineral phase.

Quantitative analyses on the amorphocity of samples used in this study were based on the internal standard addition method. This method, commonly known as 'spiking', was first proposed by LeRoux, Lennox and Kay [66]. If there is a second phase β in the sample in which a known amount of phase α (a spike phase) is added, the intensity ratio between the two phases is plotted against the known addition, and the best fit line is extrapolated to zero addition [64]. The intensity ratio, normally expressed as a function of constant "K", is then calculated and compared with the measured intensity peak of phase β to

calculate the quantity of unknown phase β . Zinc oxide was added as an internal standard (a spike mineral) for all the samples.

A traveling copy of Siroquant was obtained from Sietronics Pty. Ltd., Australia and was tried for a limited time period. All x-ray peaks of a sample were identified using identification software and using a manual method. Then, all mineral phases were refined using Siroquant until sufficient refinements were achieved. However, a few mineral entries were not established resulting in poor (but adequate) refinements. Even though all the results were dummy values due to the lack of mineral database, all values were reported in this paper to see the compositional changes in certain temperature ranges. For analyzing the amorphocity of the ash, zinc oxide was used as an internal standard. Before x-ray analyses, around 10 wt% ZnO was added into each sample and mixed thoroughly by means of hand grinding.

4.0 Metal Value Beneficiation

Since the mineralogy of both Suncor and Syncrude ash is too complicated to interpret, it is essential to concentrate some mineralogical fractions and separate them from other fractions so as to better understand the behavior of mineral phases, especially metal values. Some attempts were made to enrich iron-bearing mineral fractions and silica or silica related mineral fractions using magnetic separation, centrifuge, froth flotation and electrostatic separation techniques.

4.1 High Intensity Magnetic Separation

Several trial runs on Suncor ash were attempted using a Frantz Isodynamic Magnetic Separator. Samples were prepared by ashing Suncor coke at 700°C in order to have as many needles which contained higher iron and titanium than the matrix as possible, then by grinding by hand. Other grinding methods did not seem to be feasible since the particle size of the samples was too small (less than 3 µm) and contamination of samples would be expected. Samples were then placed in a dryer for a few hours before feeding into the separator. Due to the small particle size, ash particles tended to aggregate so that an extremely low feeding speed was selected (0.46 g/hr).

The weight fractions obtained in the non-magnetic and magnetic portions were 96.35% and 3.65%, respectively. However, chemical analyses on these fractions and SEM micrographs were unsatisfactory. Micrographs from the SEM showed that the magnetic

separation was unsuccessful since both fractions contained needles and flaky shape matrix particles, which also indicated that hand grinding was not able to liberate iron bearing minerals (Figure 4.1). EDX analysis also indicated that there was no difference between the two streams (Table 4.1).

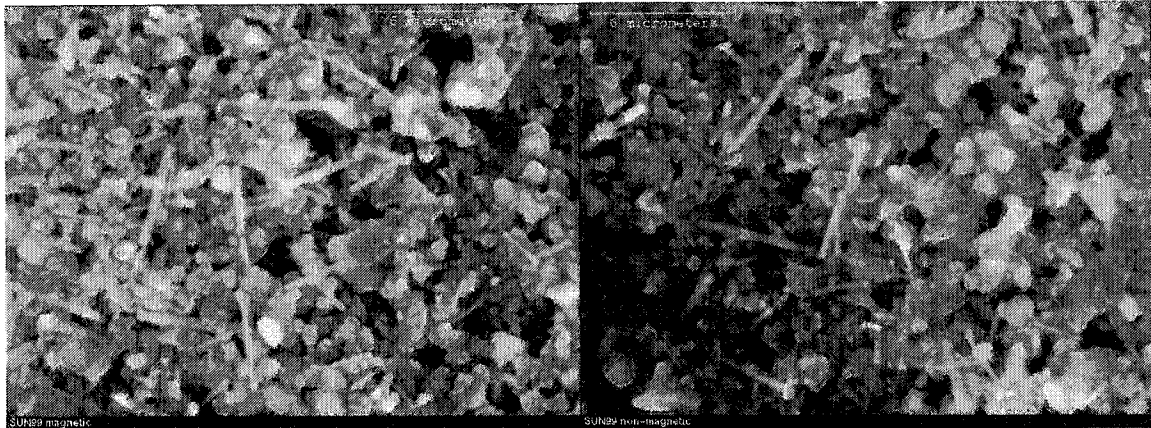


Figure 4.1 Micrographs of Magnetic Fraction (left) and Non-magnetic Fraction (right) of Suncor Fly Ash ($\times 5000$, bar: $6\mu\text{m}$)

Table 4.1 Chemical Composition of Magnetic and Non-magnetic Fractions of Suncor Ash

Elements	Magnetic fraction (%)	Non-magnetic fraction (%)
Na	0.80	0.63
Mg	1.02	0.84
Al	15.67	16.45
Si	22.93	24.43
P	0.49	0.49
S	1.70	1.88
K	1.72	1.84
Ca	2.10	2.11
Ti	4.98	5.38
V	5.31	5.58
Mn	0.46	0.45
Fe	15.36	15.15
Ni	2.05	2.38

4.2 Centrifuge

Several centrifugal concentration tests were conducted with a Falcon Concentrator #SB40 centrifuge. 30 g of sample was diluted in 300 mL of water. The rotor speed varied from 35.00 Hz to 78.25 Hz, changing the gravity from 20 G to 300 G. Back pressure also varied from 1.72 kPa (0.25 psi) to 13.79 kPa (2 psi) in order to sufficiently separate the sample into the heavy and light fractions.

Table 4.2 shows the results from centrifuge tests on as-received ash from Syncrude. Samples were first decarburized at 500°C before the tests and the chemical composition of sample was measured to calculate the recovery of each element. Chemical analyses were performed using Perkin-Elmer 4000 atomic absorption spectroscopy (AAS).

Table 4.2 Recovery from Centrifuge Tests on As-received Syncrude Ash

Conditions	20 G + 1 psi		176 G + 2 psi		300 G + 1 psi		300 G + 2 psi	
	Heavy	Light	Heavy	Light	Heavy	Light	Heavy	Light
Yield (%)	8.85	91.15	7.96	92.04	31.48	68.52	23.04	76.96
Si	13.9	86.1	8.6	91.4	51.3	48.7	39.1	60.9
Al	2.4	97.6	1.8	98.2	14.1	85.9	9.7	90.3
Ti	1.32	92.1	3.0	97.0	17.8	82.2	11.6	88.4
V	1.0	99.0	0.7	99.3	9.9	90.1	5.8	94.2
Ni	1.2	98.8	0.9	99.1	10.0	90.0	6.1	93.9
Fe	3.7	96.3	2.1	97.9	14.6	85.4	10.7	89.3
Mo	7.2	92.8	2.5	97.5	11.8	88.2	8.6	91.4

Table 4.2 indicates that Si could be separated out of fly ash when treated with the centrifuge technique. When the equipment was set to relatively higher gravity, a higher fraction of Si was collected in the heavy fraction and metal values were collected in the light fraction. At lower gravity settings, Si and other metal values were still concentrated in the light fraction.

When as-received samples from Suncor were tested, however, no good results were obtained using the centrifuge due to the lower content of free silica in Suncor ash than in Syncrude ash. Compared to the starting sample which was decarbonized at 500°C and has not been through the centrifuge, no visible separations were obtained though heavy and light fractions were produced. Table 4.3 shows the results from centrifuge tests on as-received ash from Suncor.

Table 4.3 Recovery from Centrifuge Tests on As-received Suncor Ash

Conditions	20 G + 1 psi		20 G + 1 psi	
	Heavy	Light	Heavy	Light
Yield (%)	7.49	92.51	5.24	94.76
Si	4.7	95.3	3.5	96.5
Al	11.8	88.2	9.0	91.0
Ti	19.6	80.4	12.7	87.3
V	14.6	85.4	9.4	90.6
Ni	1.19	85.1	9.4	90.6
Fe	15.7	84.3	11.3	88.07
Mo	8.9	91.1	6.2	93.8

Finally, Suncor and Syncrude cokes were ashed at 700°C and centrifuge tests were also attempted on these ashes with the same experimental settings (20 G + 1 psi). However, this method was abandoned due to extremely low yields (0 up to maximum 2%). Particle sizes of both Suncor and Syncrude ash seemed to be too small to be treated in the Falcon concentrator.

4.3 Other Separation Methods

Several electrostatic separation trials were attempted with oil sands ash derived from both Suncor and Syncrude cokes on the assumption that some particles, such as silica, which are physically free from other mineral combinations, would be nonconductive or less conductive. 5 g of a Suncor fly ash sample was fed into the rotational drum separator and both insulator and conductor fractions were collected, which were 48% and 52%, respectively. Chemical analyses on these fractions indicated no difference in concentration in both streams.

Flotation tests were also attempted on the Suncor fly ash using a mini suspension-cell flotation machine constructed at the University of Alberta. 5 g of Suncor ash was diluted and agitated for a few minutes using a magnetic stirrer without additives, followed by adding a collector and a frother at two minute interval, and floated for 5 minutes. The collector used is sodium oleate (NaOL, $C_{18}H_{33}O_2Na$) which has an anionic polar head, and MIBC (methyl isobutyl carbinol) was used as a frother. The weight fractions of froth obtained from this test varied from around 17 to 19%. However, no difference was

observed in the chemical composition of each element so that no further tests were conducted.

4.4 Discussion

Several mineral processing techniques were tried to find a better way to understand the characteristics of oil sands fly ash. However, no technique was successful to separate some fractions from other fractions. This seemed to be mainly due to the extremely small particle size of fly ash. When ashed using Suncor and Syncrude coke, both ashes consisted of particles which were very small (about 2-3 μm) and some of these particles were connected to needles which contained high Fe and Ti. These small particles appeared to be covered by aluminosilicate amorphous materials, which made separation of minerals difficult. Once needles are broken apart from the matrix, it might be possible to separate them out. However, it cannot be achieved using conventional techniques because Fe and Ti seem to be connected to (or covered by) amorphous Al and Si. XRD analyses indicate that the ash contains hematite, Fe-Ti oxides and Fe-Ti-Ni oxides so that a wet type magnetic separator might be an effective tool to obtain a higher-grade of iron bearing minerals if the ash can be ground sufficiently to liberate needle like crystals. Other recent techniques, such as selective magnetic coating, are also considered promising for these iron-bearing particles although their quantities seem to be very low.

5.0 Characterization of Suncor Fly Ash

5.1 Chemical Composition

Table 5.1 shows the chemical composition of Suncor coke ash with temperature varying from 65°C (LTA temperature) to 1200°C. All data obtained from an energy-dispersive spectrometer (EDS) attached to an SEM were normalized to 100 wt%. EDS analyses are semi-quantitative mainly due to errors in qualitative analysis, errors in instrument and errors in sample preparation. However, EDS analyses were used in this study to compare matrix composition and other microcrystal structures.

As found in the coal fly ash, aluminum, silicon and iron are the major elements. However, contrary to coal fly ash, significant amounts of V, Ni and Ti also appear as major elements in these samples. Na, Mg, K and Mn, known as network modifying elements [9], are found as minor elements. There are no significant changes in composition of each element as temperature varies. However, sulfur found in the original coke sample drastically decreases in quantity as temperature increases to 400°C and disappears at 800°C.

It appears that the loss of sulfur at lower temperature ($\leq 500^\circ\text{C}$) results from organic sulfur, which is broken apart from the organic matrix and released as SO_2 and SO_3 during combustion, whereas the loss at higher temperature (600-700°C) is attributed to complete decomposition of anhydrite found in XRD studies. When the temperature increases to

500°C, the quantity decreases from 10.78% to 1.65%. It is obvious that only a small amount (around one tenth) of the sulfur exists as calcium sulfate.

Table 5.1 Elemental Analyses of Suncor Coke Ash (wt%)

Temp (°C)	L.T.A.	400	500	600	700	800	900	1000	1100	1200
Na	0.45	0.69	0.69	0.85	0.67	0.71	0.72	0.68	1.15	0.65
Mg	0.92	0.96	1.22	1.19	1.14	0.95	1.07	1.05	1.11	1.74
Al	13.53	14.32	15.96	16.21	15.75	16.22	15.81	15.49	15.11	17.56
Si	20.97	21.51	22.70	22.68	21.78	22.00	21.03	21.84	19.36	21.76
P	0.36	0.37	0.42	0.43	0.47	0.30	0.32	0.35	0.28	0.37
S	10.78	3.80	1.65	1.30	1.65	0.00	0.00	0.00	0.00	0.00
K	2.25	1.89	1.95	2.13	2.08	2.22	1.79	1.83	1.77	2.61
Ca	1.75	1.90	2.33	2.35	2.10	2.66	2.65	2.24	1.81	2.19
Ti	5.05	4.12	4.71	5.29	5.56	6.29	5.89	5.38	4.31	3.61
V	5.40	4.10	5.00	5.32	5.59	6.57	5.95	5.67	3.92	4.59
Mn	0.23	0.36	0.43	0.55	0.37	0.36	0.51	0.38	0.30	0.93
Fe	12.33	11.14	15.46	16.62	15.83	15.07	17.23	16.85	15.35	15.82
Ni	2.24	1.76	2.43	2.48	2.42	2.82	2.69	2.79	2.97	2.84

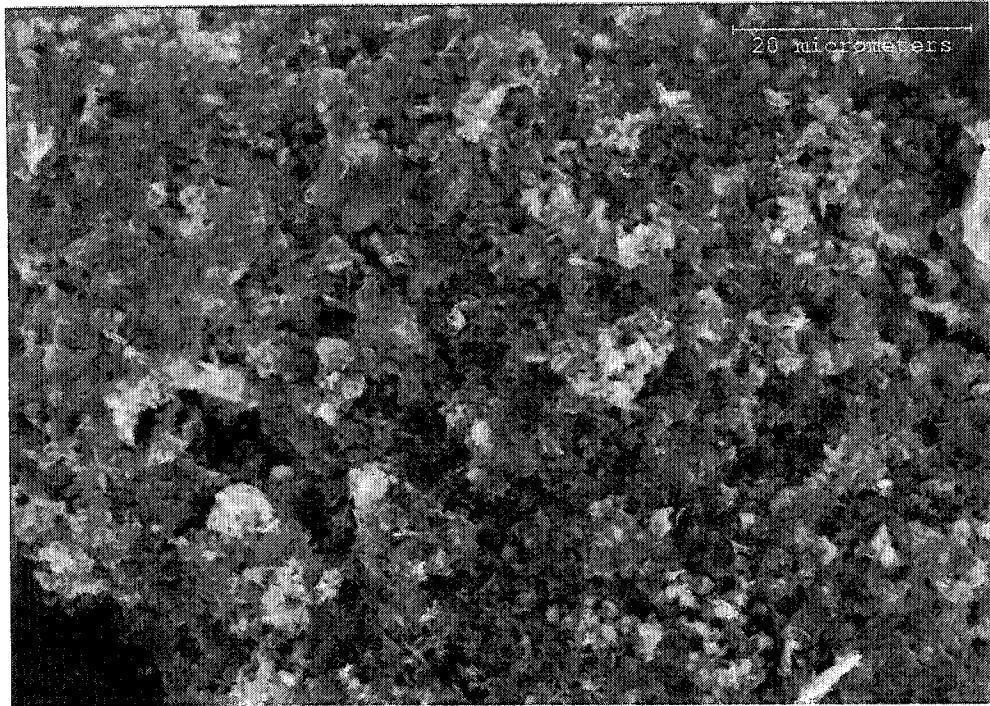
5.2 Morphology of Suncor Ash

SEM micrographs of Suncor fly ash samples show that the predominant phase in the ash samples is the amorphous aluminosilicate mineral (Figures 5.1 and 5.2). Amorphous aluminosilicate mineral refers to silicate minerals whose composition is mostly aluminum and silicon. Since minor amounts of Na, K and Ca are found in the ash, feldspar minerals such as potassium aluminum silicates and calcium aluminum silicates might be also included in the aluminosilicate mineral group. These particles are flake-like with a size

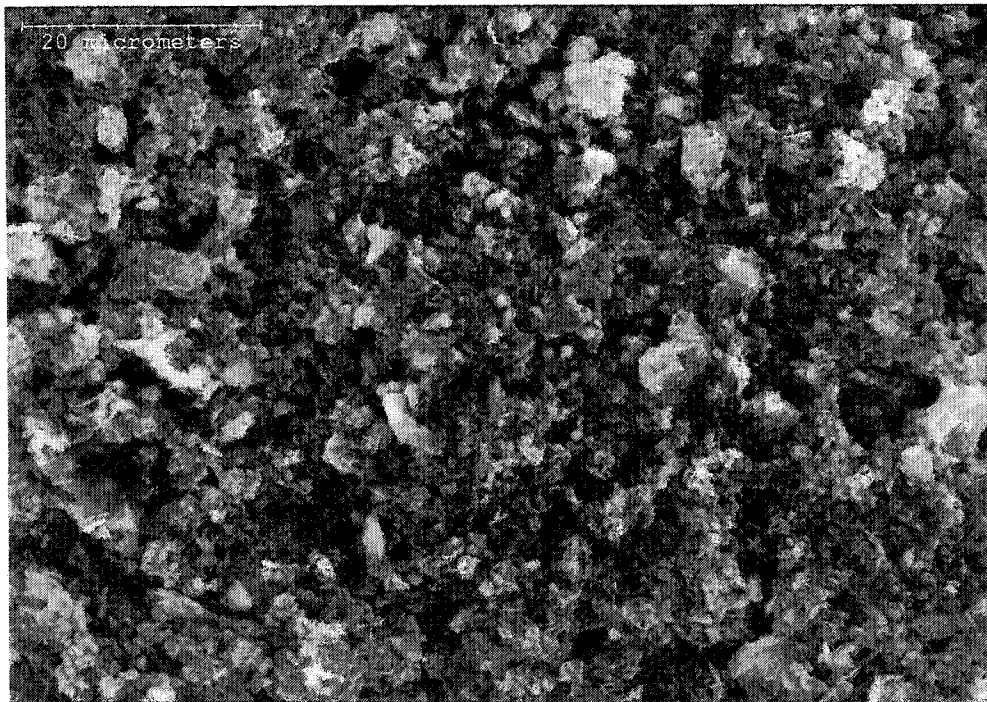
less than 4 μm for the lower temperature (from 65 to 700°C) samples. No different shapes are found in this temperature range. At 800°C, these particles seem to grow by combining with each other to make bigger particles by means of migration of glassy materials. These glassy aluminosilicate melts cover 2 to around 10 particles at 900°C and, at the later stage, they might form one big particle. Although the quantity of aluminosilicate melt is decreasing as temperature increases, their movement continues up to 1200°C leading to much bigger particles. At 1200°C, numerous small particles are entrapped in the aluminosilicate melt.

The size of the particles continuously increases as temperature increases. At 800°C, the average particle size is found to be around 6 μm , and at 1100°C, it seems to average around 15-20 μm . Around 60 μm size particles are also easily found at this temperature. At 1200°C, the particle size is even bigger and one particle shown in Figure 5.2(j) is around 300 μm when examined at low magnification.

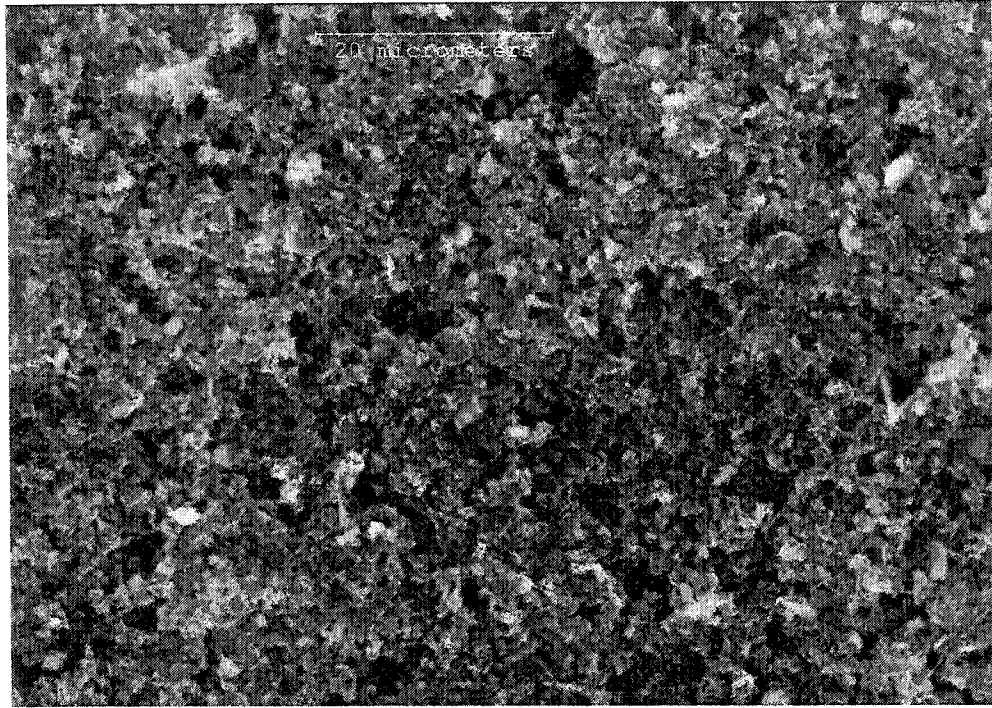
The shape of particles is also changing as temperature is changing. Very small thin flaky particles found to be predominant at low temperature become spherical when the combustion temperature is 1000°C or higher. Both cenosphere-like particles and pleurosphere-like particles were identified in this high temperature range. Figure 5.3 shows a pleurosphere-like particle and a cenosphere-like particle found in other Suncor ash samples formed at 1100°C. However, perfect spheres found in the as-received fly ash were not identified in these samples. It could be assumed that perfect spheres may be found if the ashing temperature is slightly higher than 1200°C.



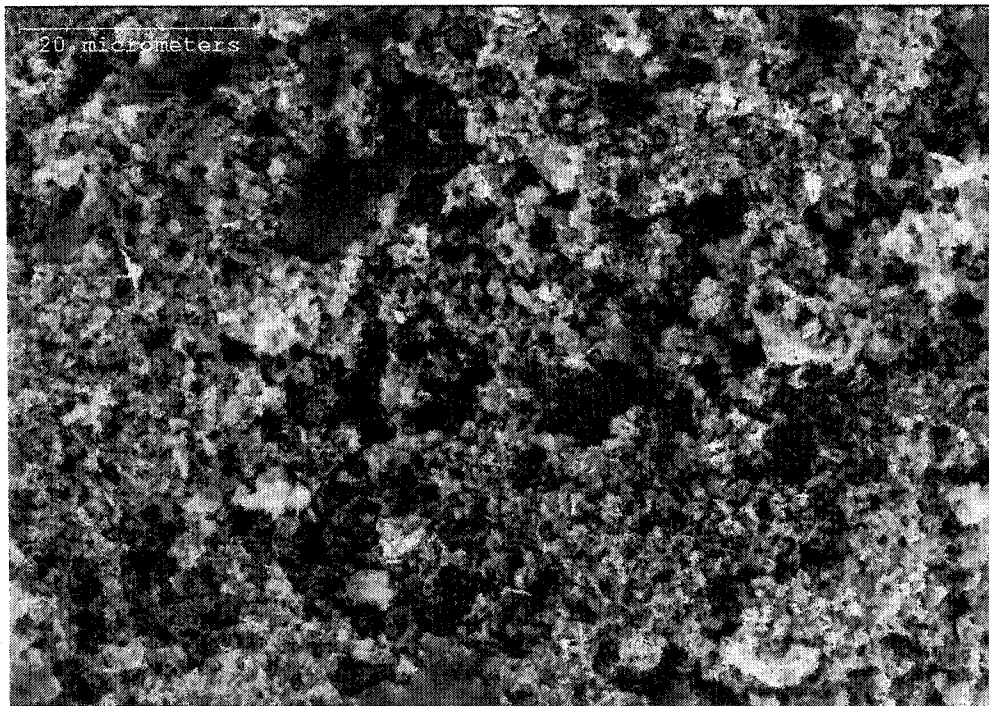
(a) Ashed at 65°C (LTA)



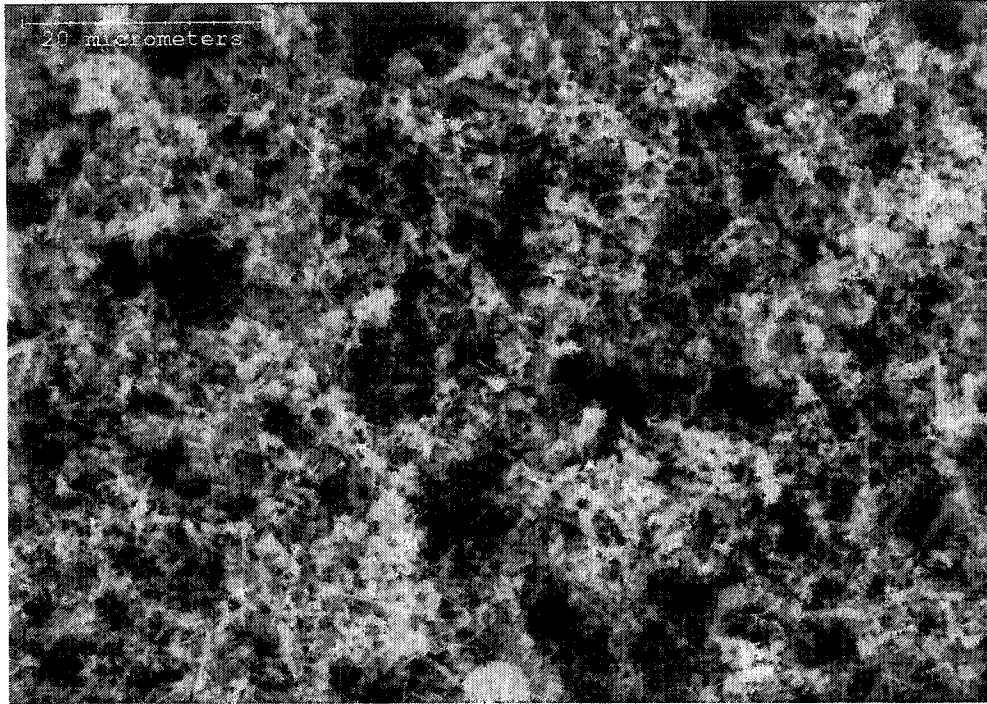
(b) Ashed at 400°C



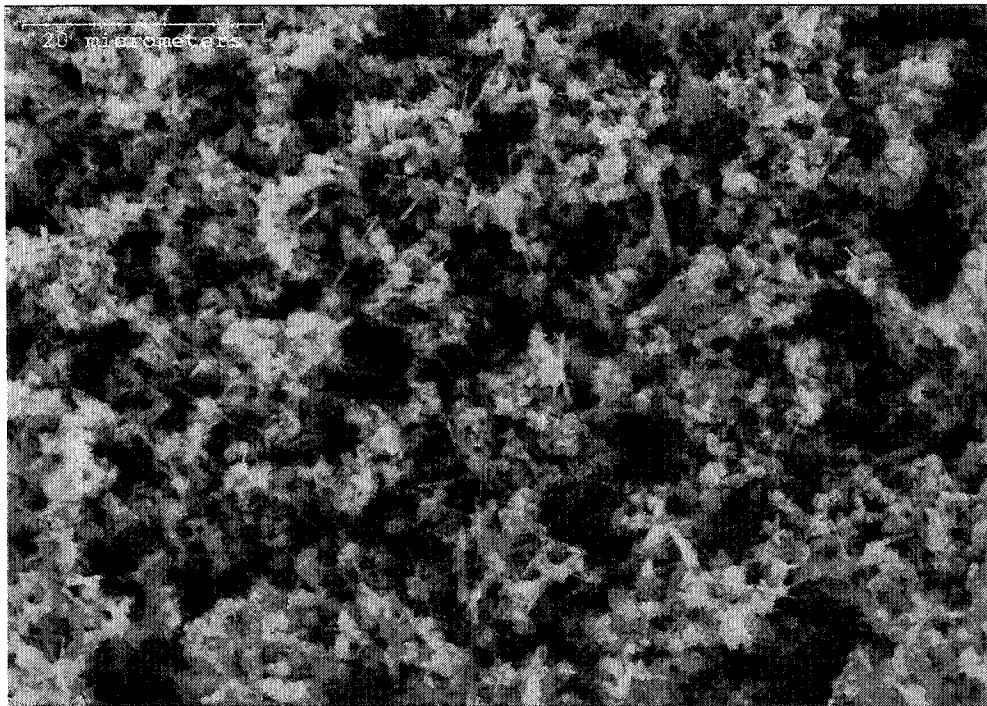
(c) Ashed at 500°C



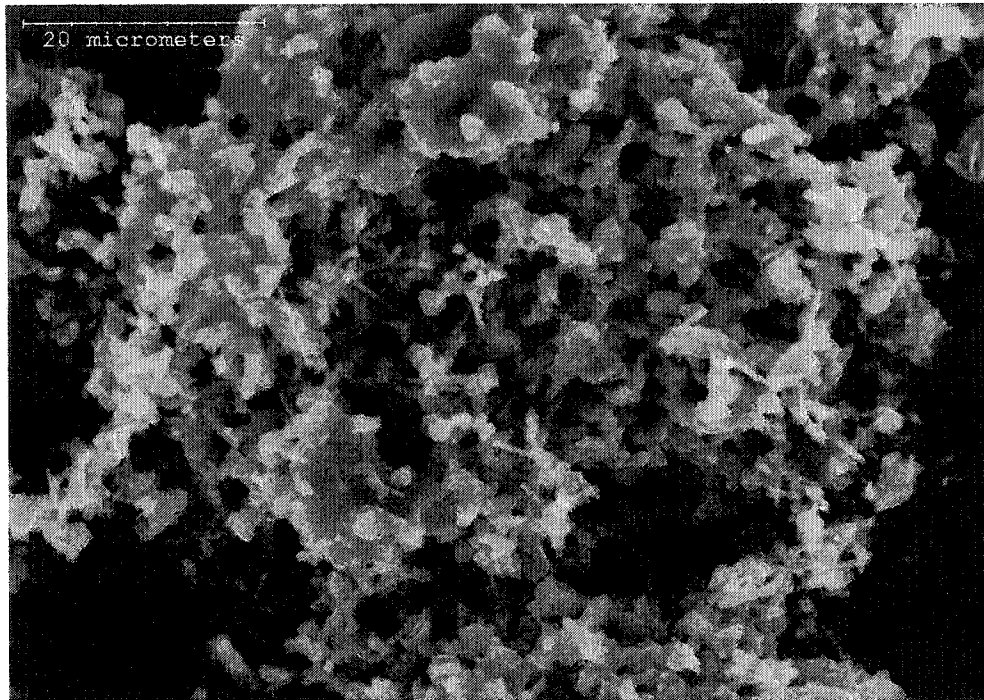
(d) Ashed at 600°C



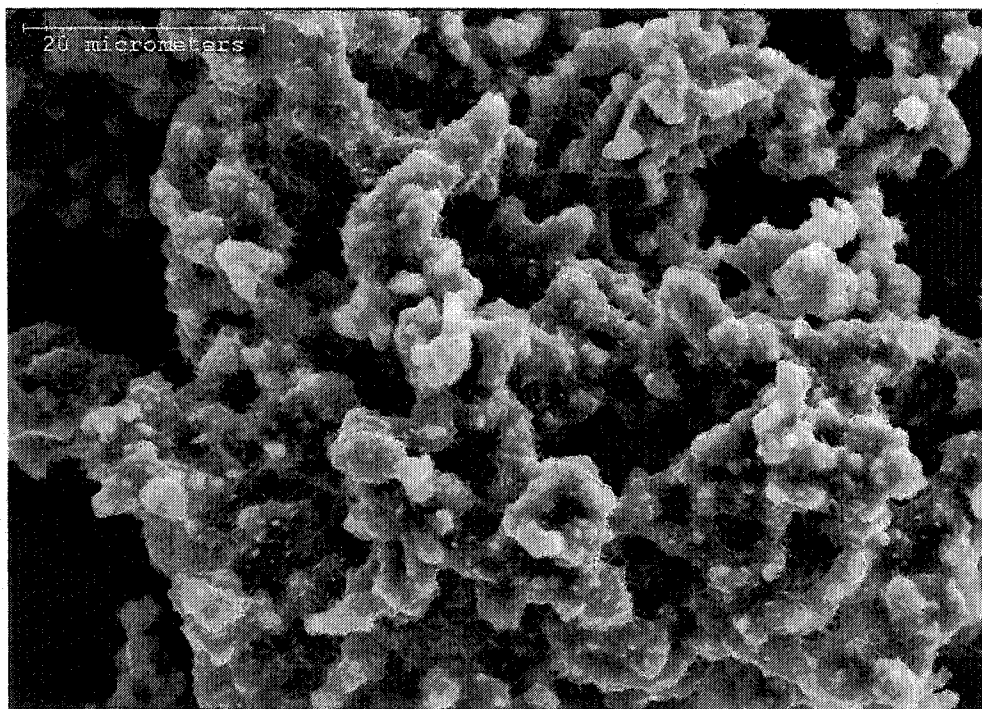
(e) Ashed at 700□



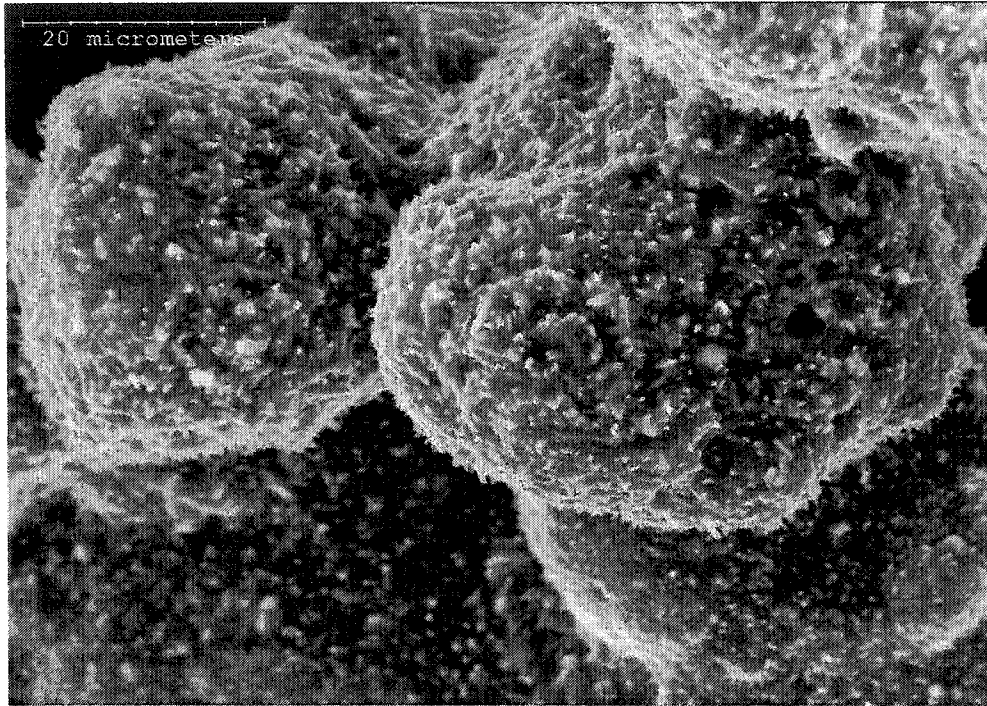
(f) Ashed at 800□



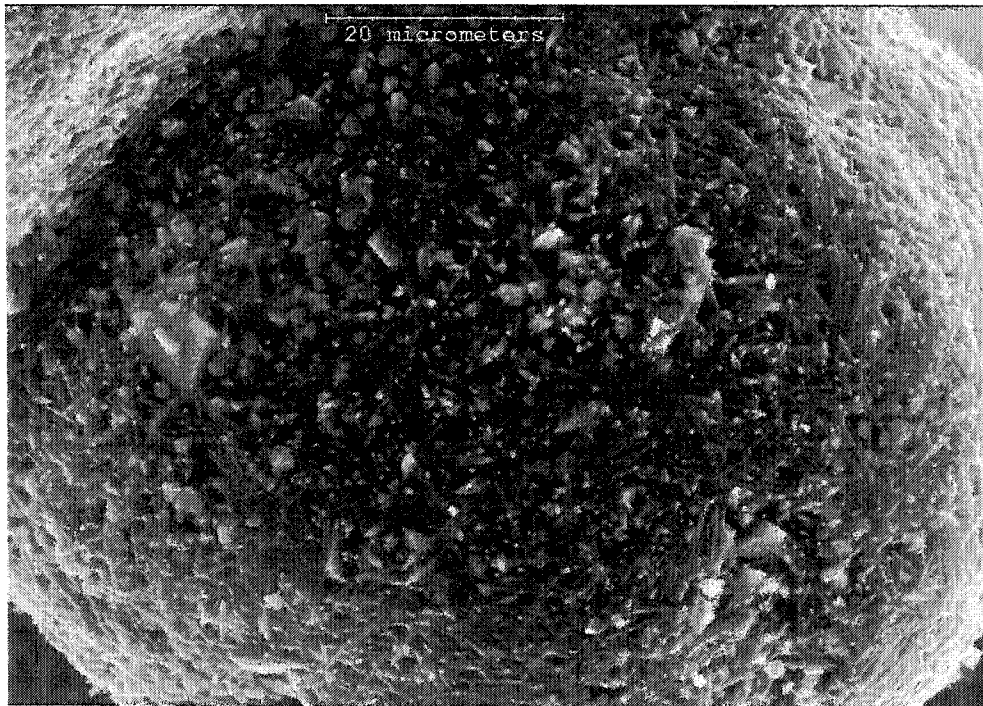
(g) Ashed at 900°C



(h) Ashed at 1000°C

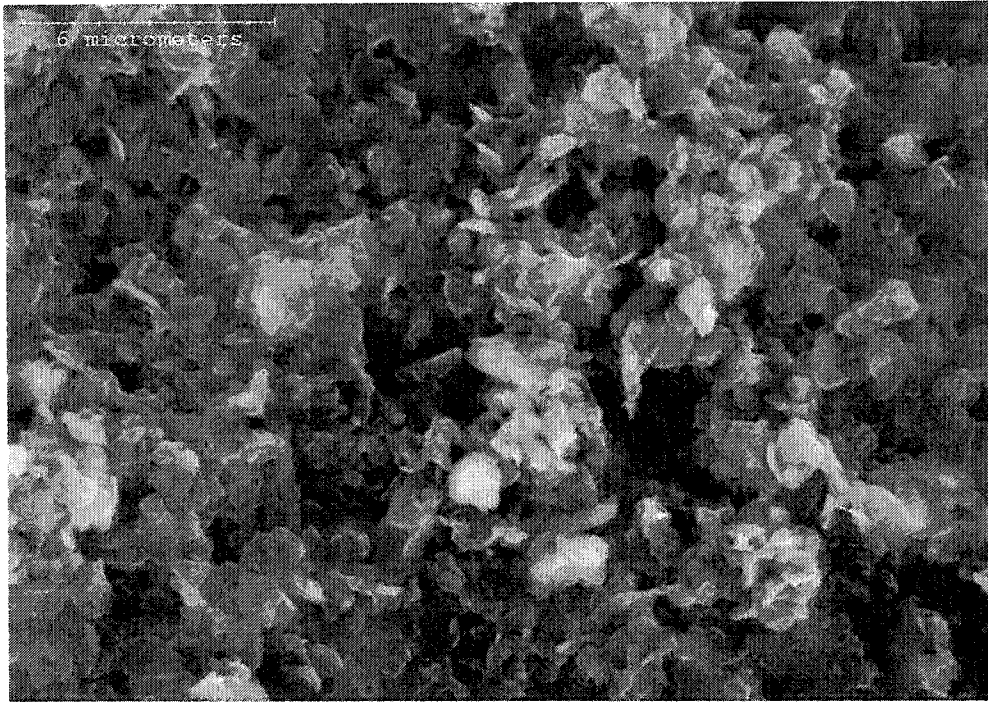


(i) Ashed at 1100°C

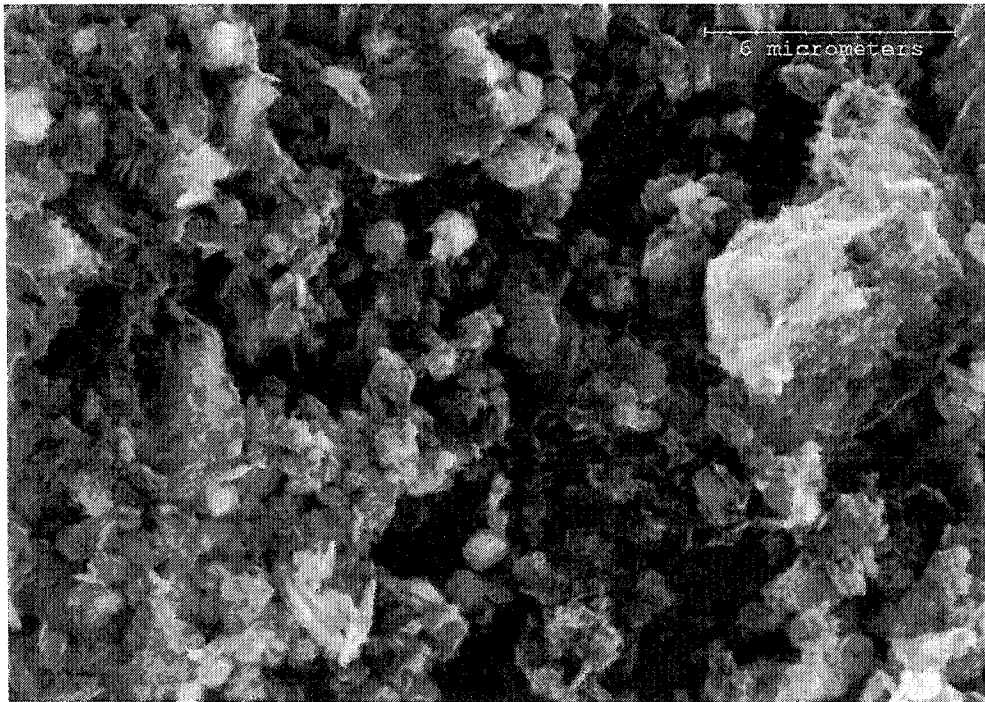


(j) Ashed at 1200°C

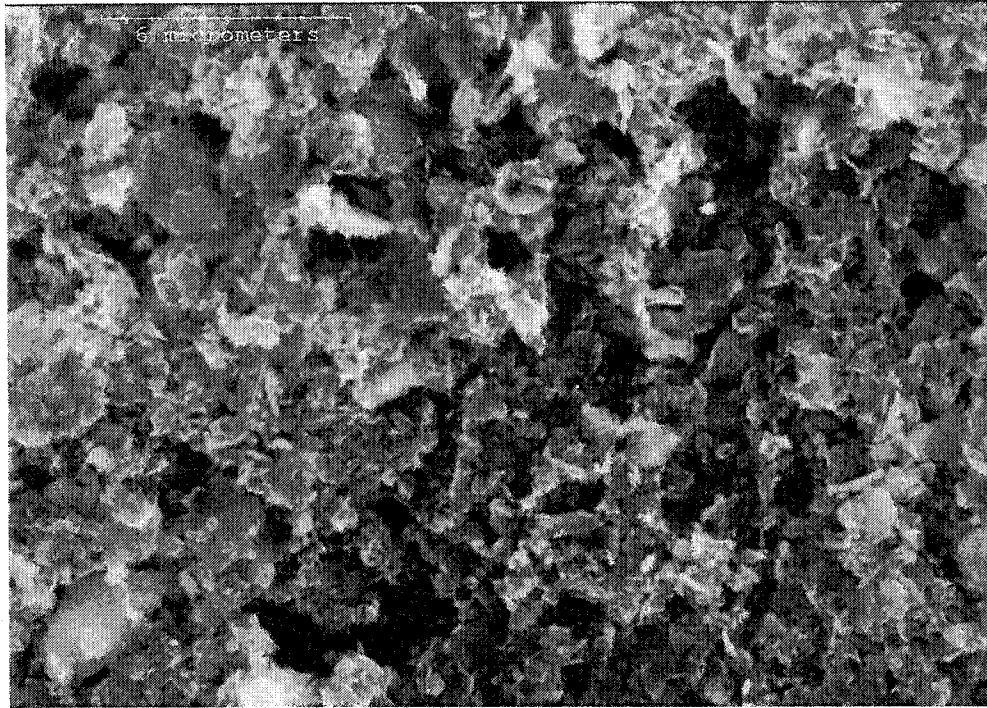
Figure 5.1 Micrographs of Suncor Fly Ash with Increasing Temperature (×1500)



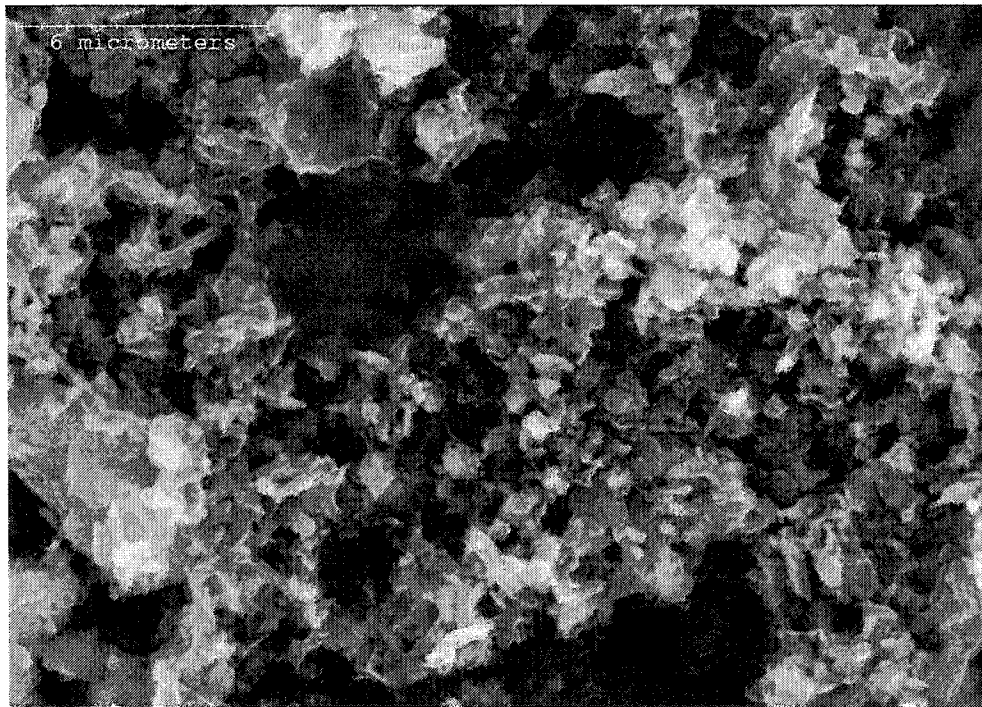
(a) Ashed at 65°C (LTA)



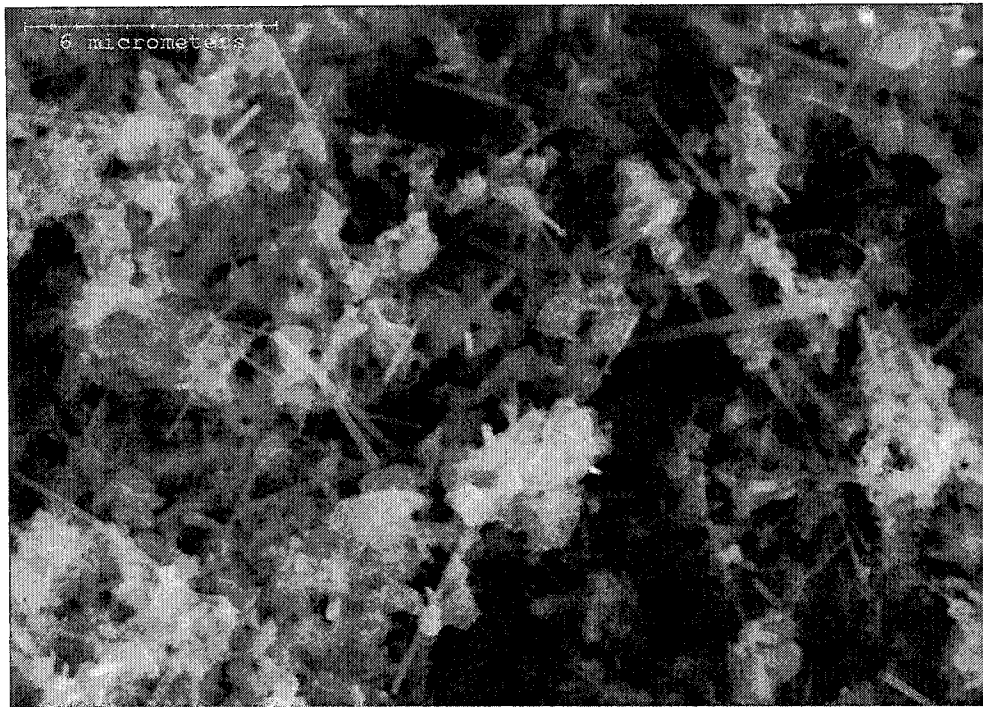
(b) Ashed at 400°C



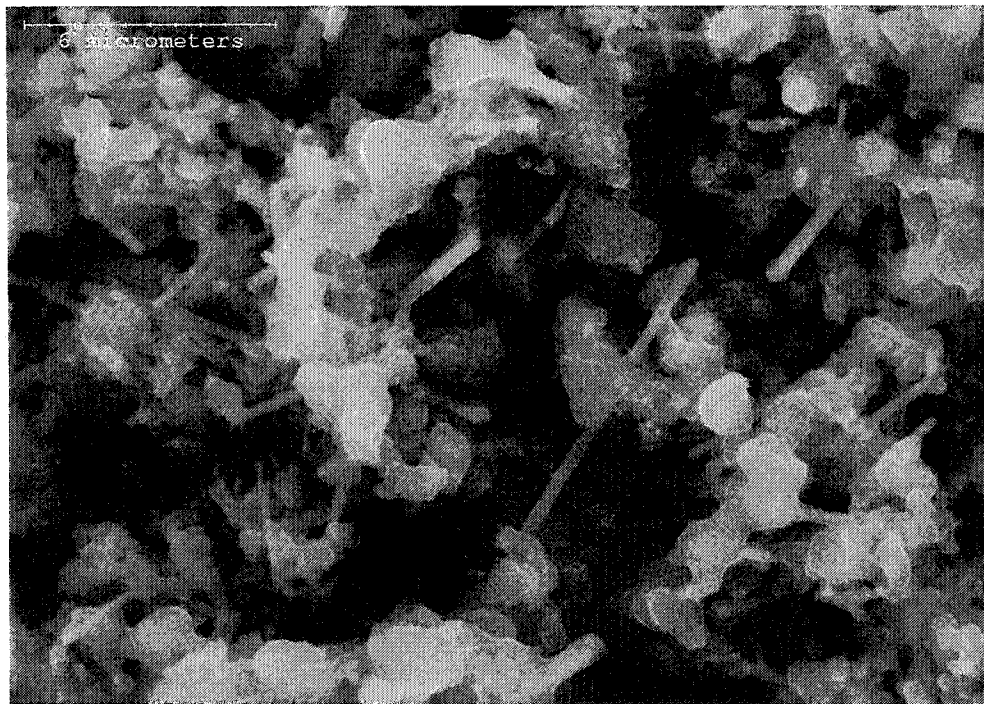
(c) Ashed at 500□



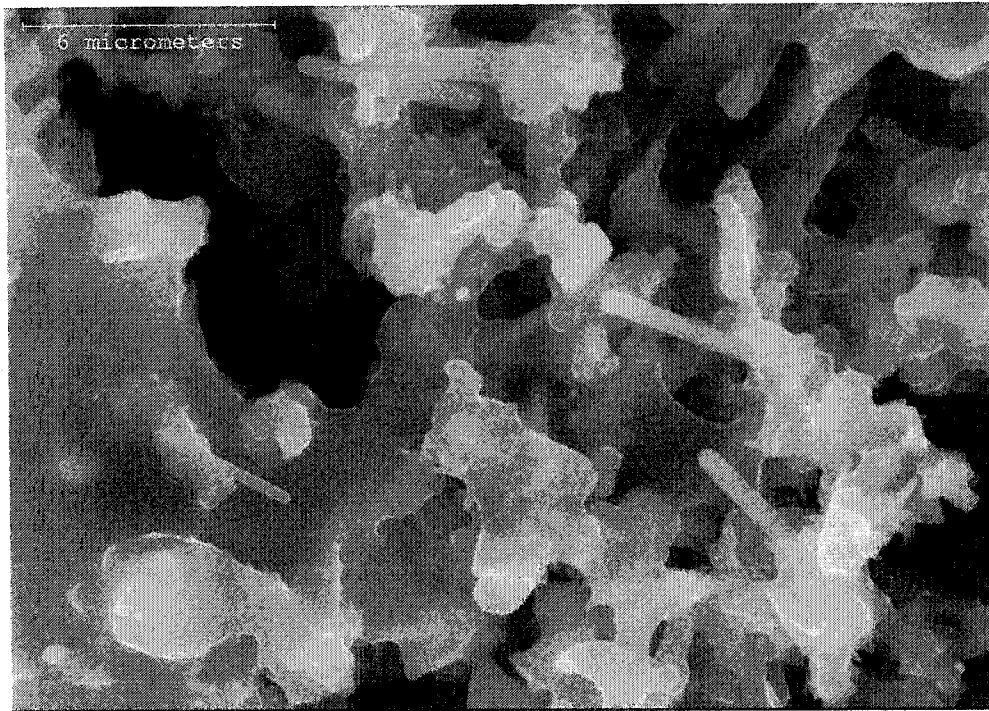
(d) Ashed at 600□



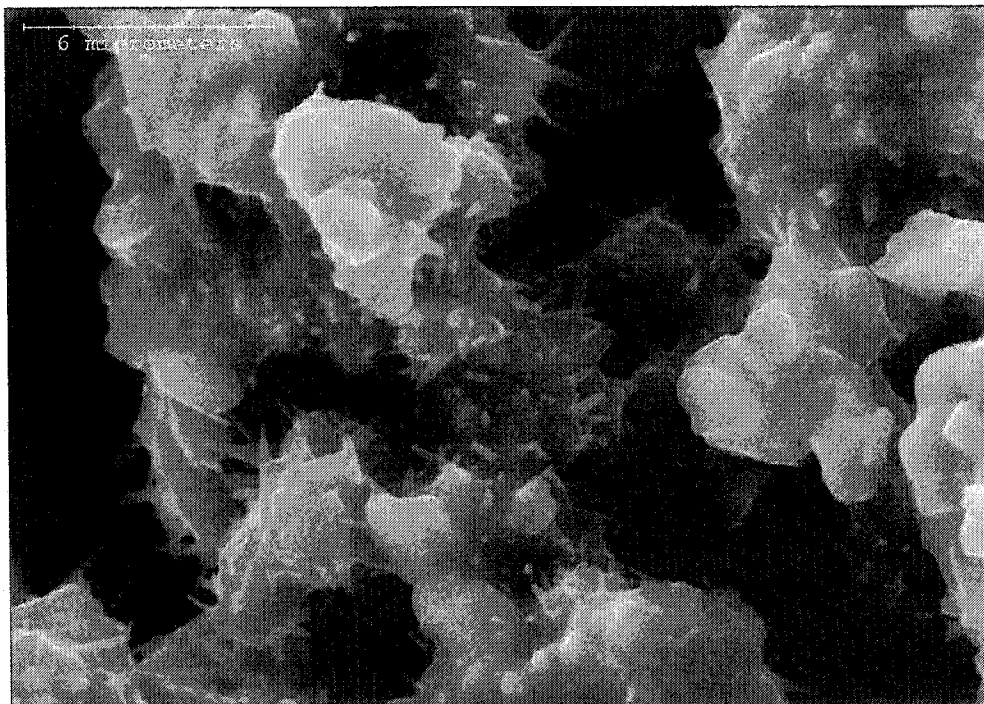
(e) Ashed at 700°



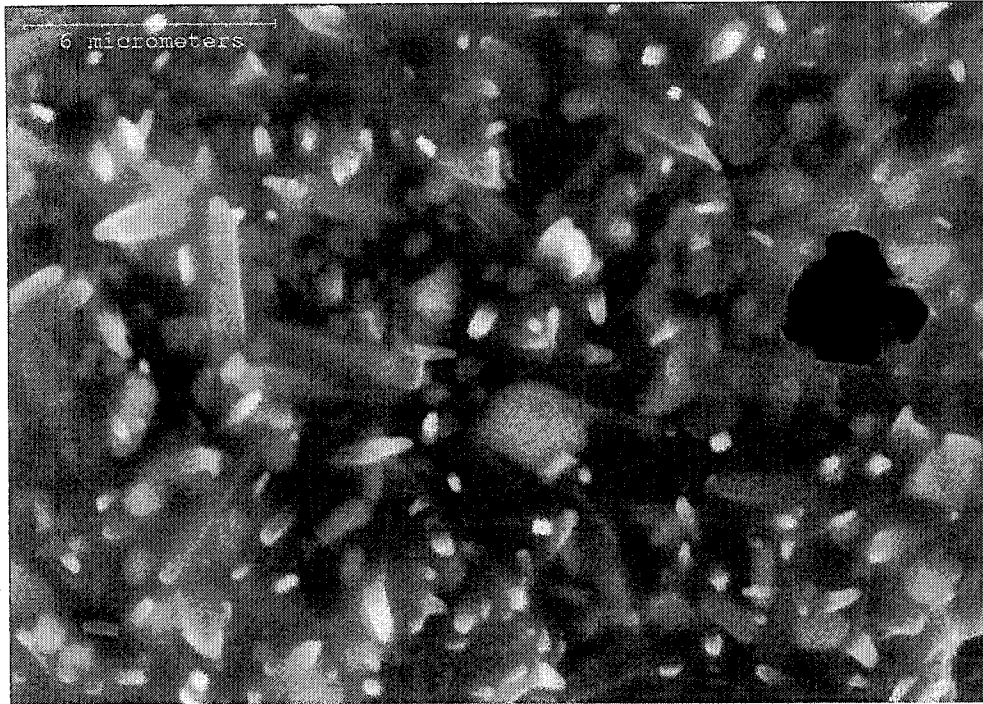
(f) Ashed at 800°



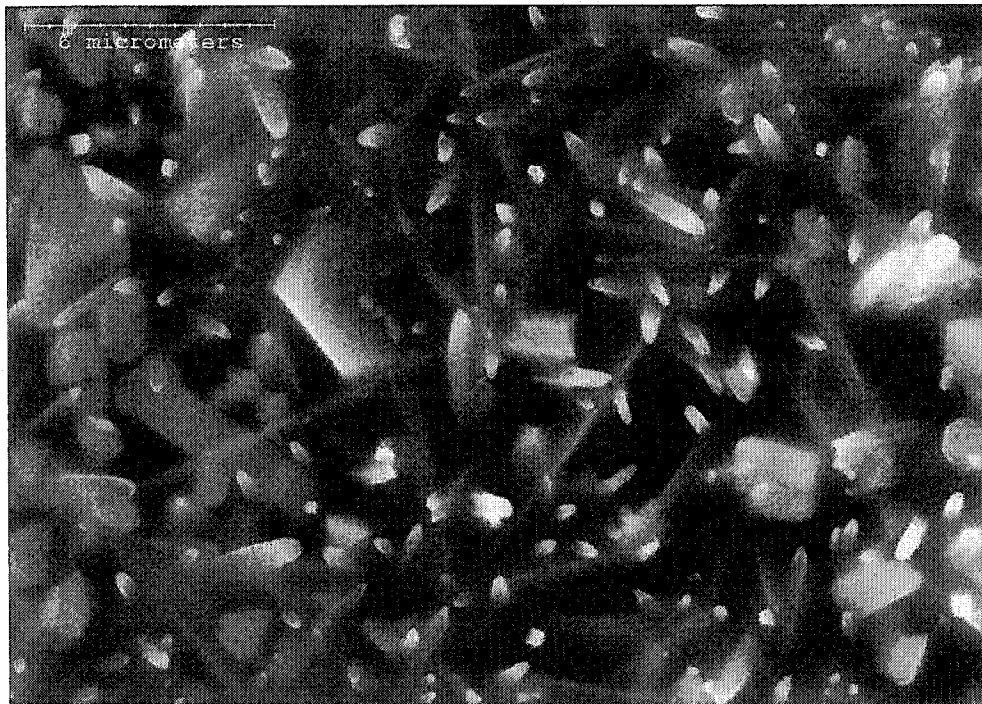
(g) Ashed at 900□



(h) Ashed at 1000□



(i) Ashed at 1100°C



(j) Ashed at 1200°C

Figure 5.2 Micrographs of Suncor Fly Ash ($\times 5000$)

If the cooling rate is high enough, it might be also possible to form perfect spheres. As-received Suncor fly ash samples contained both spheres with smooth surfaces and spheres with rough coatings. However, spheres with smooth surfaces were rarely found in this study. One would postulate that spheres with a smooth surface could form when the aluminosilicate melt solidifies rapidly right after coalescence, not allowing many microcrystals to be contacted. If the ash formation temperature is high enough (or cooling rate is sufficiently low) for microcrystals to contact the aluminosilicate melt, all the spheres might be coated with rough microcrystals.

No visible crystalline structures were found in low temperature (up to 600°C) samples. Though XRD analyses indicated that hematite crystallized at 500°C, no particles enriched in iron were found. However, thin acicular microcrystal structures were found in 700°C and higher temperature samples. At 700°C, these needles were around 1 µm in diameter, 2-6 µm long and the size seemed to be increasing as the temperature increases. When the combustion temperature was around 1000°C, these needles appeared to react with the matrix (flaky shaped aluminosilicates) which was fused and coalesced with other individual particles, and was partly covered by this melt.

At the later stages, these needles seemed to be completely entrapped in the matrix which became spherical as the aluminosilicate melt solidified around entrapped CO₂ or SO₂ gas bubbles. These needles have been also reported in many work [5, 51, 59, 67] and the composition, shapes and sizes of needles are consistent with ones found in this study. EDS analyses on needles at 900°C indicated that the needles contained higher fractions of

iron, nickel and titanium, whereas EDS analyses on melts indicated that they generally appeared to be enriched in Si, Al, Ca and K indicating that they were probably the precursors of calcium feldspars (anorthite) and potassium feldspars (microcline) (Tables 5.2 and 5.3).

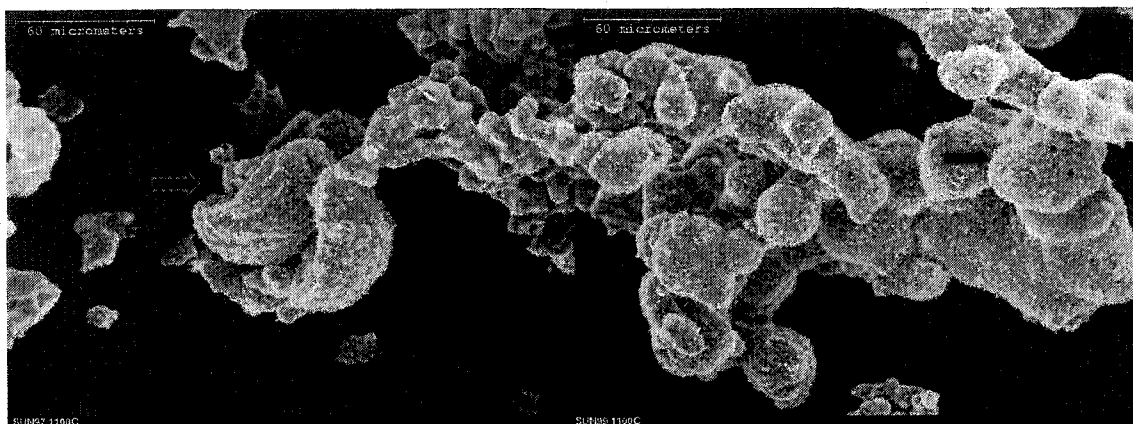


Figure 5.3 Pleurosphere-like Particle (left) and Cenosphere-like Particle (right) from 1100°C Sample ($\times 500$, bar: 60 μm)

In addition to needles, another type of microcrystal was also found in high temperature samples (1000°C or higher). These euhedral to subhedral shaped microcrystals were revealed to have large amounts of iron with an average quantity of titanium and less aluminum and silicon (points 2 and 4 in Figure 5.4 and Table 5.3). Along with needles, these microcrystals were, obviously, the major component of a spherical particle at high temperature. XRD study on this sample indicated that the possible iron-related minerals were hematite, pseudobrookite, iron-nickel-titanium oxide and hercynite (FeAl_2O_4). Stoichiometrically, the quantity of iron (53-62%) was close to that of standard hematite (69.94%).

The quantity of vanadium was found to be slightly high in needles (Table 5.2). However, no conclusion could be made since the thickness of a needle was so small that EDS results could possibly include information on the background matrix. Generally speaking, vanadium was found both in needles and in the aluminosilicate matrix in samples obtained from 700 to 1200°C. Vanadium was high in a needle found in an 1100°C sample, but no other spots throughout the sample were found to be high in vanadium. Vanadium was generally enriched in the matrix (e.g., point 3, Table 5.3) in the samples. After many attempts failed to find the vanadium-rich spots except one spot in an 1100°C sample and based on numerous spot analyses, higher fractions of vanadium appeared to be associated with the aluminosilicate melt and lower fractions were associated with Fe, Ti- rich microcrystals.

Table 5.2 Chemical Composition of a Microcrystal Found in a 900°C Sample (wt%)

Elements	Overall	Needle	Matrix
Al	14.93	12.45	13.51
Si	20.70	14.53	33.50
K	1.99	1.23	0.88
Ca	3.12	0.84	4.10
V	5.55	3.85	2.43
Fe	18.73	28.83	9.89
Ti	5.08	12.25	2.27
Ni	2.80	2.45	0.79

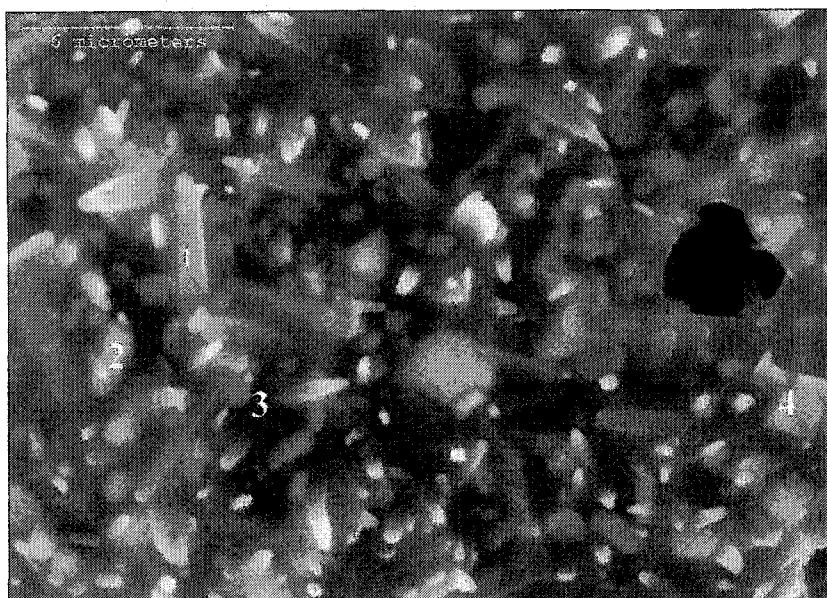


Figure 5.4 Point Analysis on Needles and Matrix of 1100°C Suncor Ash Sample

Table 5.3 Chemical Composition of Microcrystals Found in an 1100°C Sample
(wt%, Points are shown in Figure 5.4)

Elements	Overall	Pt.1	Pt. 2	Pt.3	Pt.4
Al	15.11	9.31	10.48	25.21	7.87
Na	1.15	0.00	0.71	0.00	0.00
Mg	1.11	0.00	0.69	0.27	0.63
Si	19.36	10.87	13.24	31.51	9.57
P	0.28	1.07	0.34	0.79	0.20
K	1.77	3.08	1.33	4.81	1.16
Ca	1.81	3.14	0.72	2.00	0.74
Ti	4.31	5.68	3.78	1.49	5.03
V	3.92	13.68	2.23	6.25	2.29
Mn	0.38	0.38	0.71	0.37	0.73
Fe	15.35	16.56	52.89	13.70	62.62
Ni	2.97	0.63	3.27	0.80	3.78

5.3 Mineralogy of Suncor Ash

5.3.1 Amorphocity of Suncor Ash

The amount of amorphous material in a sample often appears higher than that of the actual amorphous material present in the sample because, when XRD raw patterns are used, the amorphocity means all non-diffracting materials or mineral phases present in the sample but not classified. For amorphocity determination, fly ash samples should be mixed with an internal standard such as quartz or corundum. Non-diffracting materials present in the fly ash sample could affect the internal standard so that the XRD peaks of the internal standard will also be affected. Then, the difference can be calculated by the Rietveld refinement scale factor. This scale factor, in turn, can be used to calculate the quantity of crystalline minerals and amorphous materials. For Suncor and Syncrude fly ash samples, zinc oxide was chosen as an internal standard and 10 weight % zinc oxide was added into every fly ash sample. XRD patterns of all samples were collected and refined using the Rietveld scale factor. Figure 5.5 shows the amorphocity of Suncor fly ash.

The quantity of amorphous materials at 500°C was 79.9 wt% and kept decreasing as temperature increased. The quantity of amorphous material at 1000°C was found to be around 20 wt% which was consistent with the result of Bruhns et al. [29]. They synthesized fly ash using quartz, kaolinite, illite and 5 wt% vanadium and reported that the amorphocity of their sample at 1000°C was around 15 to 20%. The formation of mullite originating from amorphous aluminosilicates at low temperature appears to be the

major contributor. XRD patterns from high temperature Suncor ash samples also indicated many crystallites including mullite that were not found in low temperature samples.

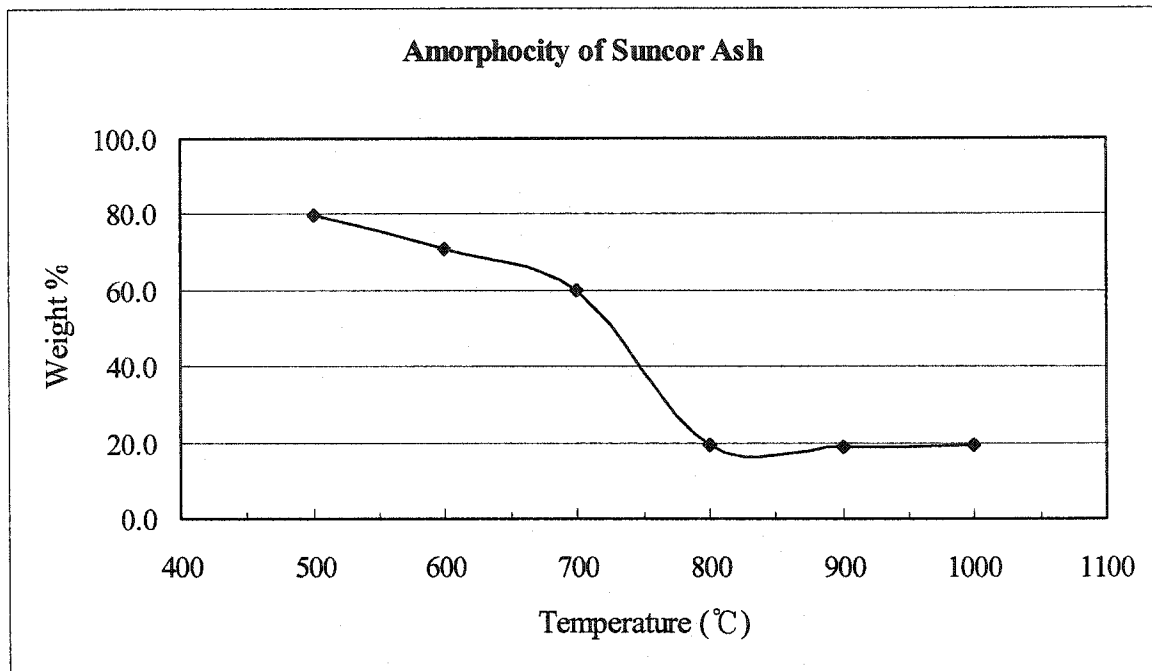
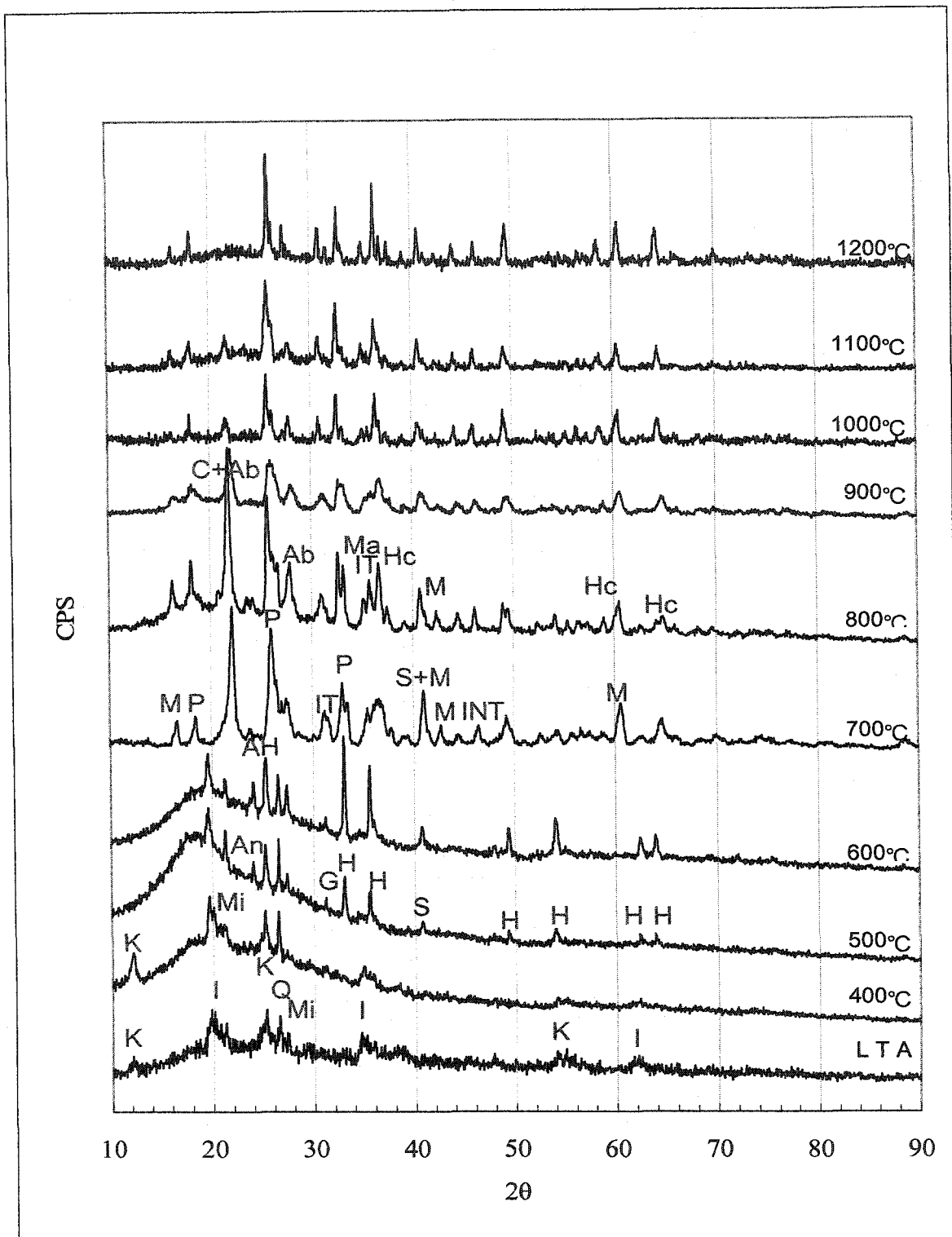


Figure 5.5 Suncor Ash Amorphocity Determination

5.3.2 Qualitative Analysis

XRD patterns have been measured for Suncor fly ash samples as temperature changes from 400 to 1200°C. XRD patterns of LTA samples (approximately 65°C) have been also measured. All x-ray raw data and mineral phases identified from the samples are shown in Figure 5.6. The XRD pattern of each sample is provided in the appendix in detail. The raw patterns from low temperature (up to 600°C) samples have amorphous humps, or diffuse scattering maxima (DSM), in the background starting at about 15° 2θ and ending at 35° 2θ.



Abbreviations used are; K: Kaolinite, I: Illite, Q: Quartz, Mi: Microcline, An: Anorthite, AH: Anhydrite, G: Gypsum, H: Hematite, S: Sillimanite, M: Mullite, P: Pseudobrookite, IT: Fe-Ti Oxide, INT: Fe-Ni-Ti Oxide, Ab: Albite, Hc: Hercynite, Ma: Mayenite, C: Cristobalite

Figure 5.6 XRD Raw Patterns of Suncor Ash

These diffuse scatterings are due to non-crystalline materials, or extremely short range ordered materials such as glass. It is also known that the position of the maximum is closely related to the amount of Ca in a fly ash sample [9]. Low-calcium fly ashes, such as bituminous coal ashes, have their DSM at lower 2θ angles, whereas high Ca samples have their DSM at much higher angles. DSM found in Suncor ash at lower temperature seems to be close to that of bituminous coal ash. These amorphous humps are not found in high temperature (700°C or higher) samples.

As mentioned earlier, more than 95% of the sulfur is of organic origin so that neither iron-sulfur-related inorganic compounds such as pyrite, marcasite (FeS_2), or pyrrhotite, nor iron sulfates are identified in LTA samples. Crystalline structures identified in LTA samples include clays, gypsum, quartz and microcline.

Clays found in LTA samples were mostly kaolinite and illite. 1Md polytype kaolinite was identified with its characteristic peaks at 12.457 2θ and 24.993 2θ which represented the (001) and (002) planes, respectively. These two peaks were also found at 400°C, but disappeared in 500°C samples. It might be postulated that the structure of kaolinite starts to transform into metakaolinite at 500°C, and finally completes its transformation by forming the mullite structure at 700°C. Illite ($\text{K}_{0.7}\text{Al}_2(\text{Si},\text{Al})_4\text{O}_{10}(\text{OH})_2$) was identified as 1M polytype with its characteristic peaks at 4.43 d and 2.56 d. While the peak at 2.56 d spacing disappeared at 500°C, the peak at 4.43 d spacing was identified up to 600°C, which probably meant that illite underwent structural deformation, or thermal expansion due to loss of water on heating, and completed dehydration at 600°C.

Grim and Bradley [68] state that dehydration of illite causes formation of either spinel or mullite, or both. These authors also report that the octahedral sheet of illite lattice which normally carries Al, Mn and Fe causes the formation of spinel, and the alkalies and silicas on tetrahedral layers yield an amorphous glass. In this study, one spinel group mineral, hercynite (FeAl_2O_4), started to form following the decomposition of illite at 700°C . Contribution to the formation of mullite could also be expected.

Other than clays, gypsum, quartz and K-feldspar identified in LTA samples, hematite (Fe_2O_3), anorthite ($\text{CaAl}_2\text{Si}_2\text{O}_8$), sillimanite (Al_2SiO_5) and anhydrite were the first mineral phases identified as predominant minerals in 500 and 600°C samples. A hydrated calcium sulfate, gypsum, was identified at LTA samples and up to 600°C samples. An intermittent phase, bassanite ($\text{CaSO}_4 \cdot 1/2\text{H}_2\text{O}$), which is believed to be dehydrated from the original gypsum at slightly higher temperature, was not identified in any samples. Some of the gypsum was dehydrated and resulted in the formation of anhydrite at 500°C . The peaks of gypsum were not identified at 700°C or higher temperature so that dehydration temperature of gypsum found in Suncor ash was confirmed to be 700°C . Complete decomposition of anhydrite was also found at this temperature. As anhydrite decomposed, Ca released from anhydrite formed mayenite at 700°C . All sulfur was completely removed at this temperature.

While gypsum and anhydrite disappeared at 700°C , traces of anorthite and sillimanite were continuously found up to 1200°C . Hematite, on the other hand, appeared to have significant distortion in its structure since only one characteristic peak was clearly shown

at elevated temperature, whereas many other peaks were broadened and overlap with others. Demir et al. [33] suggested that hematite and magnetite should partly transform to aluminosilicate glass. However, it might be concluded that hematite was a major mineral from 500 to 1200°C. Along with hematite, significant amounts of Fe in oil sands fly ash samples resulted in the formation of other oxides at relatively higher temperature (700°C). These oxides included Fe-Ni-Ti oxide ($\text{Fe}_2\text{NiTi}_3\text{O}_{10}$) and Fe-Ti oxides ($\text{Fe}_2\text{Ti}_3\text{O}_9$ and Fe_2TiO_5 ; pseudobrookite). Excess Fe resulting from the decomposition of illite was also combined with Al to form a spinel, hercynite, at 700°C or higher temperature. The characteristic peaks of these Fe-Ti and Fe-Ti-Ni oxides were found throughout the samples above 700°C. The characteristic peak of pseudobrookite was the most intense and abundant among them. Moreover, its thin, acicular shaped crystals were also identified in SEM studies.

One of the most important reactions found in oil sands fly ash was the formation of mullite, which was first observed at 700°C and was predominant up to 1200°C. The formation of mullite might be explained by the following three mechanisms. Firstly, since kaolinite was found at lower temperature, it seemed feasible that the presence of mullite could be associated with the decomposition of metakaolinite. When metakaolinite decomposed, it also resulted in cristobalite formation. Secondly, it was also possible for aluminosilicate glass to be crystallized at this temperature since the characteristic peaks of mullite were more intense at higher temperature indicating that more mullite crystals were continuously formed. Finally, many scientists showed that dehydration of illite caused the formation of mullite.

The formation temperature is significantly low compared to that of other sources, such as mullite found in coal ash. This might be related to the higher quantities of vanadium and iron in the sample since these elements are believed to enhance clay to mullite transformations. Sillimanite is also one of the main minerals which can be converted into mullite. However, the formation temperature is normally above 1300°C so that, in the Suncor ash samples up to 1200°C, sillimanite is not associated with mullite formation.

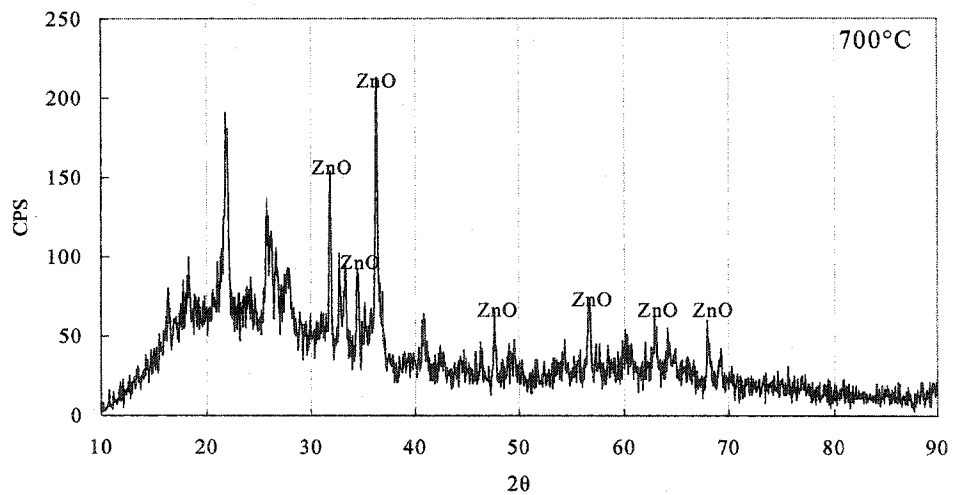
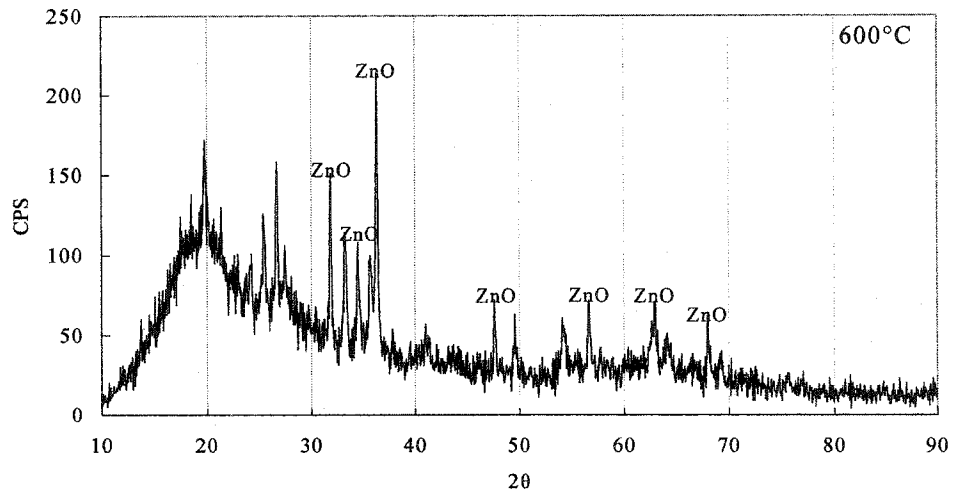
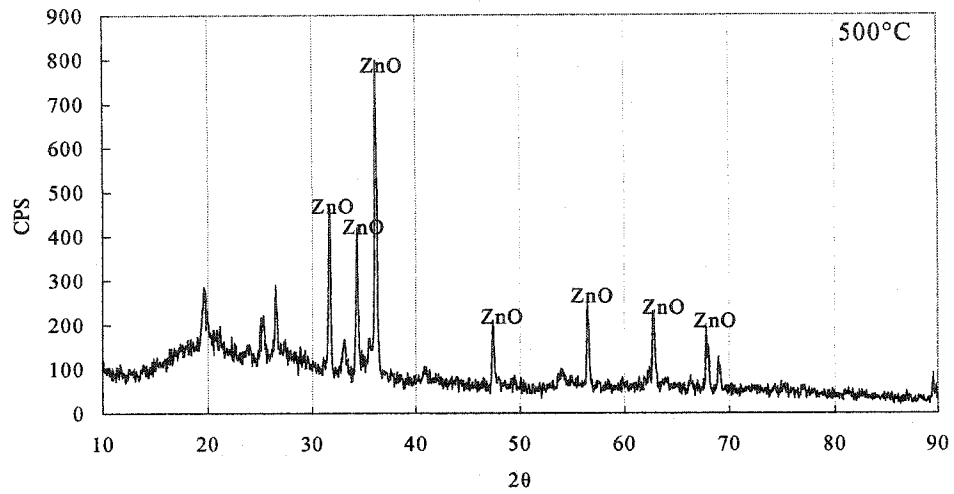
While quartz was found in the samples for the temperature ranging from LTA to 800°C, cristobalite, first found at 700°C, is the predominant silica mineral at higher temperature. Quartz, silica glass and the silica discarded from decomposition of metakaolinite might be the precursors of cristobalite. Among them, however, cristobalite formation is not associated with the presence of quartz found in lower temperature samples. Quartz shows slow reaction on combustion so that it is found in the sample unchanged. Cristobalite has a higher temperature phase called β -cristobalite; β -cristobalite is stable around 870 to 1470°C, whereas α -cristobalite is known to be stable above 1470°C. During crystallization, β -cristobalite forms first and almost instantly transforms into the α phase. Accordingly, cristobalite is not thermodynamically stable at 800 to 1200°C. However, it is known that, even when cristobalite is not a thermodynamically stable phase in the sample as found in coal ash, where tridymite should be stable instead, preferential formation of cristobalite might be highly favored [19]. Based on quantitative analysis and comparison of Suncor ash with Syncrude ash, it was concluded that when quartz decomposes at 800°C, it could only transform to silicate glass.

At 700°C, albite ($\text{NaAlSi}_3\text{O}_8$), which is classified as a plagioclase feldspar, was identified and continued to be present in samples up to 1200°C. The formation of albite may involve structural change originating from microcline. Na and K components, which are released from glass or from illite decomposition at 700°C, react with this feldspar structure to form albite.

As gypsum and anhydrite completely decompose at 700°C, mayenite is crystallized at this temperature. Ca released from gypsum and anhydrite is obviously the main component of this mineral.

5.3.3 Quantitative Analysis

In order to better understand the transition behavior of mineral phases, Suncor ash samples obtained over the temperature range of 500 to 1000°C were refined using the Rietveld method. The samples were mixed with 10 wt% ZnO and the XRD patterns were collected again. Figure 5.7 shows the XRD patterns of Suncor ash. Table 5.4 shows the quantities of each mineral phase (wt%) found in Suncor ash. Some mineral phases were unavailable to refine due to the limitation of the software database so that, even though all scale factors had relatively acceptable fit, all numeric data were dummy values. However, it is noteworthy that one can definitely see changes in the quantity of minerals as the temperature changes. Thermal transition behavior of some minerals, found at 500 and 600°C is described in Figure 5.8. Others found at 700°C or higher temperatures are described in Figure 5.9. The first group of minerals (500 and 600°C) is the phases identified during the decomposition of clay minerals and gypsum.



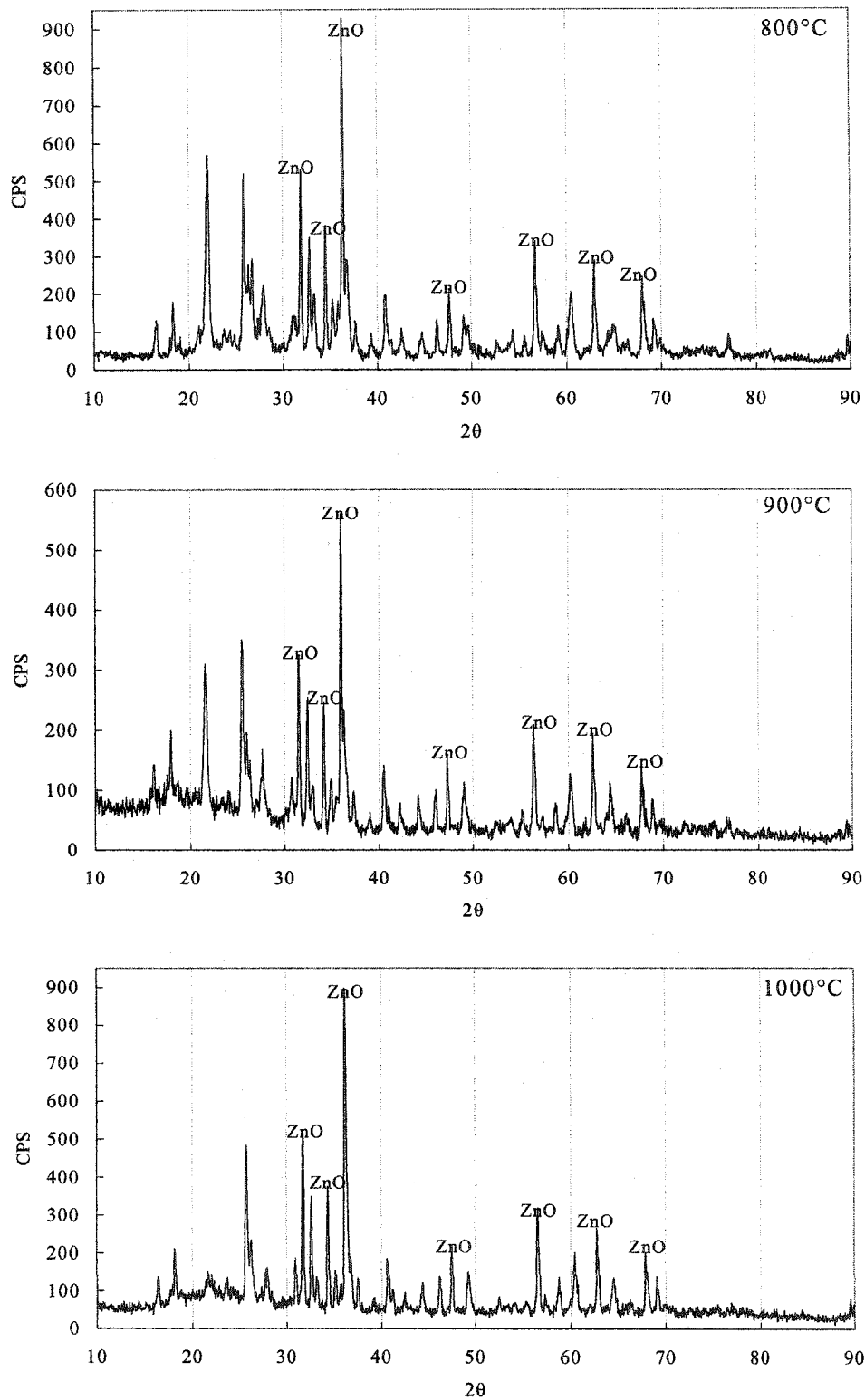


Figure 5.7 XRD Patterns of Suncor Ash Mixed with 10 wt% ZnO

Hematite, which is a predominant mineral phase at 500 and 600°C, slightly decreases in its quantity from 6.7 to 3.3%, whereas the amount of other Fe-related minerals such as pseudobrookite (and probably iron-nickel-titanium oxide as well) increases up to around 10% as temperature goes up to 1000°C. The quantity of quartz is quite unchanged up to 800°C and remains at 1.8-2.6%. This confirms that quartz is one of the most inactive minerals during combustion. It appears to be true that high temperature quartz crystals are the same ones found before combustion. Decomposition of quartz is completed at 900°C, and is not related to the formation of cristobalite since the quantity of cristobalite remains the same at 800 and 900°C, and even decreases at higher temperatures.

Table 5.4 Quantitative Analysis of Mineral Phases in Suncor Ash (wt%)

Minerals \ Temperature (°C)	500	600	700	800	900	1000
Hematite (Fe ₂ O ₃)	6.7	13.5	2.2	6.0	4.7	3.3
Pseudobrookite (Fe ₂ TiO ₅)	0.0	0.0	1.4	11.2	7.2	10.7
Hercynite (FeAl ₂ O ₄)	0.0	0.2	2.8	3.6	6.4	10.7
Cristobalite (SiO ₂ , tetragonal)	0.0	0.0	5.4	11.2	11.4	4.0
Mayenite (Ca ₁₂ Al ₁₄ O ₃₃)	0.3	0.5	1.8	2.1	3.1	1.5
Microcline (KAlSi ₃ O ₈)	1.8	1.3	2.6	2.1	3.2	5.3
Mullite (3 Al ₂ O ₃ ·2 SiO ₂)	0.0	0.0	13.5	20.1	25.7	30.4
Albite (NaAlSi ₃ O ₈)	0.0	0.0	1.2	4.0	5.4	0.1
Anhydrite (CaSO ₄)	4.7	5.6	0.6	0.0	0.0	0.0
Sillimanite (Al ₂ SiO ₅)	0.2	0.0	6.8	4.0	5.2	8.5
Quartz (SiO ₂)	2.6	1.9	0.0	1.8	0.0	0.0
Anorthite (CaAl ₂ SiO ₈)	3.5	5.3	1.6	9.9	8.9	5.8
Amorphous Contents	79.9	70.8	60.1	19.2	18.8	19.2

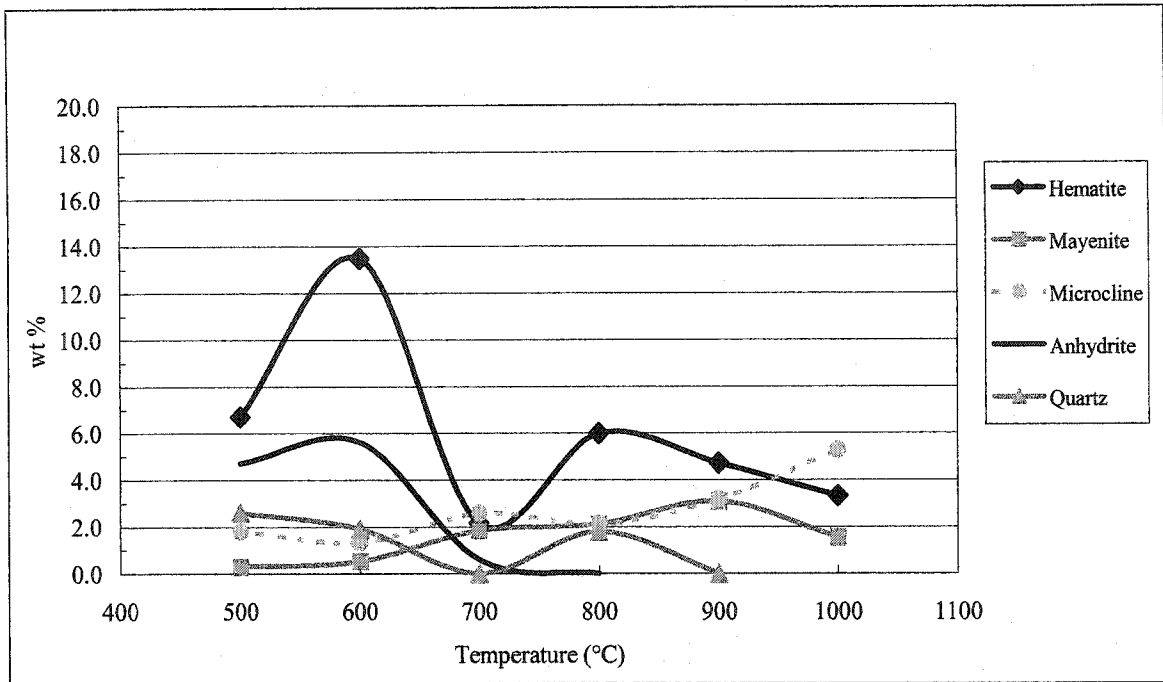


Figure 5.8 Mineral Phases Identified at Low Temperature

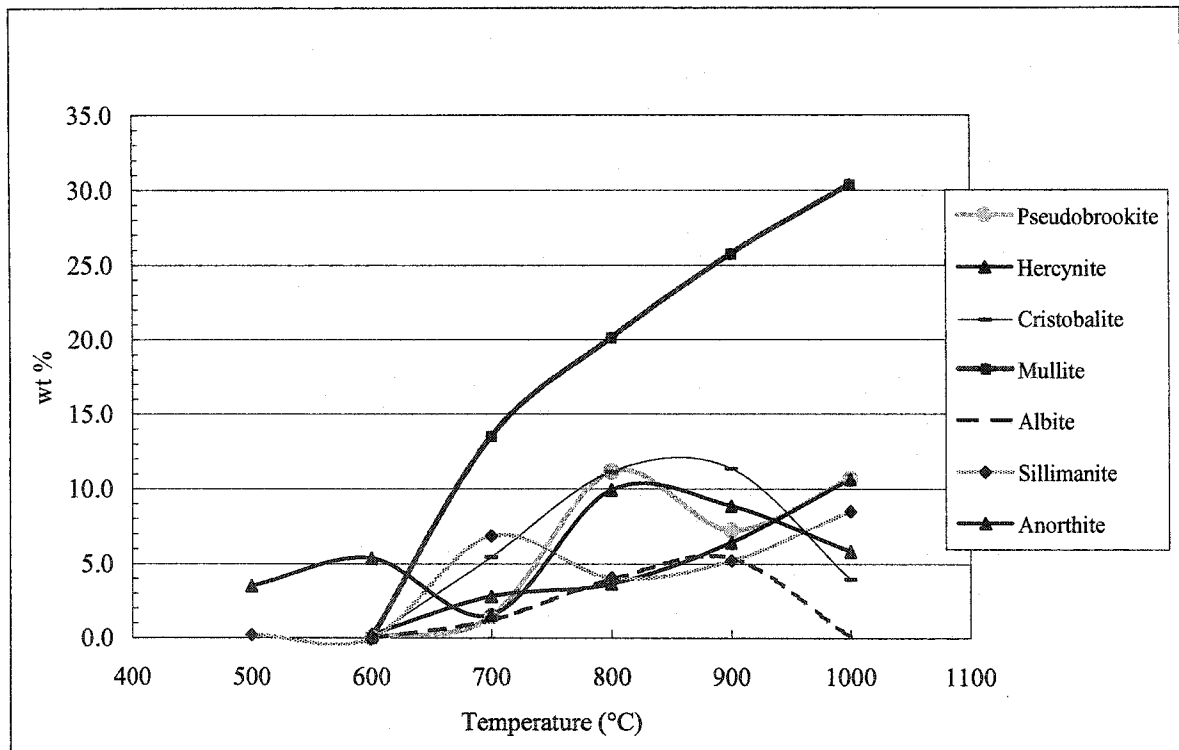


Figure 5.9 Mineral Phases Identified at High Temperature

The second group of minerals is the mineral phases found at 700°C. Microcline which is found throughout the temperature range is believed to be the most stable feldspar during combustion. The quantity ranges from 2 to 5% which indicates that it is inactive on heating and quite isolated from other chemical reactions. Its quantity slightly increases with increasing temperature as more K might be introduced into the feldspar system when aluminosilicate glasses crystallize as mullite. Ca and Na, released by the same mechanism, form anorthite and albite, respectively. However, the quantities of these two plagioclase feldspar minerals start to decrease above 900°C. The amount of mayenite is quite small at lower temperature, but the quantity increases at 700 to 900°C due to the formation of secondary mayenite from the decomposition of anhydrite. Mayenite also shows a decreasing trend at 900°C and above.

Mullite, sillimanite, hercynite and pseudobrookite keep increasing in their quantities as temperature goes up to 1000°C. As amorphous aluminosilicates continuously crystallize in this temperature range, Al oxides and Si oxides, key elements of mullite, and hercynite and sillimanite become abundant enough to form crystalline structures, while all other base elements released from the aluminosilicate structure form feldspar structures.

In order to confirm that there would be no upset situations at 600 and 700°C, more samples were refined using the Rietveld scale factor. At 600°C, the quantity of hematite was confirmed to be around 12 to 14%. At 700°C, a small amount of coke was ashed for different time period varying from 6 to 12 hr. Table 5.5 shows the relationship between chemical composition and time. Chemical composition at 24 hr is the one used in Table

5.4. These results show that, after 12 hr of ashing, the quantity of each element deviates within 1-2 wt% range. It is obvious that the data used in Table 5.4 are quite accurate.

Table 5.5 Chemical Composition of Phases in Suncor Ash for Different Time Periods (700°C, wt%)

Minerals\Time (Hr)	6	7	8	9	10	11	12	24
Hematite (Fe ₂ O ₃)	10.7	13.4	12.8	9.8	5.8	3.7	3.2	2.2
Pseudobrookite (Fe ₂ TiO ₅)	0.0	0.2	1.0	3.1	2.8	0.6	1.3	1.4
Hercynite (FeAl ₂ O ₄)	1.0	1.0	1.3	0.8	1.1	1.7	0.6	2.8
Cristobalite (SiO ₂)	0.3	0.8	2.0	2.5	5.2	5.2	6.6	5.4
Mayenite (Ca ₁₂ Al ₁₄ O ₃₃)	0.9	1.6	0.0	1.5	2.3	2.4	3.3	1.8
Microcline (KAlSi ₃ O ₈)	0.9	1.6	2.2	0.0	1.0	1.9	1.6	2.6
Mullite (3 Al ₂ O ₃ ·2 SiO ₂)	9.7	7.0	9.8	10.7	12.6	12.7	12.5	13.5
Albite (NaAlSi ₃ O ₈)	0.0	0.0	0.0	0.0	0.0	0.4	1.6	1.2
Anhydrite (CaSO ₄)	7.3	7.0	6.3	5.4	3.4	2.1	2.6	0.6
Sillimanite (Al ₂ SiO ₅)	1.6	1.0	0.4	0.6	0.8	0.0	4.1	3.4
Anorthite (CaAl ₂ SiO ₈)	4.9	5.8	3.8	5.0	4.1	2.8	1.4	1.6

It was found from this experiment that, at 700°C, hematite underwent significant phase transformation or structural distortion which was also indicated in XRD studies. The decomposition of anhydrite was completed in 24 hr at this temperature. The quantities of mullite, pseudobrookite, hercynite and cristobalite increased as time increased. Formation of mullite was quite instantaneous, whereas crystallization of albite seemed to be very difficult at this temperature. Anorthite appeared to sacrifice its Al and Si components to the formation of mullite.

5.4 Discussion and Conclusions

5.4.1 Mineral Phase Transition on Combustion

Based on qualitative and quantitative results and the knowledge obtained through the literature survey, it was partly possible to characterize the mineral phase transition behavior of Suncor ash. All minerals identified from the LTA temperature to 1200°C, and all related mineral matter and amorphous minerals not identified on XRD, were brought together in Figure 5.10

Suncor coke, in its relatively unchanged state at low temperature, normally contains a small amount of crystallites which includes clays, calcium sulfates, quartz and a potassium feldspar mineral, and a large portion of amorphous materials which may be further classified into two groups; aluminosilicate glass which is mainly made up of Al, Si, Ca, Na and K, and Fe-sulfates which contain Fe, Ni and Ti. The first group of amorphous materials is associated with the formation of sillimanite, mullite, cristobalite, hercynite and feldspars, whereas the latter amorphous materials contribute to the formation of Fe oxides, Fe-Ti oxides and Fe-Ti-Ni oxides.

Based on quantitative analyses, it is found that quartz and hematite are quite isolated from other chemical interactions occurring in the system during combustion. These two components are found to be altered to glass at high temperature (>800°C). Quartz is completely transformed into silicate glass at 900°C. It is concluded that cristobalite could form by decomposition of metakaolinite, but not by the quartz to cristobalite transition.

Hematite, on the other hand, is identified up to 1200°C, but both the structural distortion found in qualitative analysis and a slight decrease in its quantity (6.7 to 3.3%) indicate that hematite could also be partly transformed to glass.

Suncor ash is found to contain two clay minerals: illite and kaolinite. Since Suncor ash contains only a minor amount of K (around 2%), the major fraction of the ash should be kaolinite with a minor fraction of illite. However, the x-ray peaks are dominated with illite peaks. This indicates that a large part of kaolinite has been already transformed to metakaolinite, even at a temperature lower than 400°C. Its transformation to metakaolinite seems to complete at 500°C.

Illite and kaolinite found at lower temperature are the precursors of mullite formation which is found at a relatively low temperature (700°C). Cristobalite and hercynite are the associated mineral phases formed with mullite. The formation of these two minerals is initially facilitated by the decomposition of clays at a relatively low temperature (around 700°C) and the quantities increase due to the formation of secondary phases affected by amorphous to crystal transitions. Cristobalite is a polymorph of quartz, but its formation is not related to the decomposition of quartz.

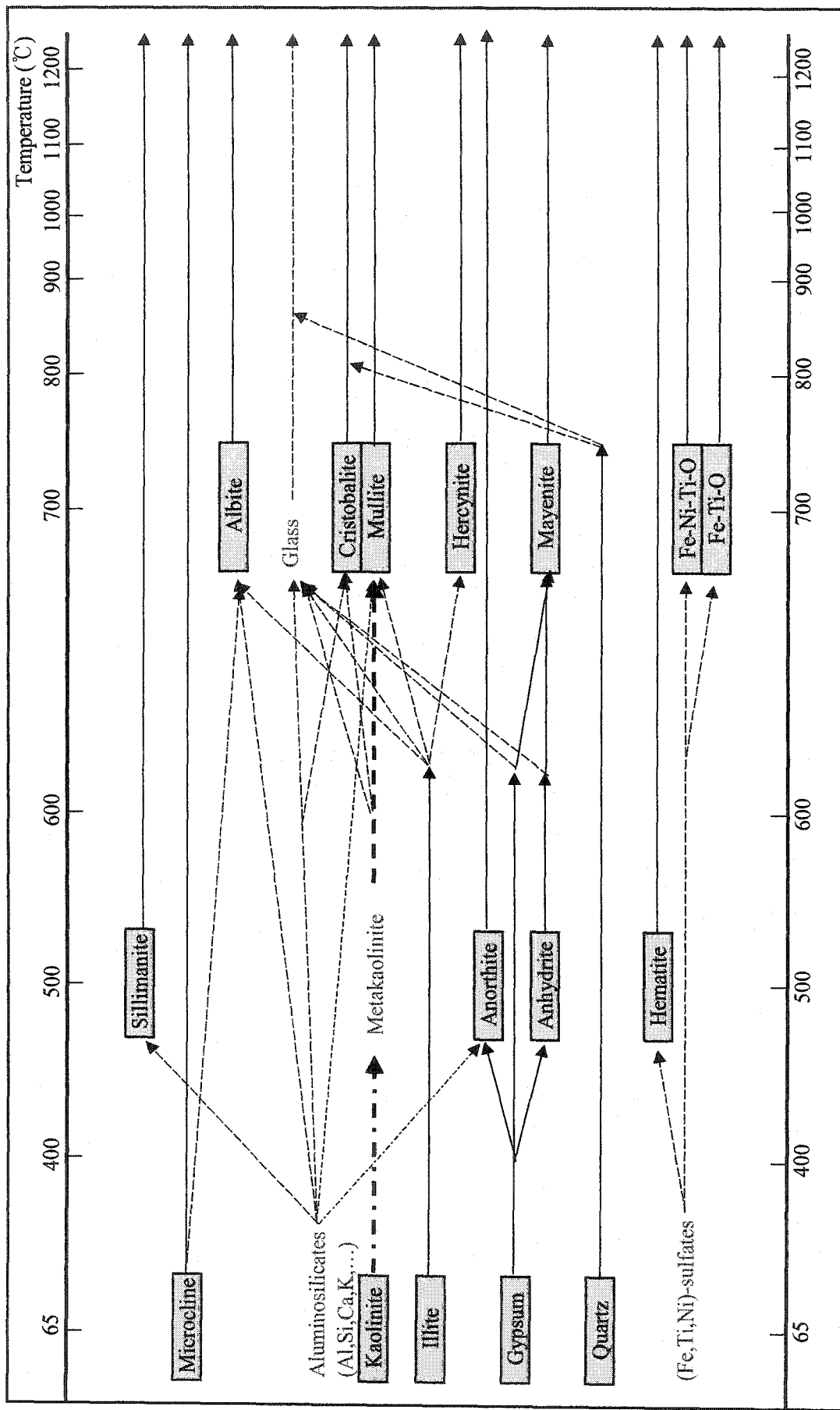


Figure 5.10 Mineral Phase Transitions of Suncor Fly Ash

For feldspars found at 700°C, aluminosilicate glass and potassium feldspar are the precursors. Both albite and anorthite might be formed when microcline absorbs more Na or Ca which are released due to the crystallization of aluminosilicates since they have similar structures, and Na, Ca and K ions are interchangeable without requiring a significant structural alteration. Compared to albite, anorthite first forms at a relatively low temperature because Ca is abundant due to the decomposition of gypsum and anhydrite.

Decomposition of gypsum and anhydrite also affects the formation of mayenite. The quantity of mayenite was quite small (< 3.5%), compared to that of anorthite. Association between anorthite and mayenite is unknown. Many researchers argue that anorthite forms when anhydrite reacts with alumina and silica, whereas mayenite forms when CaO selectively reacts with alumina. However, since no free lime was found in lower temperature Suncor ash, it appears that excess Ca released from anhydrite reacts with alumina to form mayenite.

The quantities of anorthite and albite increase as temperature goes up to 900°C, but decrease above this temperature. This appears to be mainly due to continuous transformation of aluminosilicates to mullite. As the amount of mullite reaches about 25%, Al and Si can no longer contribute to the formation of feldspars since almost all the Al element has been crystallized at 900°C and more Al atoms are required to form mullite above 900°C. Since the quantity of mullite is still in an increasing trend at 1000°C, more mullite and less feldspars are expected at 1100 and 1200°C. Above this

temperature, it might be expected that anorthite and albite, originally transformed from amorphous aluminosilicate, would transform back to glass. During this stage, Al-oxides and Si-oxides would be associated with the mullite structure, while Ca and Na would be dissolve into amorphous silicate melts. Simple stoichiometric calculations based on standard minerals [69] revealed that almost all Al was crystallized at 1000°C so that the quantity of mullite could not increase without absorbing more Al from anorthite and albite. It also suggests that the melts be enriched in silica. EDS point analyses on a melt from a 1000°C sample also support this suggestion.

5.4.2 Ash Formation and Morphology

It is known that Suncor coke contains around 79-84% C and 5-8% S as major components, Al, Si and Fe as minor elements, and 2-3% ash. At an early stage of combustion, it appears that, as all organic combinations are broken apart, Al, Si, Ca, K, Fe, V, Ti and Ni are combined all together in amorphous flaky shaped particles. These particles are somewhat homogeneous in terms of their composition. Among those, Fe, Ti and Ni are relatively active so that they crystallize as thin acicular shaped particles at low temperature (700°C). On the other hand, amorphous materials enriched in Al, Si, Ca, Na and K fuse and coalesce at higher temperature (>800°C) and cover small particles which are either flaky aluminosilicates or these particles connected to acicular particles. When these melts solidify around gas bubbles, spherical particles may form. In this case, small particles initially entrapped in the melt are lined up at the surface of the hollow spheres (cenospheres). These particles may also be covered by other hollow spheres, such that pleuroospheres form. The degree of movement, that is the activation energy required for

the melt to migrate, seems to control particle size of the ash. With this point of view, it could be concluded that the higher the temperature, the bigger the size. However, this conclusion is not considering other important factors, such as the effect of cooling rate, effect of residence time inside the furnace and the effect of individual elements, especially base elements.

It might be also concluded that surface enrichment of minor or trace elements occurs due to migration of these elements from the interior towards the surface of the particles. Deposition of smaller particles onto the surface of spheres has not been identified even in high magnification micrographs. SEM micrographs of Suncor ash clearly show that the heavy metal ions are mobile enough after being covered by the aluminosilicate melts. Compared to the ash formation mechanism of coal fly ash, the fact that the bigger particles (1-100 μm) are formed by *coalescence and coagulation* may be true for the Suncor ash. For the submicron size ash particles from coal combustion, the most widely accepted ash formation mechanism is “*vaporization of volatiles, followed by condensation*”. It may be feasible to explain the formation of Suncor ash, but no evidence has been found in this study.

5.4.3 Comparison with As-Received Ash

The XRD pattern of an as-received Suncor ash (1982) after decarburization at 500°C is shown in Figure 5.11. Figure 5.12 shows the SEM micrograph of this ash sample.

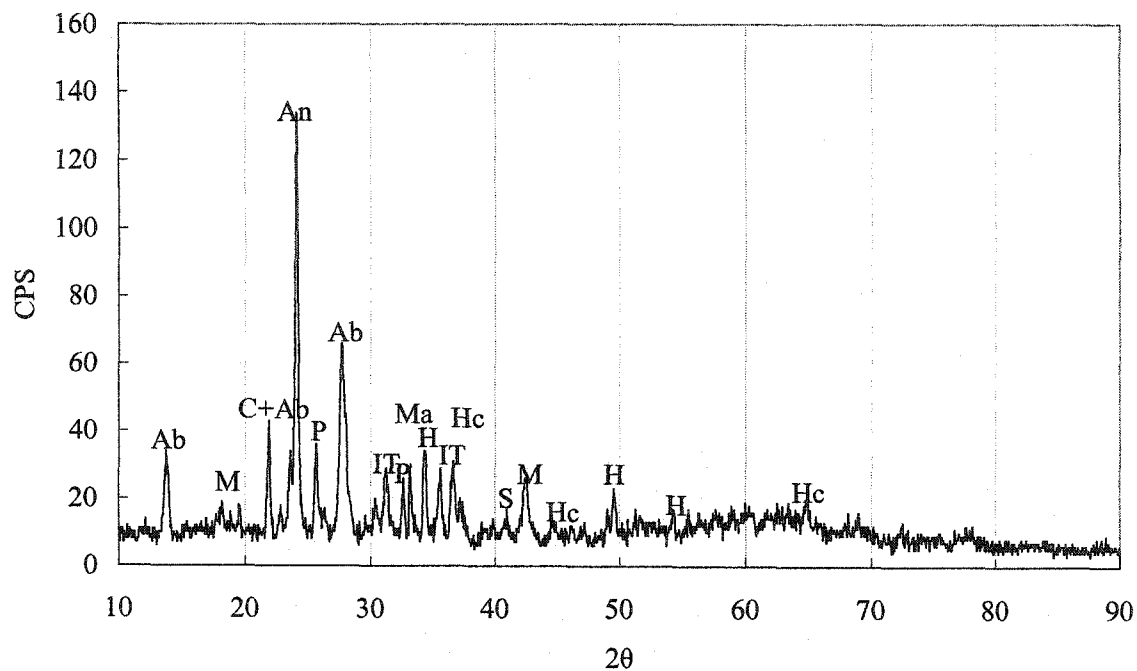


Figure 5.11 XRD pattern of As-Received Suncor Ash

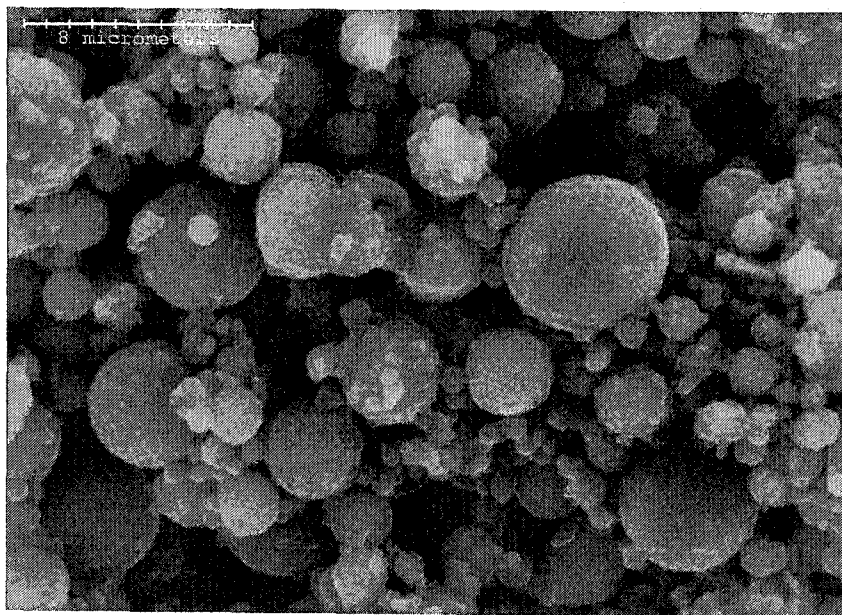


Figure 5.12 SEM Micrograph of As-Received Suncor Ash [5]

Mineral phases identified include albite, anorthite, mullite, cristobalite, hercynite, sillimanite, mayenite, hematite, pseudobrookite and iron titanium oxide. These minerals are the high temperature phases of Suncor coke which is ashed from 700 to 1200°C. Quartz found in coke ash samples from LTA to 800°C is not present in the as-received ash. The absence of quartz indicates that Suncor ash forms at 900°C or higher. The SEM micrograph of this sample shows that the ash contains numerous spherical particles, which indicates that the ash formation temperature is likely higher than 1000°C.

The major difference found in XRD analysis of an as-received ash is that the peaks of anorthite and albite are much more intense and the peaks of mullite, cristobalite and pseudobrookite are less intense compared to coke ash. This difference seems to be reasonable when the different ashing conditions of the boilers are considered. Due to the short retention times and fast cooling rates in Suncor boilers, as-received ash contains less mullite and pseudobrookite structures. More mullite, cristobalite and pseudobrookite structures would be expected at longer retention times or slower cooling rates. Also, less feldspars would be expected since they tend to transform to amorphous materials and sacrifice their alumina fractions to the formation of mullite.

6.0 Characterization of Syncrude Fly Ash

6.1 Chemical Composition

Table 6.1 shows the chemical composition of Syncrude coke ash with temperature varying from 65°C (LTA temperature) to 1200°C. All data obtained from an energy-dispersive spectrometer (EDS) attached to the SEM were normalized to 100 wt%. This method is semi-quantitative analyses due to errors in samples and instrument so that a trend of compositional change can only be considered.

Table 6.1 Elemental Analyses of Syncrude Coke Ash (wt%)

Temp (°C)	L.T.A.	400	500	600	700	800	900	1000	1100	1200
Na	0.97	1.50	1.28	1.60	1.55	1.77	1.70	1.68	1.75	1.21
Mg	0.70	0.87	0.99	1.09	1.09	0.98	0.87	1.01	1.24	0.92
Al	11.91	15.27	16.41	17.07	17.01	16.46	16.54	16.12	14.82	14.28
Si	29.02	30.09	26.16	27.29	27.53	26.75	26.36	26.69	22.17	29.35
P	0.40	0.50	0.40	0.30	0.47	0.40	0.33	0.34	0.27	0.00
S	11.41	3.66	4.66	3.54	2.36	0.00	0.00	0.00	0.00	0.00
K	2.19	2.45	2.87	2.64	2.98	2.94	2.97	2.95	2.04	2.58
Ca	5.58	6.57	6.10	5.57	6.35	7.18	7.65	6.82	4.62	5.66
Ti	2.93	3.08	3.43	3.29	3.74	3.87	3.82	3.79	2.91	3.61
V	3.68	4.33	4.26	3.62	4.24	4.26	4.23	4.39	3.47	3.84
Mn	0.27	0.40	0.33	0.35	0.41	0.45	0.52	0.45	0.34	0.59
Fe	11.13	12.48	12.29	12.03	12.70	14.17	14.52	14.98	12.44	18.60
Ni	1.63	1.92	1.82	1.76	1.78	1.98	1.62	1.87	1.85	2.24

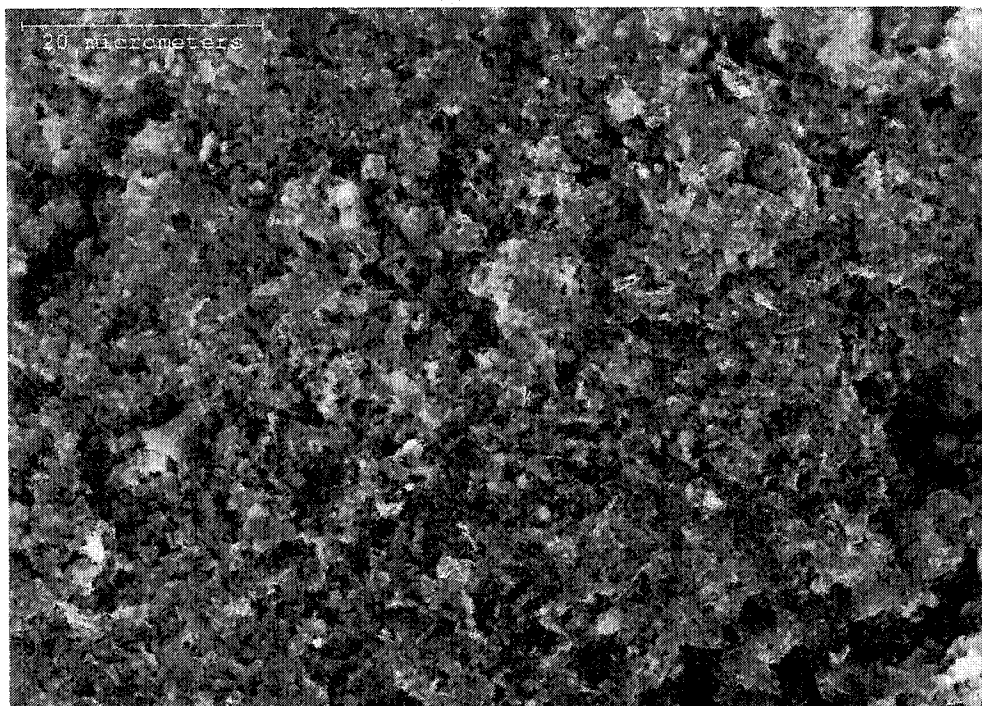
As found in coal fly ash, aluminum, silicon and iron were the major elements in Syncrude ash. However, contrary to coal fly ash, significant amounts of V, Ni and Ti were also

reported as major elements from these samples. Na, Mg, K and Mn, known as network modifying elements [9], were found as minor elements. There were no significant changes in composition of each element as temperature varied. However, sulfur found in the original coke sample decreased in quantity as temperature increased and disappeared at 700°C, probably by the same mechanism proposed for Suncor ash. Due to the higher quantity of Ca in Syncrude ash (6-7.5%, compared to 1.8-2.7% in Suncor ash), more Ca compounds were expected to be present at 500 to 600°C. This could explain the higher amount of sulfur in this temperature range.

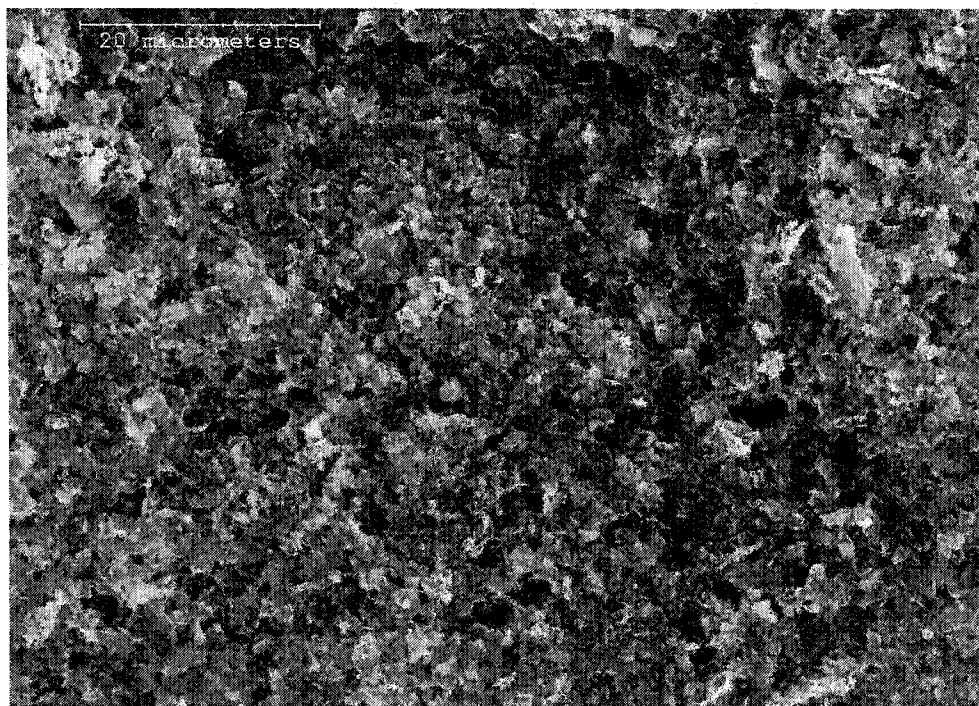
Though the quantity of each element was quite similar, slight differences in composition between Suncor and Syncrude ash were found. Compared to Suncor fly ash, much higher Si was detected (25-27 wt% vs. 20-22 wt% in Suncor ash). The amount of Al and Fe remained at the same level as that in Suncor ash, but vanadium, nickel and titanium were a bit lower in their quantities, while Ca, K and Na were slightly higher.

6.2 Morphology of Syncrude Ash

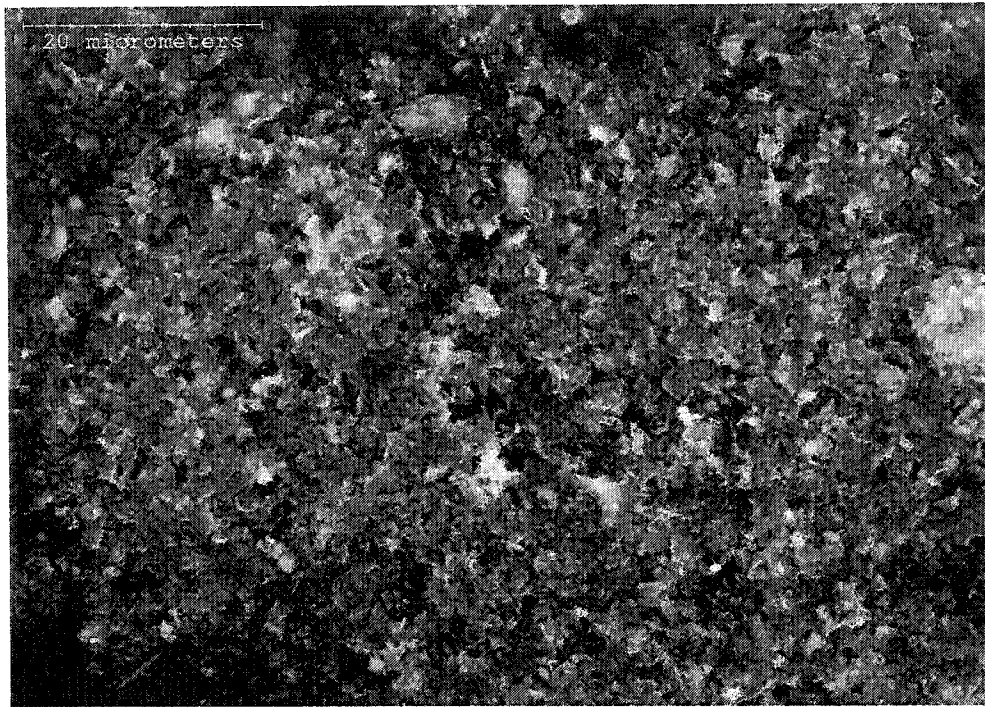
As expected, SEM micrographs of Syncrude fly ash samples (Figures 6.1 and 6.2) showed that the predominant phase in the ash samples was the amorphous aluminosilicate mineral. Particles were flake-like and the size of the particles was quite similar to that of Suncor ash (less than 4 μm) in lower temperature (from 65 to 700°C) samples. No different shapes were found over this temperature range.



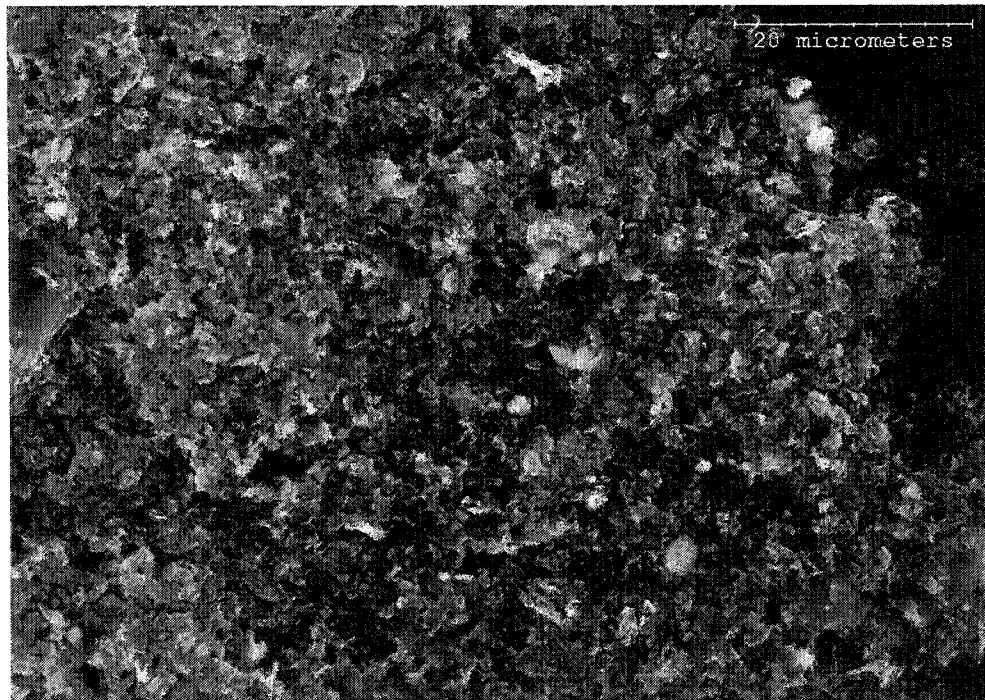
(a) Ashed at 65□ (LTA)



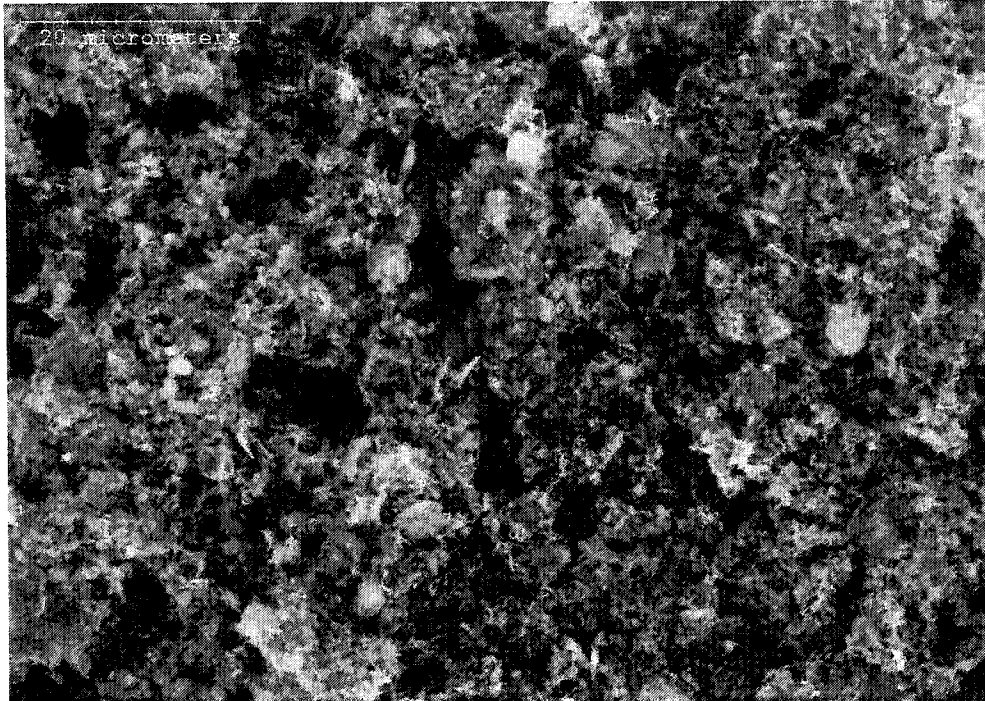
(b) Ashed at 400°C



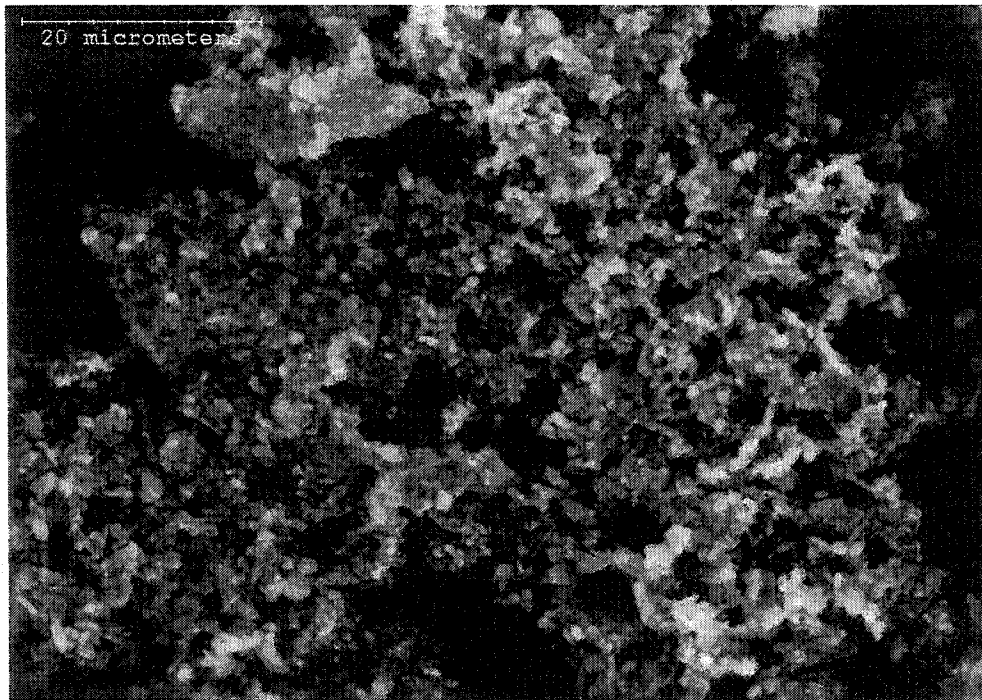
(c) Ashed at 500°C



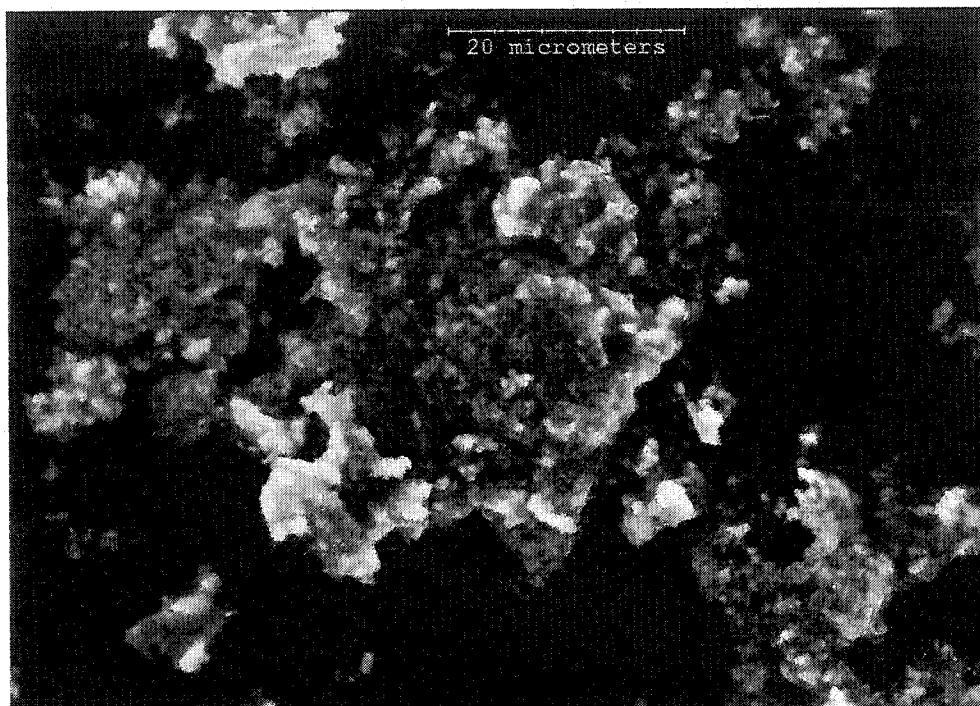
(d) Ashed at 600°C



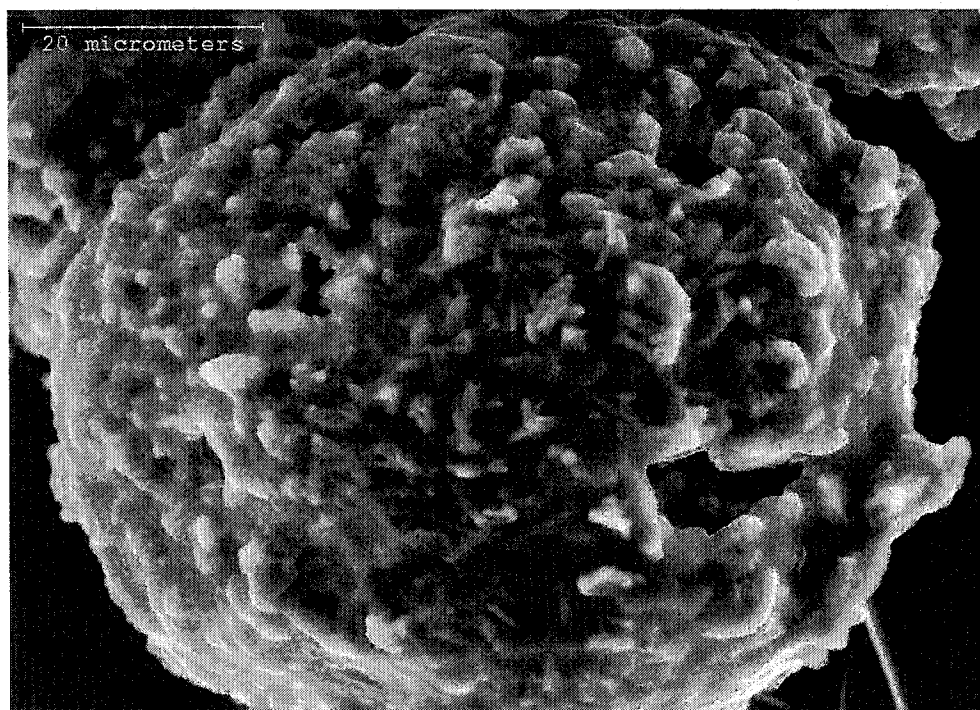
(e) Ashed at 700°C



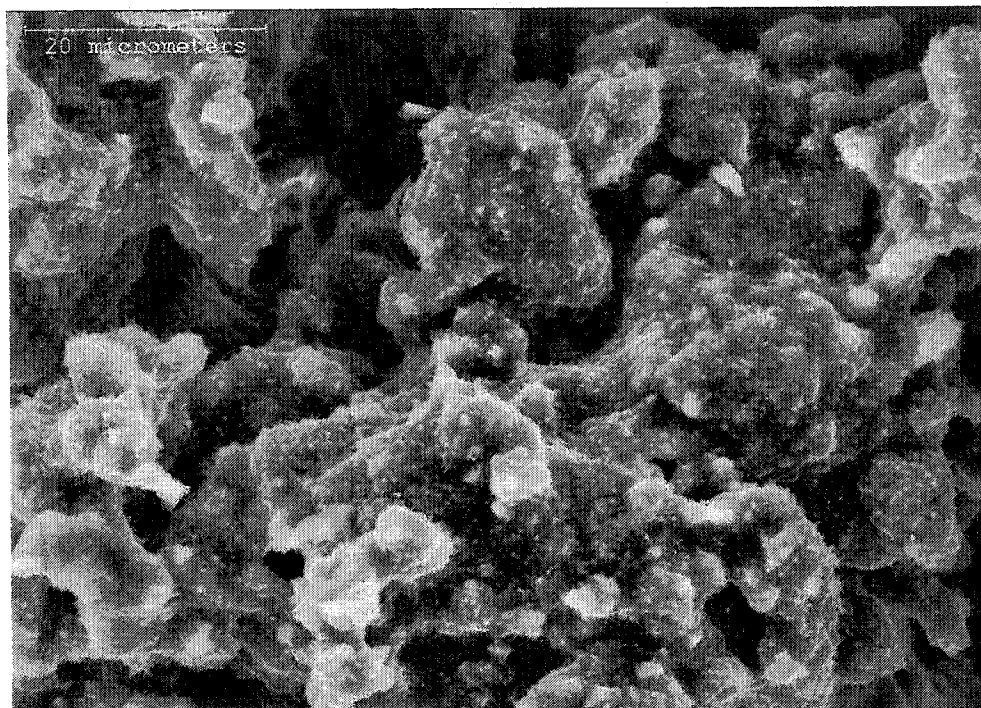
(f) Ashed at 800°C



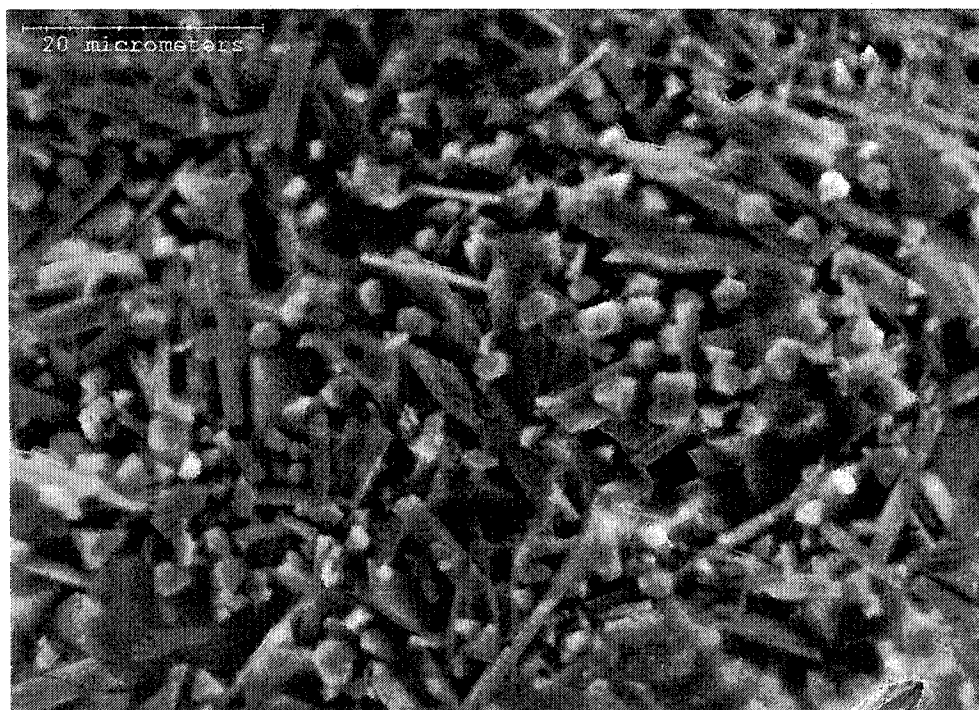
(g) Ashed at 900°C



(h) Ashed at 1000°C

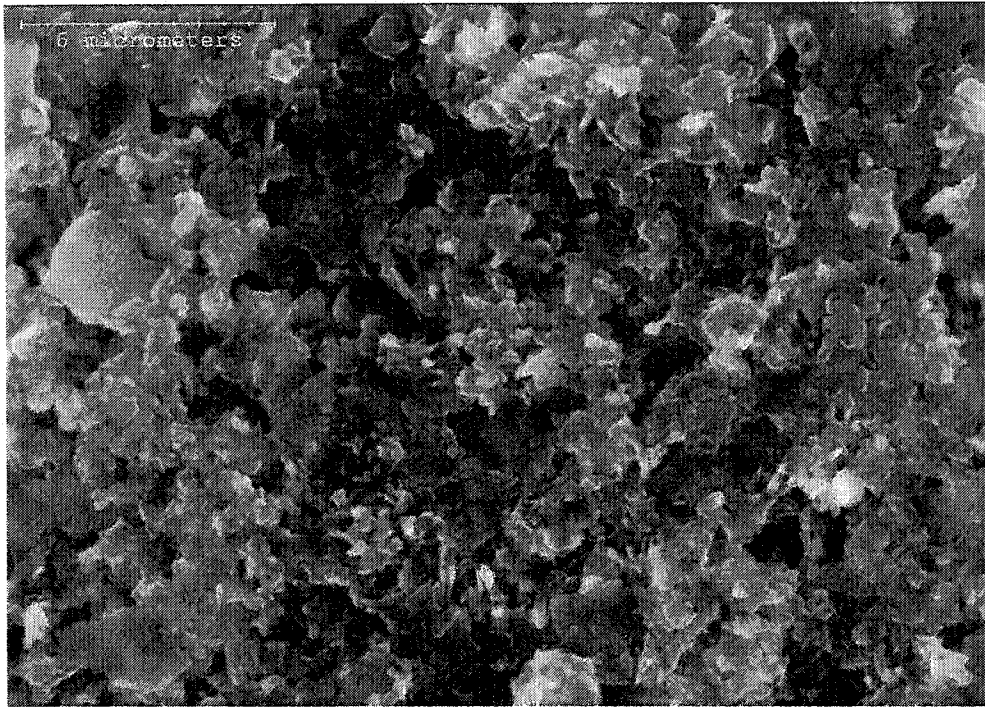


(i) Ashed at 1100°C

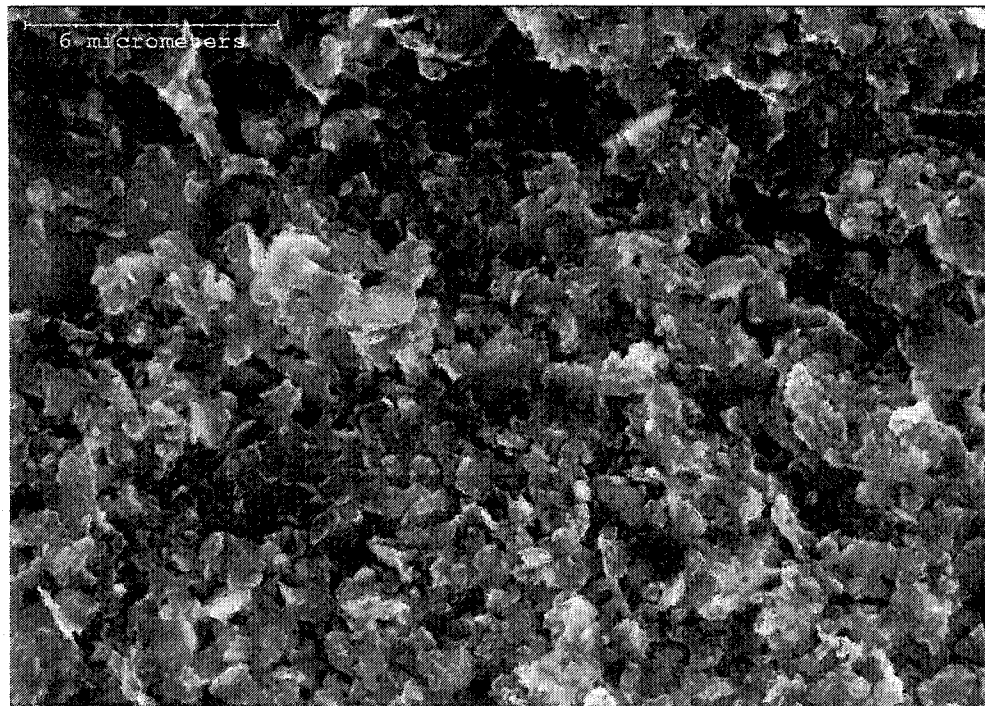


(j) Ashed at 1200°C

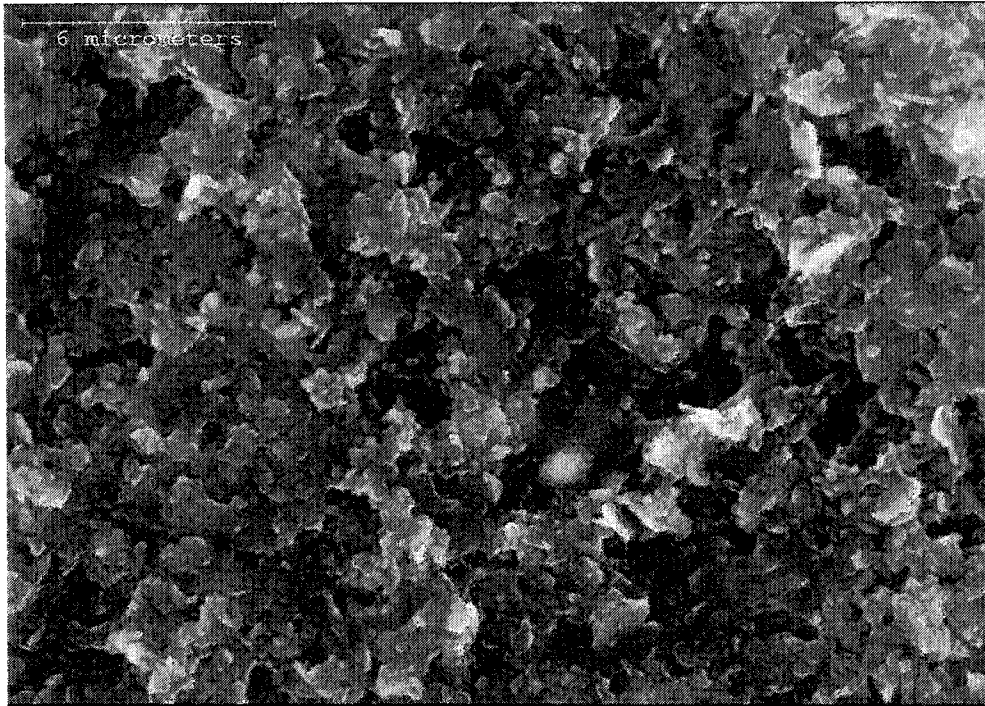
Figure 6.1 Micrographs of Syncrude Fly Ash ($\times 1500$)



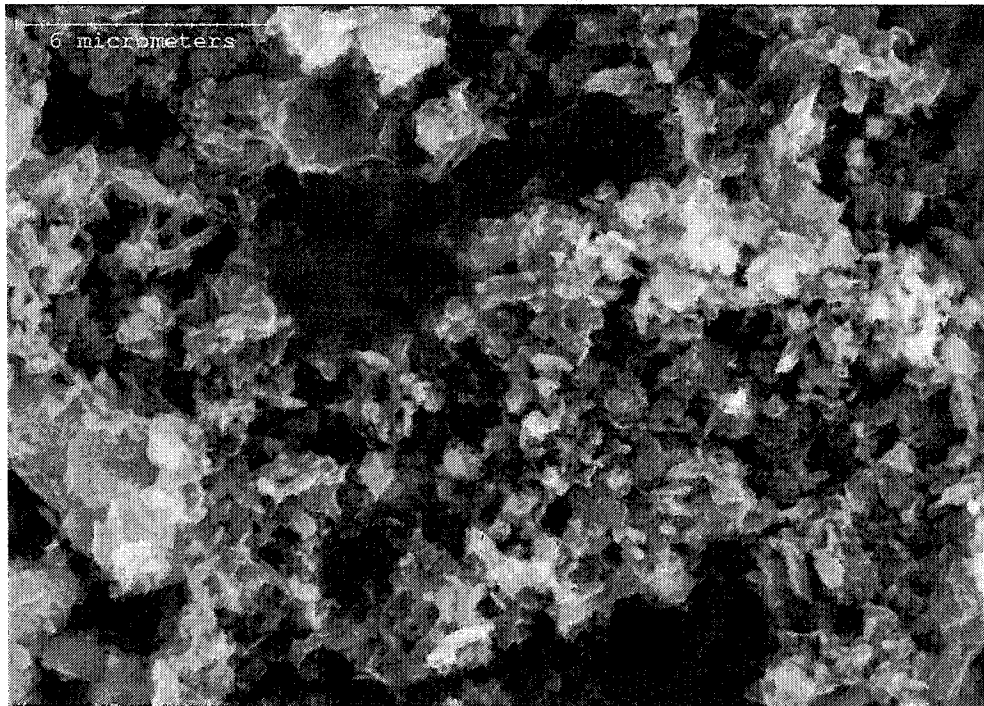
(a) Ashed at 65°C



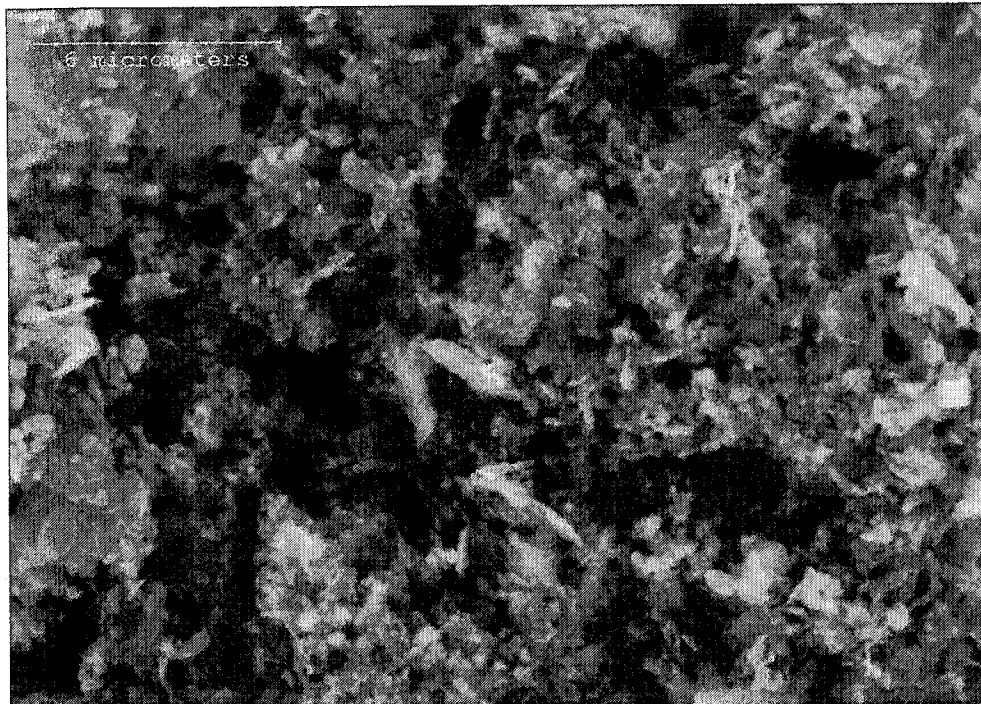
(b) Ashed at 400°C



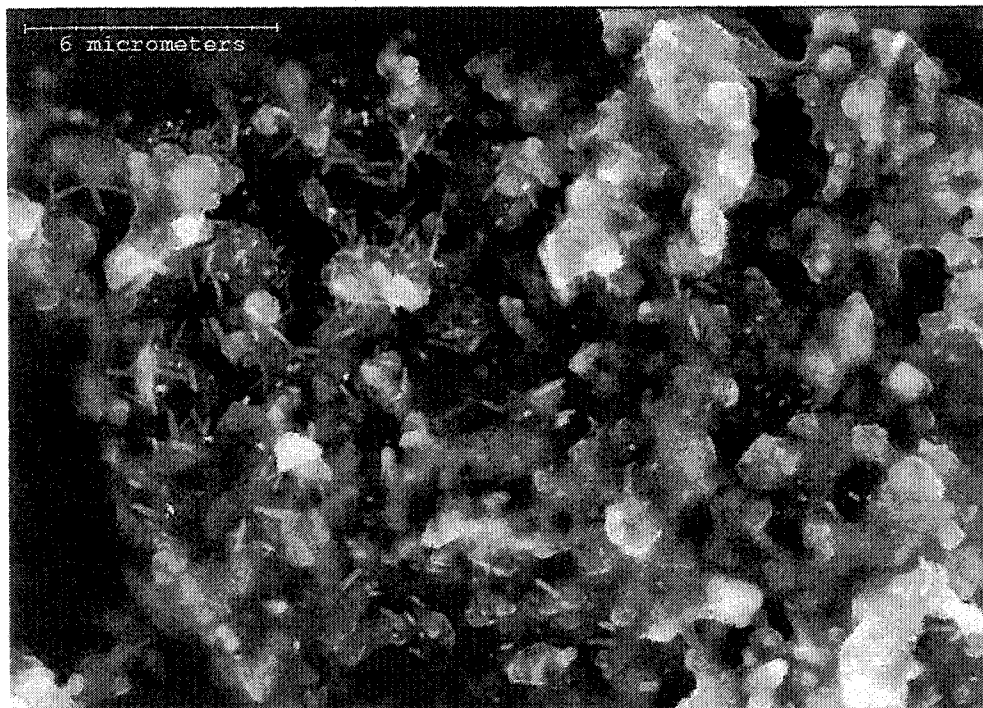
(c) Ashed at 500°C



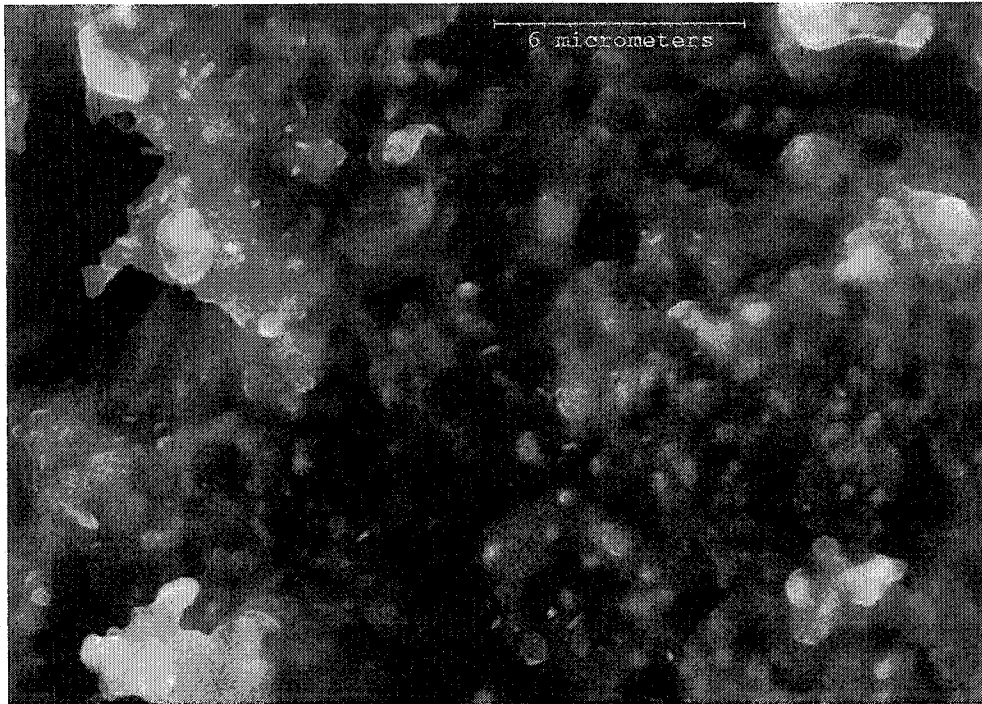
(d) Ashed at 600°C



(e) Ashed at 700°C



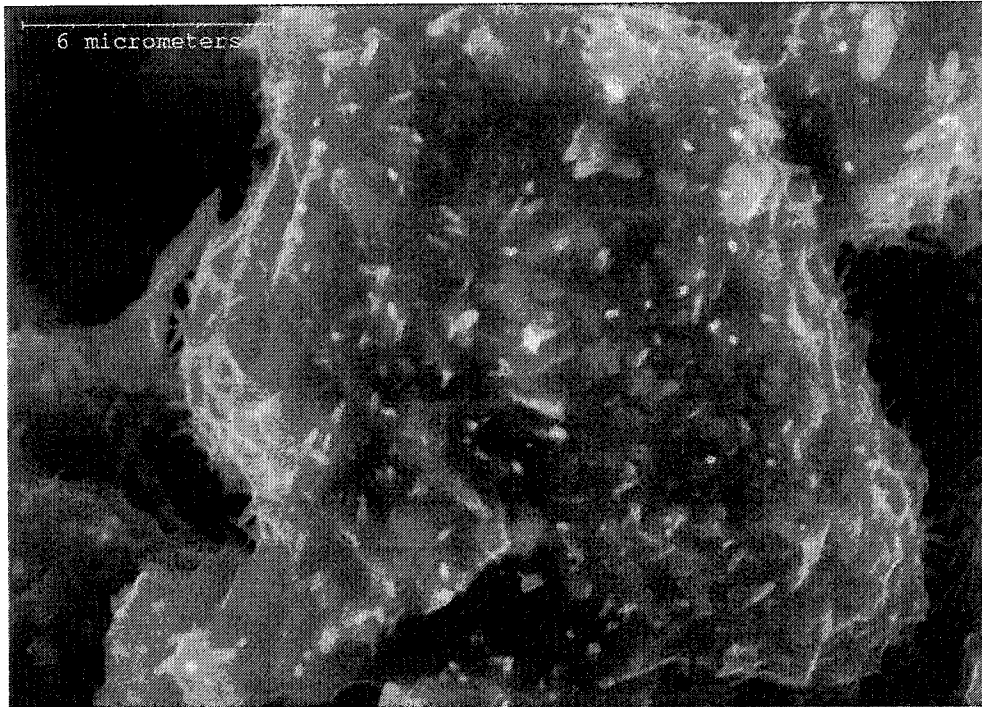
(f) Ashed at 800°C



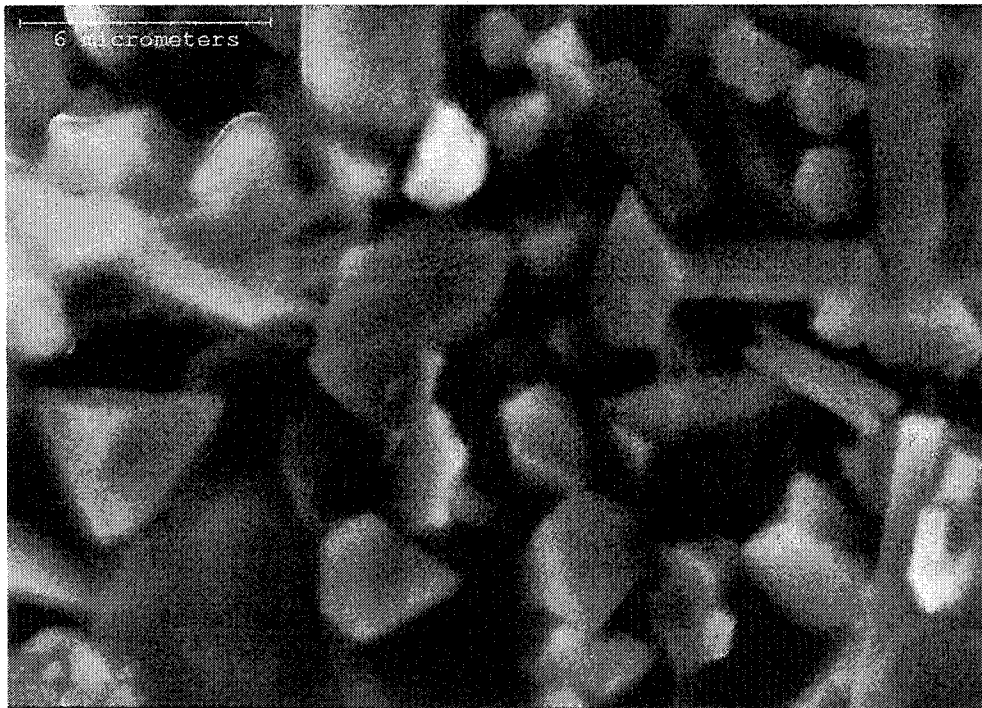
(g) Ashed at 900°C



(h) Ashed at 1000°C



(i) Ashed at 1100°C



(j) Ashed at 1200°C

Figure 6.2 Micrographs of Syncrude Fly Ash ($\times 5000$)

At 800°C, the aluminosilicate melt started to flow and combined with neighbors, then covered small particles. When at high temperature, the movement was much faster so that the melt could possibly interact with more particles resulting in bigger particles when cooled down.

The presence of microcrystals was found at 800°C which was retarded by about 100°C compared to Suncor ash. The size of needles was very small, less than 0.2 μm in diameter and 1 μm long. Fe, Ti, Ni and other elements that might be combined in needles were obviously less mobile compared to Suncor ash. This is probably because the higher silica content, which is normally forming amorphous materials, and higher Ca, K and other base elements are interfering with the movement of needles. Point analyses using EDS indicated that their composition was quite similar to that of Suncor ash needles. These needles were completely entrapped in the aluminosilicate melt above 1000°C so that the particle size was getting bigger.

6.3 Mineralogy of Syncrude Ash

6.3.1 Amorphocity of Syncrude Ash

Syncrude ash samples were collected over the temperature range from 500 to 1000°C and mixed with 10 wt% ZnO. Compared to Suncor ash, a much higher fraction of amorphous materials remained even at high temperature. Starting with 75.5 wt% at 500°C, the amorphous fraction was 48.8 wt% at 1000°C (Figure 6.3). It appeared that high fractions of Ca and K, and amorphous silicates found in Syncrude ash interfered with the

transformation of aluminosilicate glass into crystallites such as mullite. XRD raw patterns of Syncrude ash also indicated the higher amorphocity in Syncrude ash than in Suncor ash (Figure 6.4). The amorphous humps were visible in all samples up to 1000°C, and the humps which were intense and sharp started at about 15° 2θ and ended at 25° 2θ. The diffuse scattering maxima (DSM) of Syncrude ash centers at 18° 2θ approximately, and the shape of the DSM is very sharp compared to that of Suncor which is dull and broad. This is due to the higher quantity of calcium as mentioned earlier.

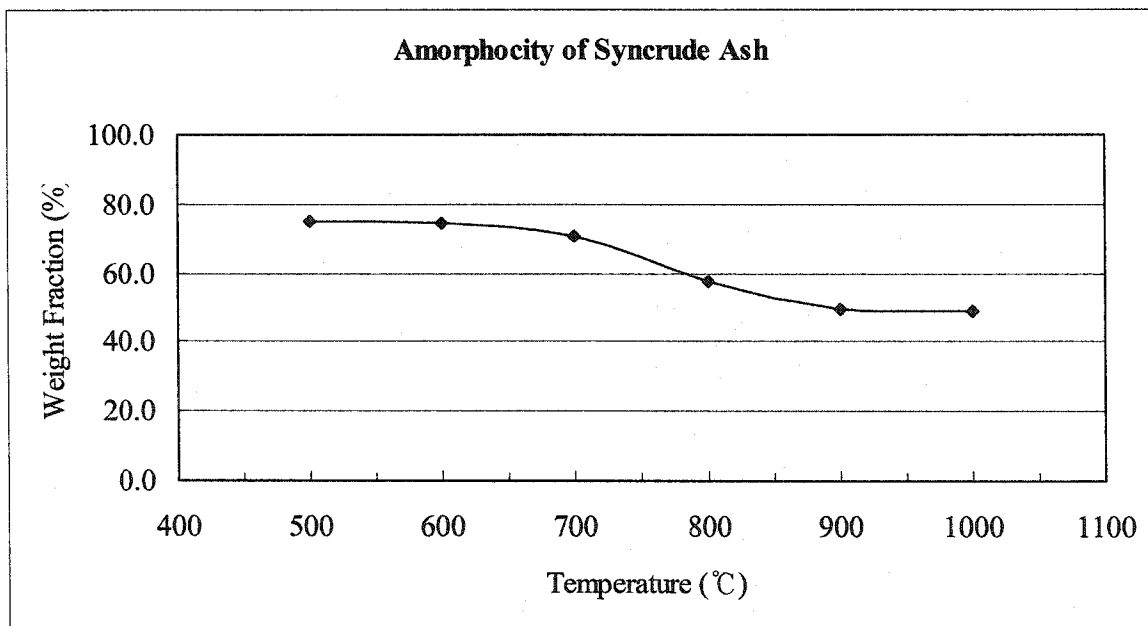
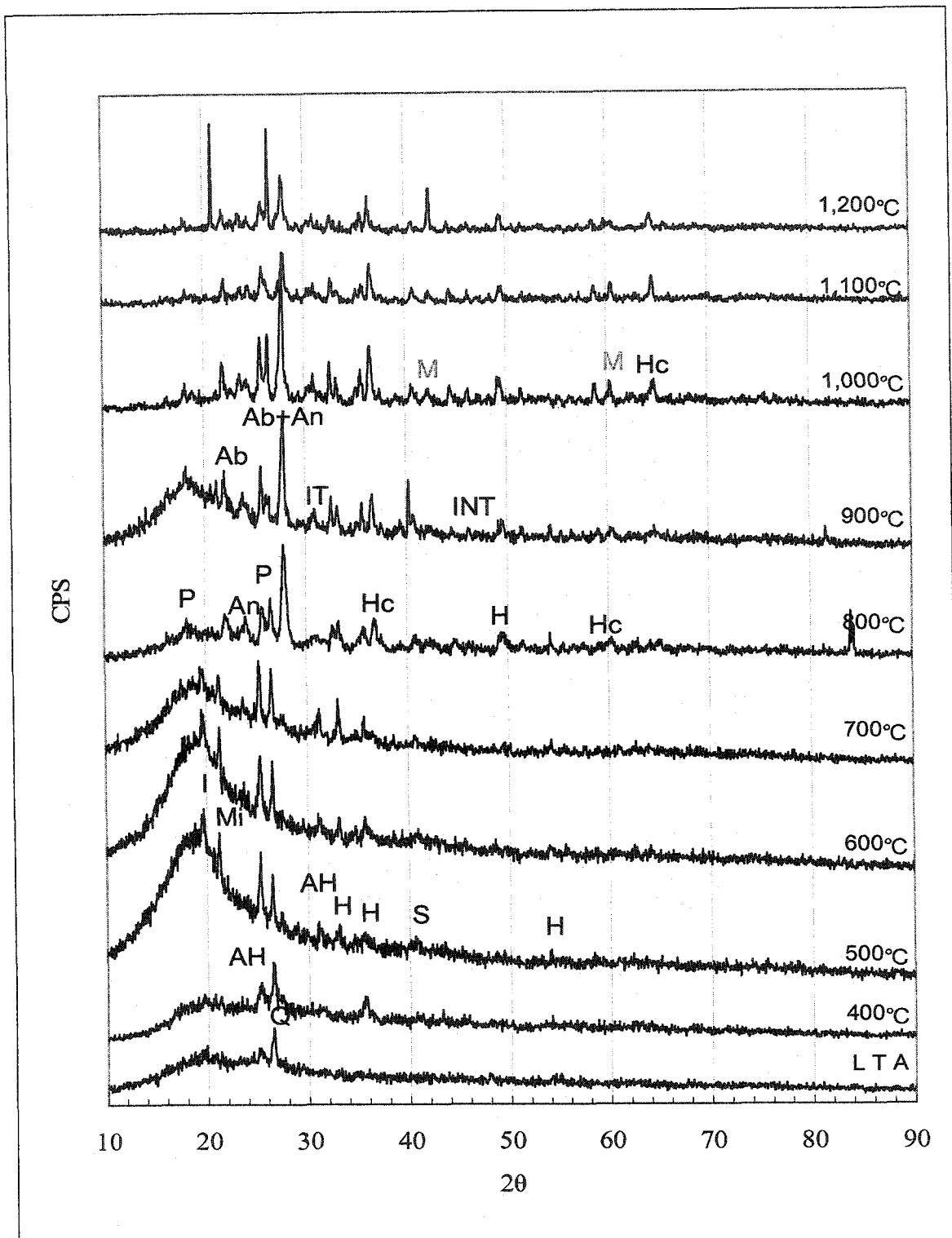


Figure 6.3 Syncrude Ash Amorphocity Determination

6.3.2 Qualitative Analysis

XRD patterns have been measured for Syncrude fly ash samples as temperature changes from 400 to 1200°C. XRD patterns of LTA samples (approximately 65°C) have been also measured (Figure 6.4). The XRD pattern of each sample is provided in the appendix in detail. Strong peaks of quartz, along with moderate peaks of illite and anhydrite were identified in LTA samples. Microcline was also found in this sample with very low intensity peaks. As in Suncor ash, illite ($K_{0.7}Al_2(Si,Al)_4O_{10}(OH)_2$) identified in Syncrude ash was the 1M polytype with its characteristic peaks at 4.43 d and 2.56 d, and was found up to 700°C. No characteristic peaks of kaolinite were found at low temperature. As a result, no mullite structure was identified at high temperature and no cristobalite structure was identified. Characteristic peaks of quartz seemed to remain unchanged. The peaks of microcline found from the LTA temperature to 700°C disappeared at 800°C. Anhydrite was found even at the LTA temperature indicating that gypsum was completely dehydrated at this temperature.

Compared with anhydrite which completely disappeared at 700°C in Suncor ash, anhydrite was found to be present up to 800°C in Syncrude ash, which indicated decomposition of anhydrite was retarded by about 100°C by elemental effects. The higher amount of calcium in Syncrude ash might be mainly responsible for these elemental effects.



Abbreviations used are; I: Illite, Q: Quartz, Mi: Microcline, An: Anorthite, AH: Anhydrite, H: Hematite, S: Sillimanite, P: Pseudobrookite, IT: Fe-Ti Oxide, INT: Fe-Ni-Ti Oxide, Ab: Albite, M: Mullite

Figure 6.4 XRD Raw Patterns of Syncrude Ash

Along with these mineral phases, sillimanite was crystallized at 400°C. Weak intensity peaks of sillimanite were found throughout the temperature range. The presence of sillimanite at 400°C indicated that, among the amorphous materials of fly ash, aluminum was the easiest component to be crystallized. Reacting with Ca released from either the amorphous matrix or gypsum, continuous crystallization of Al also affected the formation of anorthite identified at 600°C.

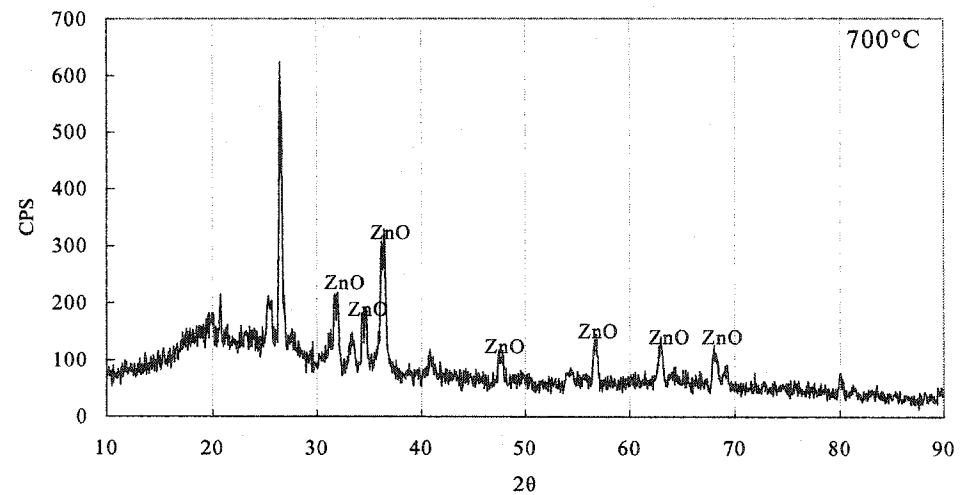
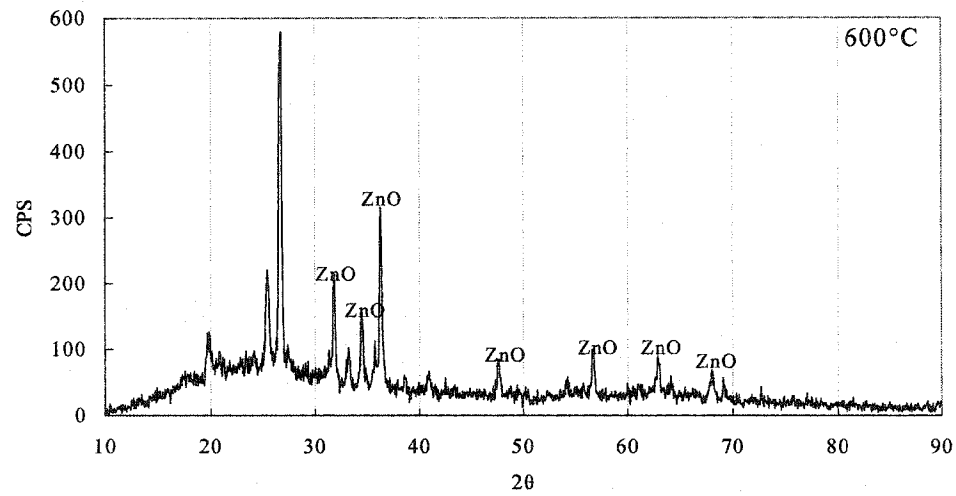
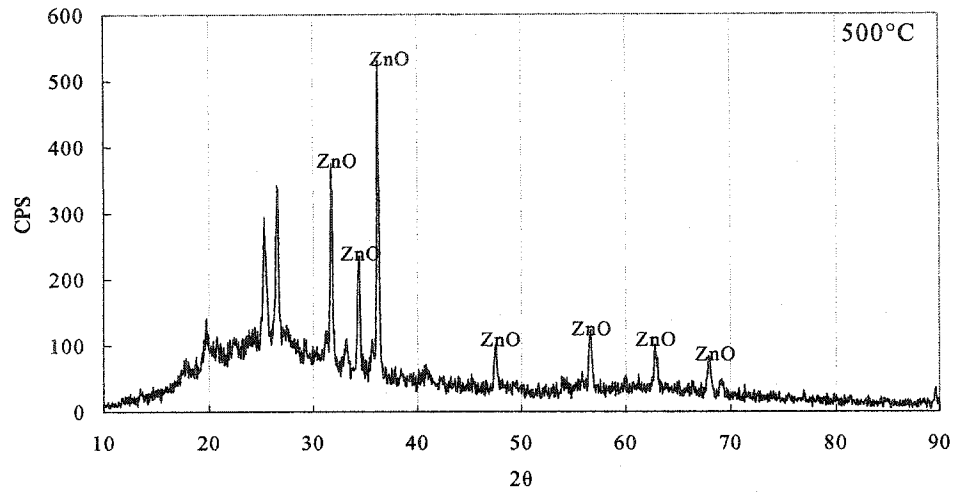
Hematite was first identified at 500°C, and the peaks remained up to 1200°C. Unlike Suncor ash, the peaks were quite obvious up to 1000°C and slowly broadened and overlapped above 1000°C. Other Fe-bearing oxides found from 700 to 1200°C included pseudobrookite (identified at 800°C and higher), other Fe-Ti oxides (identified at 800°C and higher temperature) and Fe-Ni-Ti oxides (identified at 900°C and higher). As found in Suncor ash, the peaks of pseudobrookite were the most intense among these mineral phases. While all these mineral phases containing Fe possibly originated from amorphous Fe-Ni-Ti compounds, hercynite found at 800°C and above appeared to contain Fe originating from illite which contained a significant amount of Fe (normally 1.43% or higher) as an impurity in its interlayers.

Unlike Suncor ash, no mullite structure was identified even at high temperature. Suspicious peaks at $16.6 2\theta$ and $60.5 2\theta$, which are among the characteristic peaks of mullite were found at 900°C and above, but quantitative analysis was unable to detect this phase. None of the associated minerals such as cristobalite were found. Instead, the intensity peaks of albite and anorthite were getting stronger as temperature increased

from 800 to 1000°C. At 1100 and 1200°C, these peak intensities slightly decreased. The peak intensity of pseudobrookite continuously increased up to 1200°C.

6.3.3 Quantitative Analysis

To obtain quantitative information, Syncrude ash samples were mixed with ZnO and the XRD patterns were collected again. Figure 6.5 shows the raw patterns of Syncrude ash. As seen in Table 6.2 and Figure 6.6, the quantities of sillimanite and hematite were quite consistent (sillimanite: 2.8-4.4%, hematite: 2.8-4.3%), which indicated these mineral phases were inactive on combustion. The quantity of sillimanite displayed an increasing trend with temperature in Syncrude ash. Quartz was in a decreasing trend and disappeared at 900°C. Compared with quartz in Suncor ash, quartz in Syncrude ash disappeared at a slightly higher temperature. The absence of cristobalite along with disappearance of quartz indicated again that quartz could not transform into cristobalite. Instead, quartz appeared to transform into amorphous silicates. Mayenite which was regarded as a second phase following the decomposition of anhydrite in Suncor ash was not found in Syncrude ash. The amount of albite and anorthite were significantly increasing at 800°C as much more alkali elements were released from the amorphous aluminosilicate materials at this temperature. The quantity of albite decreased when the temperature was over 1000°C, whereas the quantity of anorthite continuously increased. Pseudobrookite (and possibly other Fe-Ti-Ni oxides) continuously increased in quantity. It might be increasing up to 1200°C since more needle-shaped particles were found in the SEM studies.



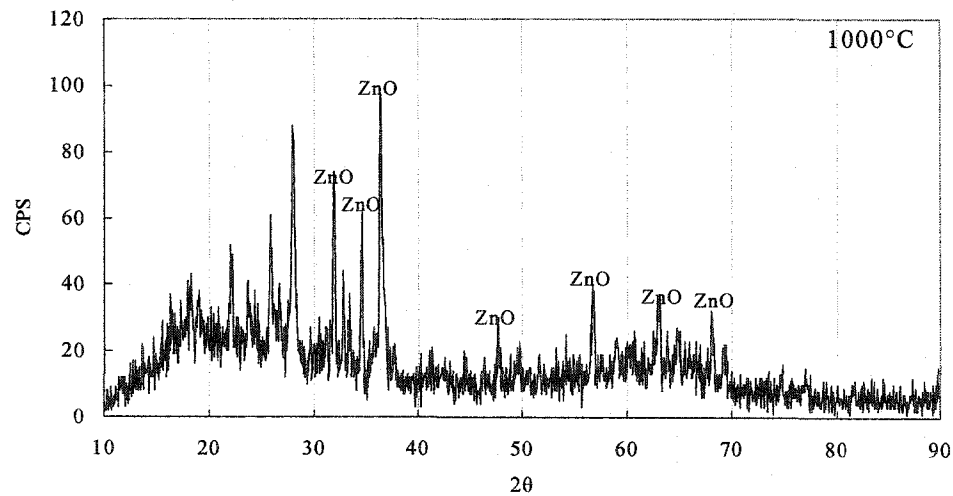
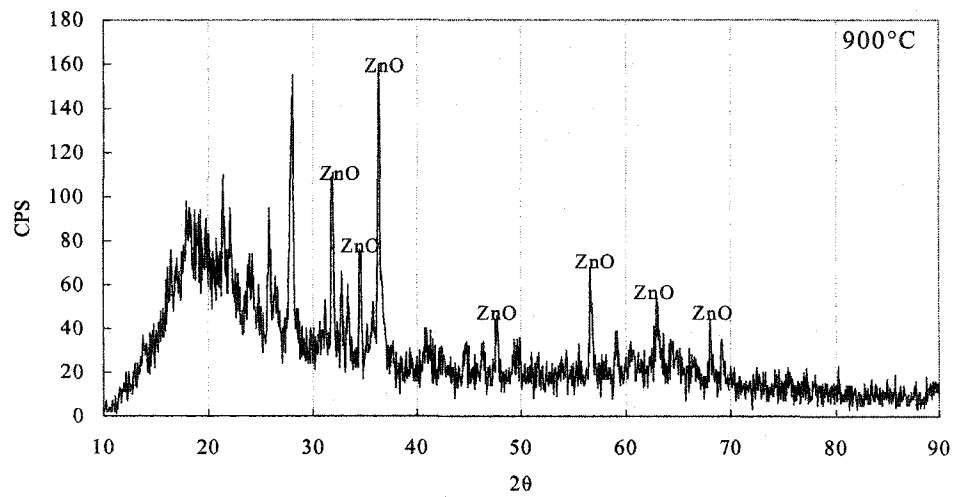
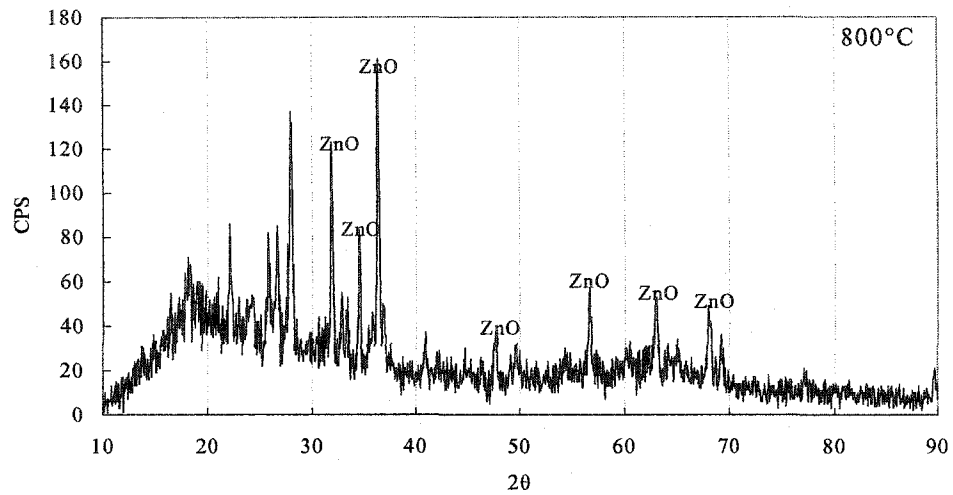


Figure 6.5 XRD Patterns of Syn crude Ash Mixed with 10 wt% ZnO

Table 6.2 Quantitative Analysis of Mineral Phases in Syncrude Ash (wt%)

Minerals \ Temperature (°C)	500	600	700	800	900	1000
Hematite (Fe ₂ O ₃)	2.8	2.1	4.3	3.9	4.0	2.9
Pseudobrookite (Fe ₂ TiO ₅)	0.0	0.0	0.0	3.2	5.9	6.8
Quartz (SiO ₂)	7.5	16.1	9.4	2.9	0.2	0.7
Cristobalite (SiO ₂)	0.0	0.0	0.0	0.0	0.0	0.6
Sillimanite (Al ₂ SiO ₅)	3.0	1.6	3.5	4.4	2.8	3.7
Anorthite (CaAl ₂ SiO ₈)	4.8	2.2	2.1	13.4	19.5	21.7
Albite (NaAlSi ₃ O ₈)	0.1	0.0	2.0	14.7	18.0	14.8
Anhydrite (CaSO ₄)	6.6	3.6	7.9	0.0	0.0	0.0
Amorphous Content	75.2	74.4	70.9	57.4	49.5	48.8

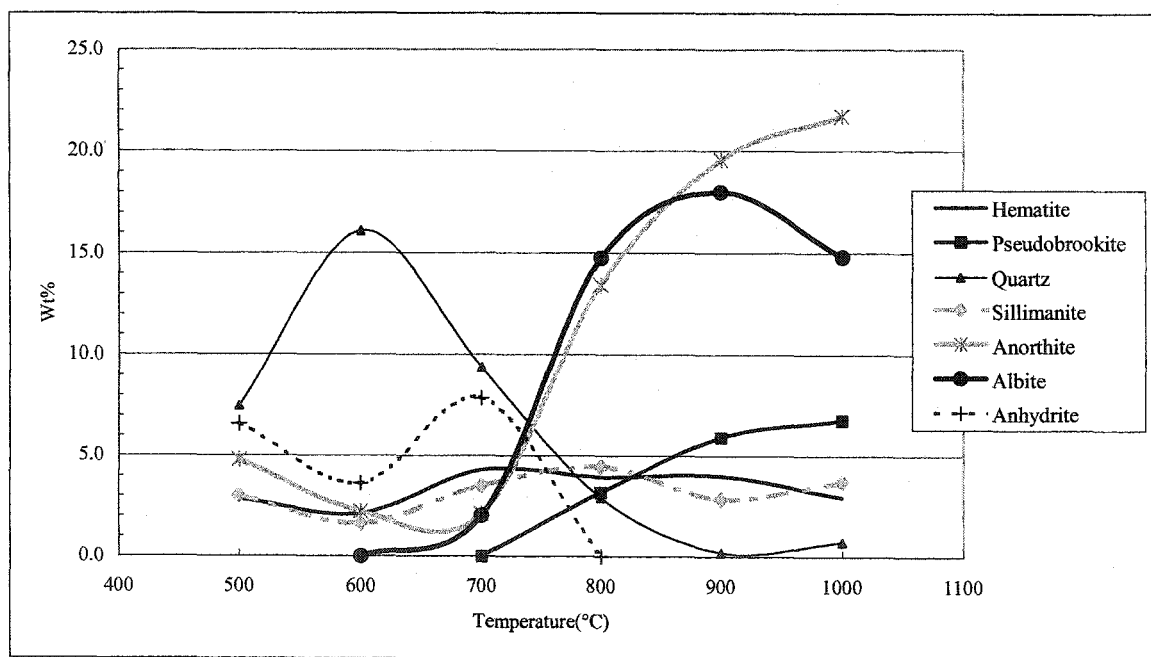


Figure 6.6 Mineral Phases Identified in Syncrude Ash

6.4 Discussion and Conclusions

6.4.1 Mineral Phase Transitions on Combustion

Figure 6.7 illustrates the mineral phase transition behavior of Syncrude ash. Crystalline phases found in the aluminosilicate matrix of Syncrude ash are illite, quartz, microcline and anhydrite. Except quartz, the other three phases undergo significant phase transition. As illite decomposes at 700°C, Al and Si seem to contribute to the formation of albitic feldspars while its impurities such as Fe and Mg are related to the formation of a spinel group mineral, hercynite. However, its potassium fraction which may not form a crystallite seems to be either absorbed in the amorphous materials or inserted in the interstitial sites of crystallites as an impurity. Microcline found from 400 to 700°C also disappears at higher temperature. Quartz transforms at 800°C into amorphous silicates.

Anhydrite rather than gypsum is found in LTA samples. Gypsum has a transition sequence of gypsum-bassanite-anhydrite with increasing temperature, and this transition which accompanies the loss of water could begin at a temperature above 60°C [37]. This transition temperature is highly affected by the presence of alkali or alkaline impurities such as Na₂SO₄ [70]. Bayat [71] also states that the presence of calcium promotes the dehydration of gypsum and forms sulfates easily. One could note that, due to higher concentrations of Ca, Na and K, gypsum in Syncrude coke undergoes a phase transition to anhydrite at a very low temperature on combustion.

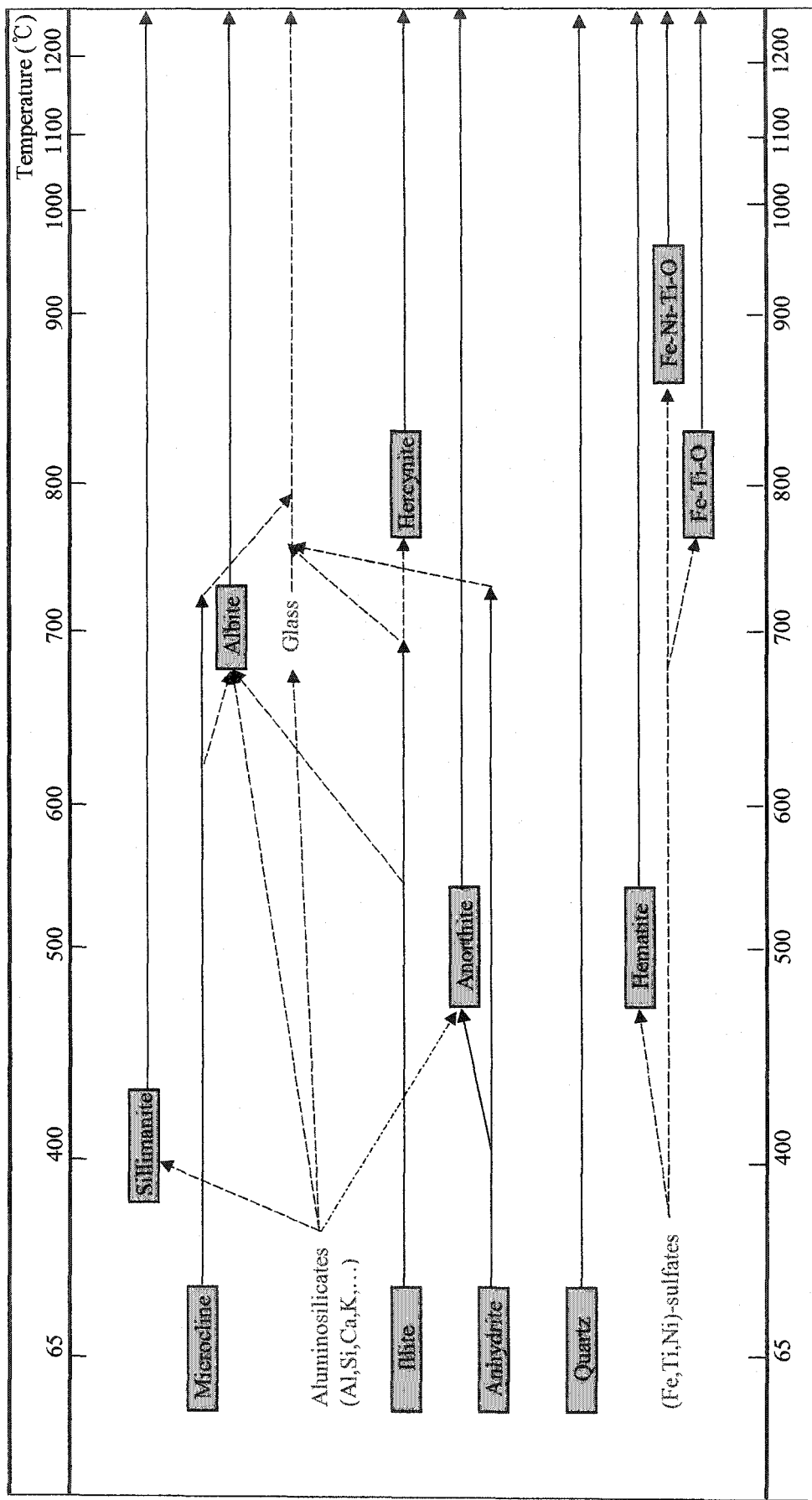


Figure 6.7 Mineral Phase Transitions of Syncrude Fly Ash

It is quite interesting that peaks for kaolinite are not found in this sample. It was anticipated because similarity of mineralogy was expected due to similarity in coking temperature which was about 580°C at Suncor and 630°C at Syncrude, and the proximity of the production mines. It appears that the difference in elemental composition of the fly ash mainly controls the mineralogy of fly ash, especially the occurrence of kaolinite. Less volatiles due to slightly higher coking temperature, less Ni, Ti and V, higher silica and higher Ca could be the main factors that retard the formation of kaolinite in Syncrude ash.

As seen in Suncor ash, formation of mullite and feldspars are the most preferable reactions in the ash, and they are competing with each other. Since mullite could not form in Syncrude ash, it is obvious that feldspars would be crystallized instead. Al-oxides and silica released from amorphous aluminosilicates react with Ca and Na to form these phases. However, if mullite forms at higher temperature, the quantity of feldspars will decrease.

6.4.2 Ash Formation and Morphology

As-received Syncrude ash is derived from the fluid coker which is held at around 630°C so that the ash has no spheres. SEM micrographs show that it only contains flaky shaped aluminosilicate particles. It is consistent with the ash made directly from coke at 600°C. Other Syncrude ashes are found to contain a small amount of needles indicating that the local temperature of the fluid coker might exceed 700°C.

At 800°C, plagioclase feldspars, rather than mullite, start to crystallize from the aluminosilicate matrix and the remaining amorphous material also starts to fuse and coalesce. While these amorphous aluminosilicate melts cover a few small particles, minor elements continuously flow towards the surface of the melts. However, their movement is slower than that of Suncor ash.

When the melts solidify around the gas bubbles, spheres result. At 1100°C, the evidence of spherical particle formation is found. The diameter of a sphere is relatively small compared to that of Suncor ash indicating that the migration of melt is slower. Higher silica, rather than higher Ca, Na and K, might be responsible for slower movement of both aluminosilicate melts and minor elements. It is noteworthy that acidic components, such as silica and ferric oxide, increase the viscosity of melts, whereas basic components such as alkali or alkaline earth minerals decrease their viscosity [20]. It is also found that, when anorthite and mullite are crystallized from glass, the residual melts become enriched in amorphous silica, becoming more viscous. Raask [72] reported that significant amounts of Na and K oxides dissolved in the aluminosilicate melts resulted in the low viscosity of melts. Syncrude ash which contains higher Ca, Na and K might have low viscosity melts at high temperature. However, since Syncrude ash has more amorphous silica materials than Suncor ash, the speed of melt migration may be quite low even at 1200°C or higher.

As explained for Suncor ash, at an early stage of combustion, ash would be formed by simple fragmentation of coke particles. For the ash formed at higher temperature, ash

formation behavior can be explained by the coalescence and coagulation model. Spherical particles, particle size and the surface enrichment of metal elements might also be explained by the melt migration and coagulation model.

6.4.3 Comparison with As-Received Ash

The XRD pattern of an as-received Syncrude ash (1998) after decarburization at 500°C is shown in Figure 6.8. Figure 6.9 shows the SEM micrograph of this ash sample. Mineral phases which are present in an as-received ash include microcline, albite, quartz, anhydrite, sillimanite and hematite. The presence of hematite and anhydrite suggests that Syncrude ash should form between 500 and 800°C. The micrograph and a high temperature phase, albite, indicates that the ash formation of given sample is likely close to 800°C.

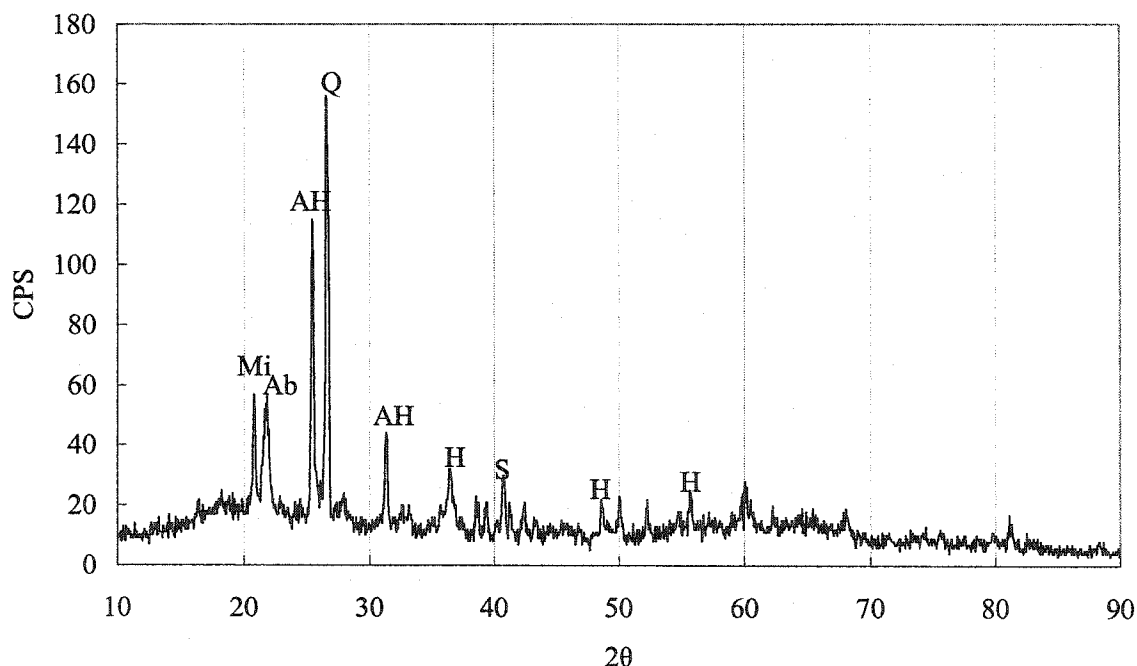


Figure 6.8 XRD pattern of As-Received Syncrude Ash

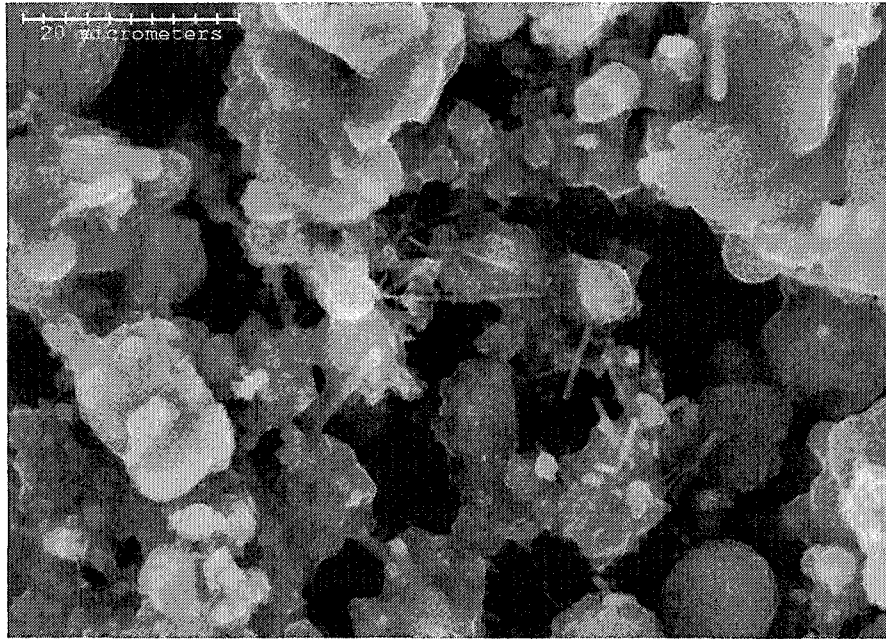


Figure 6.9 SEM Micrograph of As-Received Suncor Ash [5]

7.0 Comparison between Suncor Ash and Syncrude Ash

7.1 Mineralogy of Oil Sands Fly Ash

Due to the proximity of the actual production mines, some mineralogical information obtained from Suncor and Syncrude cokes is quite similar. For both Suncor and Syncrude cokes, the main constituents of fly ash were aluminosilicate minerals and amorphous Fe-Ti-Ni compounds. Aluminosilicate minerals are mainly associated with the formation of mullite and feldspars, while Fe-Ti-Ni compounds lead to the crystallization of hematite, Fe-Ti oxides, pseudobrookite and Fe-Ti-Ni oxides. For both cokes, no pyritic sulfur is identified supporting the fact that almost all the sulfur in oil sands coke is of organic origin. Hematite and quartz are relatively unchanged, but quartz is altered to amorphous silicates at high temperature (800-900°C). Anhydrite originating from gypsum is decomposed at low temperature (700-800°C). Anorthite is formed both by decomposition of anhydrite and by crystallization from amorphous aluminosilicates. A minor amount of hercynite is found as a secondary phase of illite decomposition.

However, since Suncor and Syncrude Canada employ different upgrading and coking processes, the mineralogy of their coke is quite different, as is the mineralogy of fly ash. Chemical analyses reveal that, compared to Suncor ash, Syncrude ash is characterized by its high Ca, Na, K and Si fractions and its low Fe, Ti and V fractions. This elemental difference results in some differences in mineral phases and their thermal behavior:

1. Crystalline phases found in Suncor coke are mainly kaolinite, illite, gypsum, microcline and quartz, whereas illite, microcline, quartz and anhydrite are the main

crystallites in Syncrude coke. Based on the assumption that the same bitumen is treated at both Suncor and Syncrude, which means the mineral phases should be similar, this difference indicates that kaolinite undergoes significant structural distortion during fluid coking processes at Syncrude.

2. Occurrence of mullite is characterized only in Suncor ash. Mullite formation found at 700°C in Suncor ash is not found in Syncrude ash which has no kaolinite to serve as the precursor for mullite formation in its coke samples. Formation of cristobalite results from the decomposition of metakaolinite in Suncor ash, but not in Syncrude ash. This difference confirms the fact that the amorphous silica-to-cristobalite transformation or quartz-to-cristobalite transformation is not possible in oil sands fly ash. The only possible way for cristobalite to form is the decomposition of metakaolinite.

3. Phase transitions of mineral phases are relatively slow in Syncrude ash. Compared to about 20% amorphous materials at 1000°C in Suncor ash, approximately 50% of the ash samples remained amorphous for Syncrude. Formation of needles which is identified as formation of Fe-Ti oxides and Fe-Ti-Ni oxides is delayed around 100°C. Crystallization of feldspar minerals are also retarded for about 100°C. However, dehydration of gypsum is surprisingly fast so that even at a temperature of less than 100°C, anhydrite is found instead of gypsum in Syncrude ash.

4. While mullite is the main mineral phase in Suncor ash, anorthite and albite are the main mineral phases in Syncrude ash. As seen in Suncor ash, the formation of these feldspar minerals competes with the formation of mullite. It is obvious that mullite formation is the preferable reaction on combustion of oil sands fly ash. However, when the ash contains high amounts of Ca, K and Na, as in Syncrude ash, feldspar minerals preferentially crystallize instead of mullite.

7.2 Ash Formation and Morphology of Oil Sands Fly Ash

SEM micrographs of both Suncor and Syncrude ash are not overly different. They indicate that oil sands fly ash is entirely made up of flaky aluminosilicate particles. Iron-titanium related minerals starts to crystallize from these flaky particles at 700°C in Suncor ash and at 800°C in Syncrude ash. When the temperature increases slightly more, the amorphous aluminosilicates starts to fuse and coalesce. Then, at a higher temperature, these melts covers the small particles which are originally flaky flat but irregularly spheroidized somewhat. The thin acicular shaped particles which grow out of flaky particles are also covered by these melts. These needles have a tendency to continuously grow so that they appear on the surface of melts. The growth of needles is much more active in Suncor ash which contains higher amounts of metal elements. With less metal values, Syncrude ash shows weak movements of needles. The growth of needles, which results from migration towards the surface of melts, is the direct evidence of surface enrichment of heavy metals found in many research work.

When the temperature reaches approximately 1100°C in Suncor ash and 1200°C in Syncrude ash, the melts seem to form spherical shaped particles as they solidify around the entrapped gas bubbles. It is concluded that spherical shaped particles form at a temperature which is high enough for melts to flow and coalesce. Obviously, their viscosity should be adequate to form spheres. At lower temperatures, however, the ash seems to form only by the fragmentation of coke particles since it is found that the coke particle itself had a multi-layered “onion skin” structure [58]. The thin flat particles are layered to form a chunk of coke particles. The evidence of “*particle deposition onto the surface*” mentioned by many scientists [23, 39, 58] was not found in the oil sands fly ash. Also, other mechanisms such as “*vaporization of volatiles to form a sub-micron sphere*”, might be accepted, but seems unable to properly explain the formation mechanism of oil sands fly ash.

The degree of melt migration seems to control the size of a particle. When the melts move farther, bigger particles are formed. The factors affecting the speed of melt migration may include temperature, chemical distribution of each element which affects the viscosity of melts, and the amorphocity of the ash.

8.0 Future Work

Several areas would require further study to characterize oil sands fly ash in order to develop its commercial usage. Especially, in order to commercialize vanadium extraction, vanadium speciation is urgently required. It is not known which mineral phases are related with vanadium. To solve this problem, much effort would be required in several areas. These areas will include:

1. Development of mineral processing techniques to obtain more knowledge on mineral phases as well as to increase the efficiency of metal extraction,
2. Chemical treatment of ash to selectively dissolve a certain mineral fraction (e.g., desilication using diluted HF solution),
3. Metal value speciation to establish the relations between metal elements and amorphous materials, and metal elements and crystalline phases,
4. Structural information on important mineral phases (e.g., the solubility of vanadium into Al sites of mullite),
5. Thermodynamic equilibrium study to explain the transition of mineral phases and to develop equilibrium phase diagrams,
6. Mineralogical phase changes upon addition of some chemicals.

7. Ashing Syncrude coke in a reducing atmosphere to check the difference in properties between the ash obtained from the oxidizing atmosphere and the ash obtained from the reducing environment, and
8. Ashing bitumen from LTA temperature to 600°C to clarify the difference in the properties between coke ash and the bitumen ash.

In order to overcome the limitation of conventional techniques, usage of some recently developed technology must be considered. Extended x-ray absorption fine structure (EXAFS) and x-ray absorption near edge structure (XANES) are some of the key techniques used in metal value speciation since these can be used for amorphous materials. The Rietveld refinement technique is also promising to obtain structural information.

9.0 Conclusions

Oil sands fly ash obtained from Suncor and Syncrude were characterized mainly as to chemical composition, mineralogy and morphology. In the temperature range of 65-1200°C, numerous characteristics of fly ash were collected and compared. As well, along with high temperature ashing, a low temperature ashing technique revealed the nature of oil sands coke. Mineral phases and their thermal transition in oil sands ash were uncovered qualitatively and quantitatively based on XRD raw data. The ash formation behavior during combustion was also explained in detail for the first time.

The ash obtained in the low temperature asher was revealed to have significant amounts of amorphous aluminosilicate materials along with minor amounts of illite and kaolinite, a minor amount of calcium sulfate and quartz. Aluminosilicates were further classified into two forms: aluminosilicates combining alkaline earth elements and aluminosilicates combining transition metal elements. The former aluminosilicates were the precursors of feldspars, mullite and sillimanite, and the latter were attributed to the crystallization of hematite, Fe-Ti oxides and Fe-Ti-Ni oxides. Clays contributed to the formation of mullite, cristobalite and hercynite, while quartz was not associated with chemical interactions. Gypsum underwent dehydration resulting in the formation of anhydrite which also contributed to the formation of anorthite at a later stage of combustion. It was found that, though the mineralogy of Suncor and Syncrude coke was supposed to be the same, minor differences in chemical composition between two plants greatly affected the phase transitions at elevated temperature.

Ash formation behavior of oil sands fly ash was quite similar to that of coal fly ash. At an early stage of combustion, ash was formed by the fragmentation of coke particles whereas, at a later stage of combustion, the ash was found to form by coalescence and coagulation. However, SEM micrographs indicated that a vaporization-condensation model which included surface deposition of volatiles was not feasible to explain the formation of oil sands ash. Surface enrichment of metallic elements (and probably trace elements as well) was rather explained by the flow of melts and the migration of needle shaped particles. The extent of melt migration was closely related to the size of particles. It was also found that the migration of both melts and crystallites was governed by the temperature, amorphocity and the chemical composition of fly ash. Spherical particles were found at over 1100°C and their formation was identified when the melts were cooled down around the entrapped gas bubbles.

A good understanding of the mechanism of mineral phase transition during combustion and the mechanism of ash formation behavior of oil sands fly ash could lead to future improvements and optimization of recovery of metal values from oil sands ash. As well, the results from this thesis could be a useful source for acceptable disposal of oil sands fly ash or successful gasification of oil sands coke.

References

1. Cameron Engineers, "*Oil Sands*", Synthetic Fuels Data Handbook, 1978, Colorado, Cameron Engineers Inc.
2. Gray, M.R. and Masliyah, J.H., "*Extraction and Upgrading of Oilsands Bitumen*", 2001, Edmonton, University of Alberta.
3. Furimsky, E., "*Gasification of Oil Sand Coke: Review*", Fuel Processing Technology, 1998, 56, p. 263-90.
4. Griffin, P.J. and Etsell, T.H., "*Extraction of vanadium and nickel from Athabasca Oil Sands Fly Ash*", in Future Heavy Crude Tar Sands, Int. Conf., 2nd., 1982, Calgary, McGraw-Hill, New York, p.1286-93.
5. Holloway, Preston C., "*Vanadium Recovery from Oil Sands Fly Ash*", M.Sc. Thesis, 2002, University of Alberta, Edmonton.
6. Carrigy, M.A., "*Mesozoic Geology of the Fort McMurray Area*", Guide to the Athabasca Oil Sands Area, ed. Carrigy, M.A. and Kramers, J.W., 1973, Alberta Research Council, Edmonton, p.77-103.
7. Holloway, P. and Etsell, T.H., "*Recovery of Vanadium from Oil Sands Fly Ash*", in Proceedings of the International Symposium on Vanadium, 2002, Montreal, p.227-42.
8. Torrey, S., "*Coal Ash Utilisation; Fly Ash, Bottom Ash and Slag*", Coal Ash Characterization, 1978, New Jersey, Noyes Data Corporation.
9. McCarthy, G.J., "*Energy: By-Products of Coal Combustion in Power Plants*", Industrial Applications of X-Ray Diffraction, ed. Chung, F.H. and Smith, D.K., 2000, Marcel Dekker, Inc., New York, p.555-72.
10. Denoyer, E., Natusch, D.F.S., Surkyn, P. and Adams, F.C., "*Laser Microprobe Mass Analysis (LAMMA) as a Tool for Particle Characterization: A Study of Coal Fly Ash*", Environ. Sci. Technol., 1983, 17, p. 457-62.
11. Vincze, L., Somogyi, A., Osan, J., Vekemans, B. and Adams, F.C., "*Quantitative Trace Element Analysis of Individual Fly Ash Particles by means of X-ray Microfluorescence*", Anal. Chem., 2002, 74, p. 1128-35.
12. Hassett, D.J. and Eylands, K.E., "*Mercury Capture on Coal Combustion Fly Ash*", Fuel, 1999, 78, p. 243-48.

13. Sakulpitakphon, T., Hower, J.C., Trimble, A.S., Schram, W.H. and Thomas, G.A., "Mercury Capture by Fly Ash: Study of the Combustion of a High-Mercury Coal at a Utility Boiler", *Energy & Fuels*, 2000, 14, p. 727-33.
14. Hower, J.C., Trimble, A.S., Eble, C.F., Palmer, C.A. and Kolker, A., "Characterization of Fly Ash from Low-Sulfur and High-Sulfur Coal Sources: Partitioning of Carbon and Trace Elements with Particle Size", *Energy Sources*, 1999, 21, p. 511-25.
15. Querol, X., Fernandez-Turiel, L. and Lopez-Soler, A., "Trace Elements in Coal and Their Behavior during Combustion in a Large Power Station", *Fuel*, 1995, 74, p. 331-43.
16. Yan, R., Gauthier, D., Flamant, G. and Gautrin, M., "An Equilibrium Analysis to Determine the Speciation of Trace Elements in the Flue Gas from a Coal-Fired Fluidized-Bed Boiler", in *Proceedings of the 15th International Conference on Fluidized Bed Combustion*, 1999, New York, ASME, p.730-61.
17. O'Gorman, J.V. and Walker Jr., P.L., "Mineral Matter and Trace Elements in U.S. Coals", Pennsylvania State University, University Park, PA, 1972, 61, p.81-101.
18. Levin, E.M., Robbins, C.R. and McMurdie, H.F., "Phase Diagrams for Ceramists", 3 ed., ed. Reser, Margie K., 1964, Columbus, Ohio, The American Ceramic Society, Inc.
19. Mollah, M.Y.A., Promreuk, S., Schennach, R., Cocke, D.L. and Guler, R., "Cristobalite Formation from Thermal Treatment of Texas Lignite Fly Ash", *Fuel*, 1999, 78, p. 1277-82.
20. Kalmanovitch, D.P. and Williamson, J., "Crystallization of Coal Ash Melts", *Mineral Matter and Ash in Coal*, ed. Vorres, K.S., 1986, American Chemical Society, Washington DC, p.234-55.
21. Falcone, S.K. and Schobert, H.H., "Mineral Transformations during Ashing of Selected Low-rank Coals", *Mineral Matter and Ash in Coal*, ed. Vorres, K.S., 1986, American Chemical Society, Washington DC, p.114-27.
22. Biggs, D.L. and Lindsay, C.G., "High Temperature Interactions among Minerals Occuring in Coal", *Mineral Matter and Ash in Coal*, ed. Vorres, K.S., 1986, American Chemical Society, Washington DC, p.128-37.
23. Sarofim, A.F., Howard, J.B. and Padia, A.S., "The Physical Transformation of the Mineral Matter in Pulverized Coal Under Simulated Combustion Conditions", *Combust. Sci. Technol.*, 1977, 16, p. 187-204.

24. Renton, John J., "*Semiquantitative Determination of Coal Minerals by X-Ray Diffractometry*", Mineral Matter and Ash in Coal, ed. Vorres, Karl S., 1986, American Chemical Society, Washington DC, p.53-60.
25. Hulett, L.D. and Weinberger, A.J., "*Some Etching Studies of the Microstructure and Composition of Large Aluminosilicate Particles in Fly Ash from Coal-burning Power Plants*", Environ. Sci. Technol., 1980, 14, p. 965-70.
26. Grim, Ralph E., "*Clay Mineralogy*", 2nd. ed., 1968, New York, McGraw-Hill Book Company.
27. Spears, D.A., "*Role of Clay Minerals in UK Coal Combustion*", Appl. Clay Sci., 2000, 16, p. 87-95.
28. Kerrick, Derrill M., "*The Al₂SiO₅ Polymorphs*", Reviews in Mineralogy, ed. Ribbe, Paul H., Vol. 22, 1990, Washington DC, Mineralogical Society of America.
29. Bruhns, Petra and Fischer, Reinhard X., "*Phase Reactions in the Brick Firing Process of V-doped Clay*", Eur. J. Mineral., 2001, 13, p. 611-19.
30. Sainz, M.A., Serrano, F.J., Bastida, J. and Caballero, A., "*Microstructural Evolution and Growth of Crystallite Size of Mullite During Thermal Transformation of Kyanite*", J. Eur. Ceram. Soc., 1997, 17, p. 1277-84.
31. Rahman, S., Feustel, U. and Freimann, S., "*Structure Description of the Thermal Phase Transformation Sillimanite-Mullite*", J. Eur. Ceram. Soc., 2001, 21, p. 2471-78.
32. Hatt, R.M. and Bull, D.L., Mineral Matter and Ash Deposition from Coal, ed. Bryers, R.W. and Vorres, K.S., 1990, Engineering Foundation, New York, p.215.
33. Demir, I., Hughes, R.E. and DeMaris, P.J., "*Formation and Use of Coal Combustion Residues from Three Types of Power Plants Burning Illinois Coals*", Fuel, 2001, 80, p. 1659-73.
34. McCarthy, G.J., Swanson, K.D., Keller, L.P. and Blatter, W.C., "*Mineralogy of Western Fly Ash*", Cement and Concrete Research, 1984, 14, p. 471-78.
35. Mitchell, R.S. and Gluskoter, H.J., "*Mineralogy of Ash of Some American Coals: Variations with Temperature and Source*", Fuel, 1976, 55, p. 90-96.
36. Akhtar, S.S. and Schlorholtz, S.M., "*Characterization of Fluidized Bed Combustion Fly Ashes Produced from High Sulfur Coals*", Coal Science and Technology, 1993, 21(Processing and Utilisation of High-Sulfur Coals), p. 345-60.

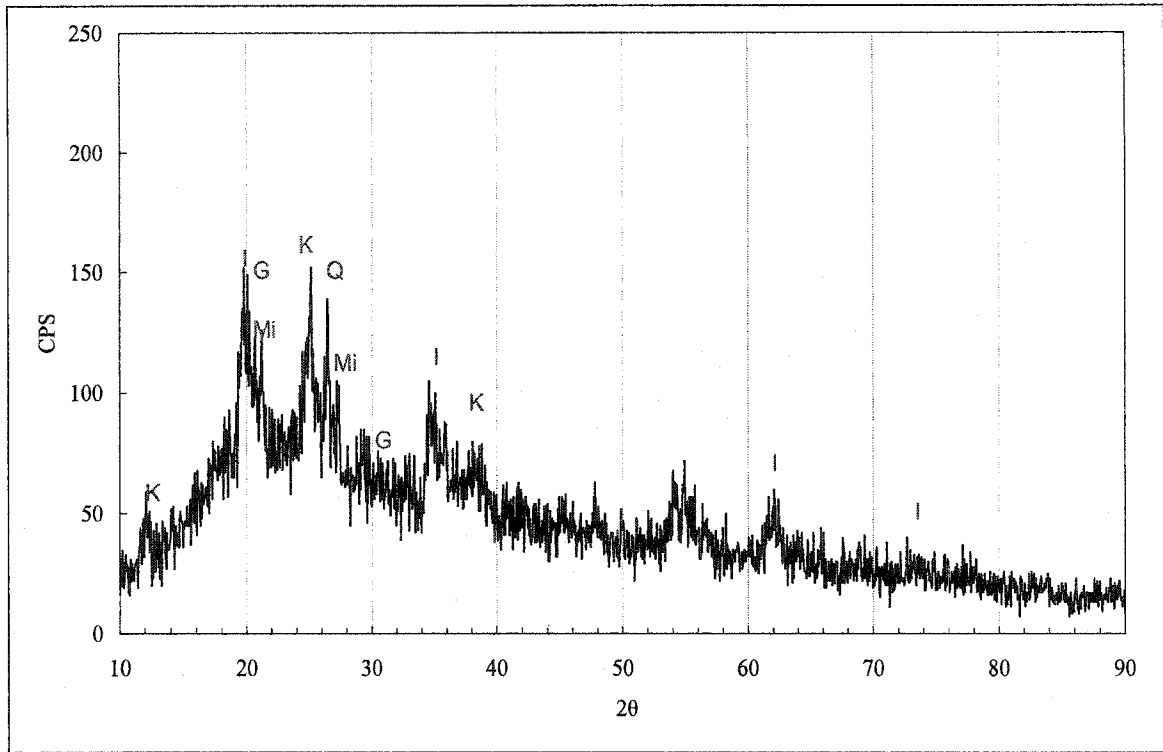
37. Knittle, E., Phillips, W. and Williams, Q., "*An Infrared and Raman Spectroscopic Study of Gypsum at High Pressures*", *Phys. Chem. Minerals*, 2001, 28, p. 630-40.
38. Vassilev, S.V., Braekman-Danheux, C. and Laurent, P., "*Characterization of Refuse-derived char from Municipal Solid Waste: 1. Phase-mineral and Chemical Composition*", *Fuel Processing Technology*, 1999, 59, p. 95-134.
39. Flagan, R.C. and Friedlander, S.K., "*Particle Formation in Pulverized Coal Combustion - a Review*", in *Symposium of Aerosol Science and Technology-Recent Developments in Aerosol Science*, 1976, Pasadena, CA, Wiley, New York, p.25-59.
40. Couch, G., "*Understanding Slagging and Fouling in pf Combustion*", IEA Coal Research, London, 1994, CR/72, p.118.
41. Yan, L., Gupta, R.P. and Wall, T.F., "*The Implication of Mineral Coalescence Behavior on Ash Formation and Ash Deposition during Pulverized Coal Combustion*", *Fuel*, 2001, 80, p. 1333-40.
42. McLennan, A.R., Bryant, G.W., Stanmore, B.R. and Wall, T.F., "*Ash Formation Mechanisms during pf Combustion in Reducing Conditions*", *Energy & Fuels*, 2000, 14, p. 150-59.
43. Wu, H., Bryant, G. and Wall, T., "*The Effect of Pressure on Ash Formation during Pulverized Coal Combustion*", *Energy & Fuels*, 2000, 14, p. 745-50.
44. Kang, S.G., Sarofim, A.F. and Beer, J.M., "*Effect of Char Structure on Residual Ash Formation During Pulverized Coal Combustion*", in *Proceedings of 24th International Symposium on Combustion*, 1992, Sydney, The Combustion Institute, p.1153-59.
45. Kaakinen, J.W., Jordan, R.M., Lawasani, M.H. and West, R.E., "*Trace Elements Behavior in Coal Fire Power Plant*", *Environ. Sci. Technol.*, 1975, 9, p. 862.
46. Klein, D.H., "*Pathways of Thirty-Seven Trace Elements through Coal-fire Power Plants*", *Environ. Sci. Technol.*, 1975, 9, p. 973.
47. Kaufherr, N. and Lichtman, D., "*Comparison of Micron and Submicron Fly Ash Particles Using Scanning Electron Microscopy and X-ray Elemental Analysis*", *Environ. Sci. Technol.*, 1984, 18, p. 544-47.
48. Fishman, N.S., Rice, C.A., Breit, G.N. and Johnson, R.D., "*Sulfur-bearing Coatings on Fly Ash from a Coal-fired Power Plant: Composition, Origin, and Influence on Ash Alteration*", *Fuel*, 1999, 78, p. 187-96.

49. Vassilev, S.V., Menendez, R., Alvarez, D., Diaz-Somoano, M. and Martinez-Tarazona, M.R., "*Phase-mineral and Chemical Composition of Coal Fly Ash as a Basis for Their Multicomponent Utilization. 1. Characterization of Feed Coals and Fly Ashes*", *Fuel*, 2004, 82, p. 1793-811.
50. EUB, "*Alberta's Reserves 2002 and Supply/Demand Outlook 2003-2012*", Alberta Energy & Utilities Board, 2002, Statistical Series 2003-98.
51. Griffin, Peter J., "*Extraction of Vanadium and Nickel from Athabasca Oil Sands Fly Ash*", Ph.D Thesis, 1981, University of Alberta, Edmonton.
52. Smith, A.J., Rice, J.O., Shaner, Jr. W.C and C.C, Cerato, "*Trace Analysis of Iron, Nickel, Copper and Vanadium in Petroleum Products*", *The Role of Trace Metals in Petroleum*, ed. Yen, T.F., 1975, Ann Arbor Science, Michigan, p.149-60.
53. Filby, R.H., "*The Nature of Metals in Petroleum*", *The Role of Trace Metals in Petroleum*, ed. Yen, T.F., 1975, Ann Arbor Science, Michigan, p.31-58.
54. Hitchon, B., Filby, R.H. and Shah, K.R., "*Geochemistry of Trace Elements in Crude Oils, Alberta, Canada*", *The Role of Trace Metals in Petroleum*, ed. Yen, T.F., 1975, Ann Arbor Science, Michigan, p.111-22.
55. Valkovic, Vlado, "*Trace Elements in Petroleum*", 1978, Tulsa, OK, The Petroleum Publishing Company.
56. Yen, T.F., "*Vanadium and its Bonding in Petroleum*", *The Role of Trace Metals in Petroleum*, ed. Yen, T.F., 1975, Ann Arbor Science, Michigan, p.167-82.
57. Boduszynski, M.M., "*Composition of Heavy Petroleums. 1. Molecular Weight, Hydrogen Deficiency, and Heteroatom Concentration as a Function of Atmospheric Equivalent Boiling Point up to 1400F*", *Energy & Fuels*, 1987, 1, p. 2-11.
58. Har, S. H., "*Characterization of Oil Sands Fluid Coke*", M.Sc. Thesis, 1981, University of Alberta, Edmonton.
59. Gomez-Bueno, C.O., Spink, D.R. and Rempel, G.L., "*Extraction of Vanadium from Athabasca Tar Sands Fly Ash*", *Metall. Trans.*, 1981, 12B, p. 341-52.
60. LFE Corporation, "*Operation and Maintenance of LTA-302*" 1978, No. 255539, Waltham, Massachusetts.
61. Perkin Elmer Corp., Model 4000 Atomic Absorption Spectroscopy Manual, "*Analytical Methods for Atomic Absorption Spectroscopy*" 1982, Norwalk, CN.

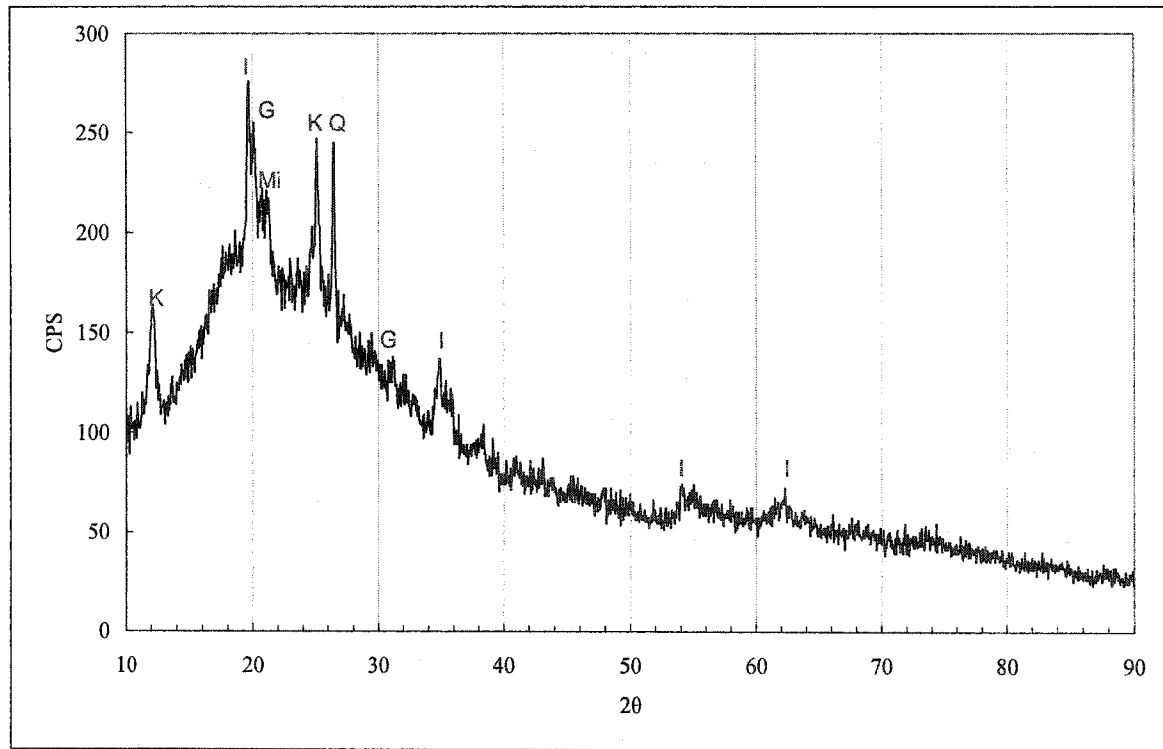
62. Rietveld, H.M., "*Line Profiles of Neutron Powder-diffraction Peaks for Structure Refinement*", Acta Cryst., 1967, 22, p. 151-52.
63. Rietveld, H.M., "*A Profile Refinement Method for Nuclear and Magnetic Structures*", J. Appl. Cryst., 1969, 2, p. 65-71.
64. Chung, F.H. and Smith, D.K., "*Industrial Applications of X-Ray Diffraction*", 2000, Marcel Dekker, Inc., New York.
65. Young, R.A., "*The Rietveld Method*", International Union of Crystallography. 5., 1995, Oxford University Press, New York.
66. LeRoux, J.,Lennox, D.H. and Kay, K., "*Direct Quantitative X-ray Analysis by Diffraction-Absorption Technique*", Anal. Chem., 1953, 25, p. 740-43.
67. Schneider, Linda G., "*Extraction of Vanadium from Oil Sands Fly Ash*", M.Sc. Thesis, 1983, University of Alberta, Edmonton.
68. Grim, Ralph E. and Bradley, W.F., "*Investigation of the Effect of Heat on the Clay Minerals Illite and Montmorillonite*", J. Am. Ceram. Soc., 1940, 23, p. 242-48.
69. Anthony, J.W.,Bideaux, R.A.,Bladh, K.W. and Nichols, M.C., "*Handbook of Mineralogy*", Vol. 2, 1995, Tucson, AZ, Mineral Data Publishing.
70. Prasad, P.S.R.,Ravikumar, N.,Krishnamurthy, A.S.R. and Sarma, L.P., "*Role of Impurities in Gypsum-Bassanite Phase Transition: A Comparative Raman Study*", Current Science, 1998, 75, p. 1410-14.
71. Bayat, Oktay, "*Characterization of Turkish Fly Ashes*", Fuel, 1998, 77, p. 1059-66.
72. Raask, Enrich, "*Flame Vitrification and Sintering Characteristics of Silicate Ash*", Mineral Matter and Ash in Coal, ed. Vorres, K.S., 1986, American Chemical Society, Washington DC, p.138-55.

APPENDIX

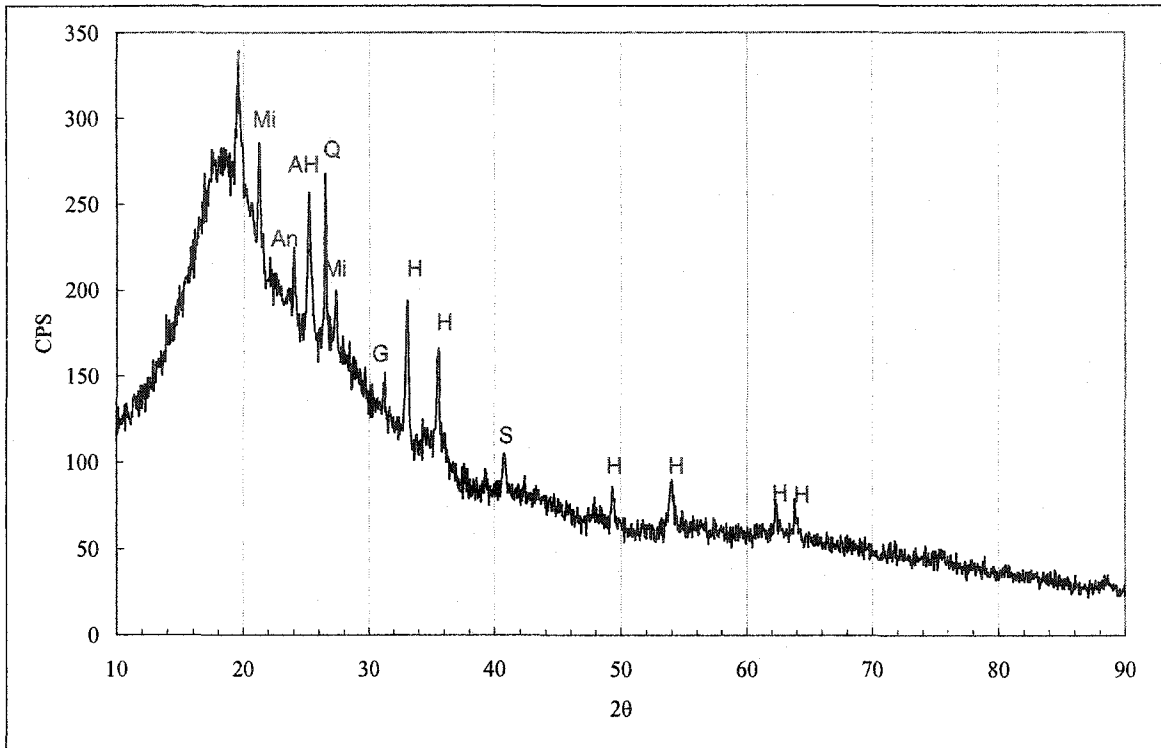
1. XRD Raw Patterns and Mineral Phases Identified in Suncor Ash



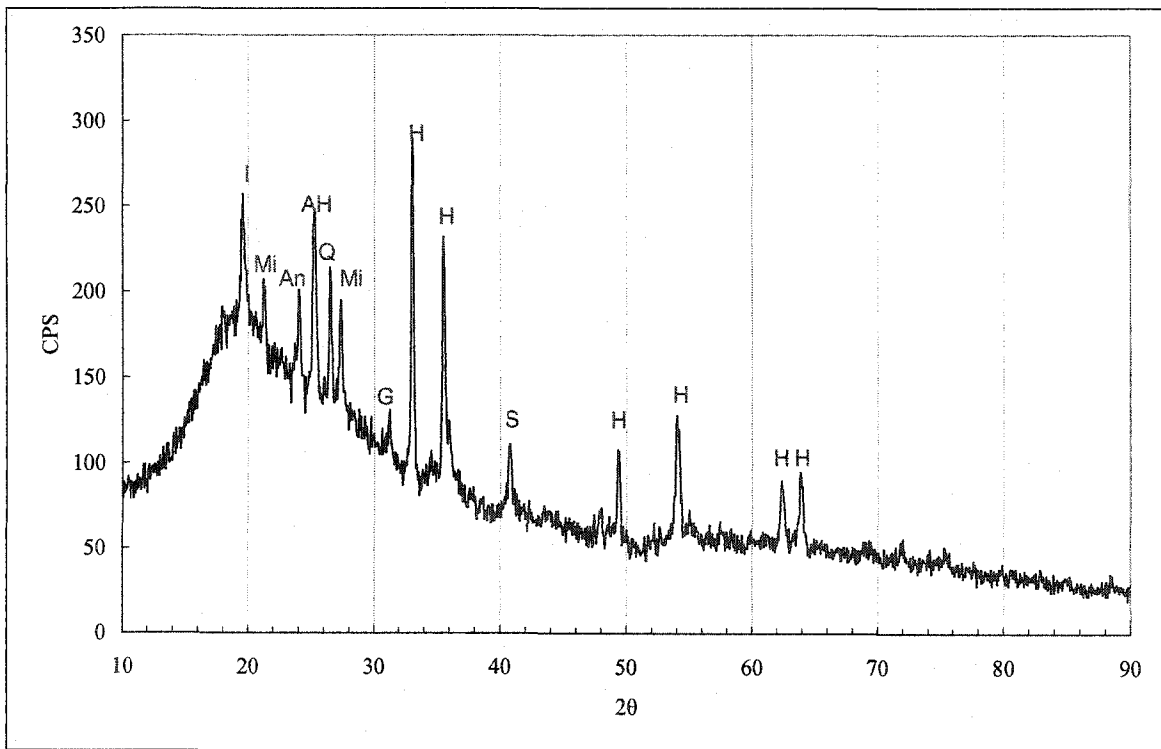
(A 1.1) XRD Raw Pattern of Suncor Ash at LTA Temperature (65°C)



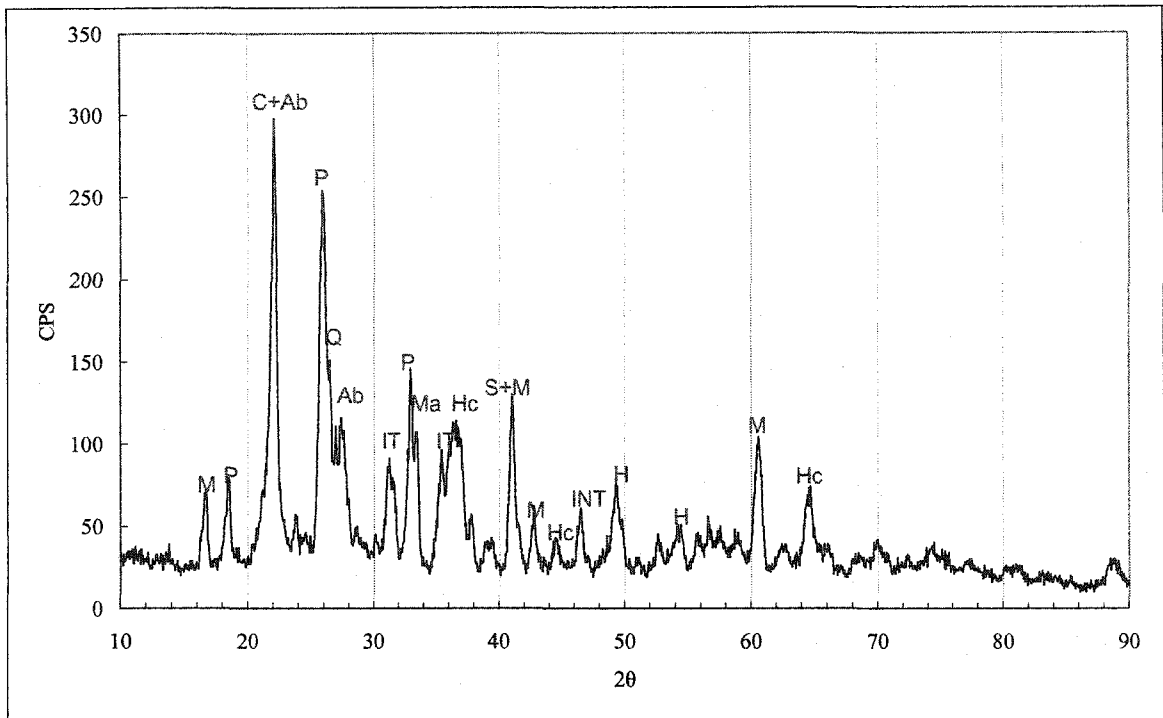
(A 1.2) XRD Raw Pattern of Suncor Ash at 400°C



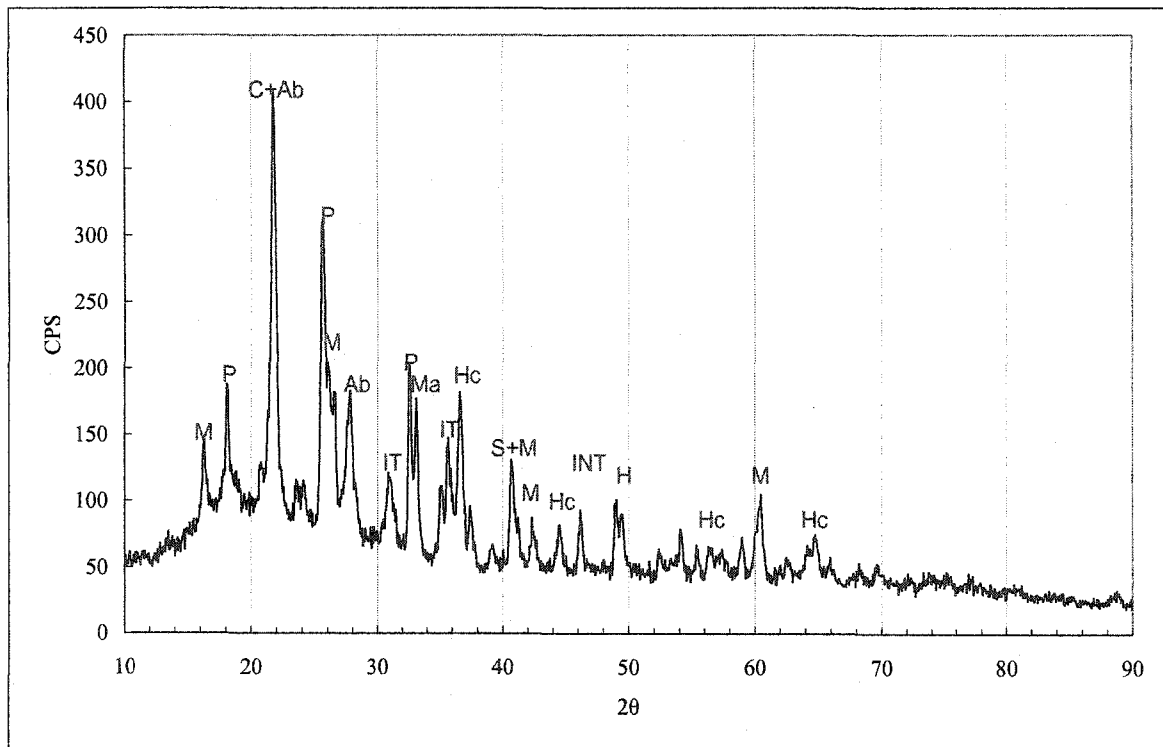
(A 1.3) XRD Raw Pattern of Suncor Ash at 500°C



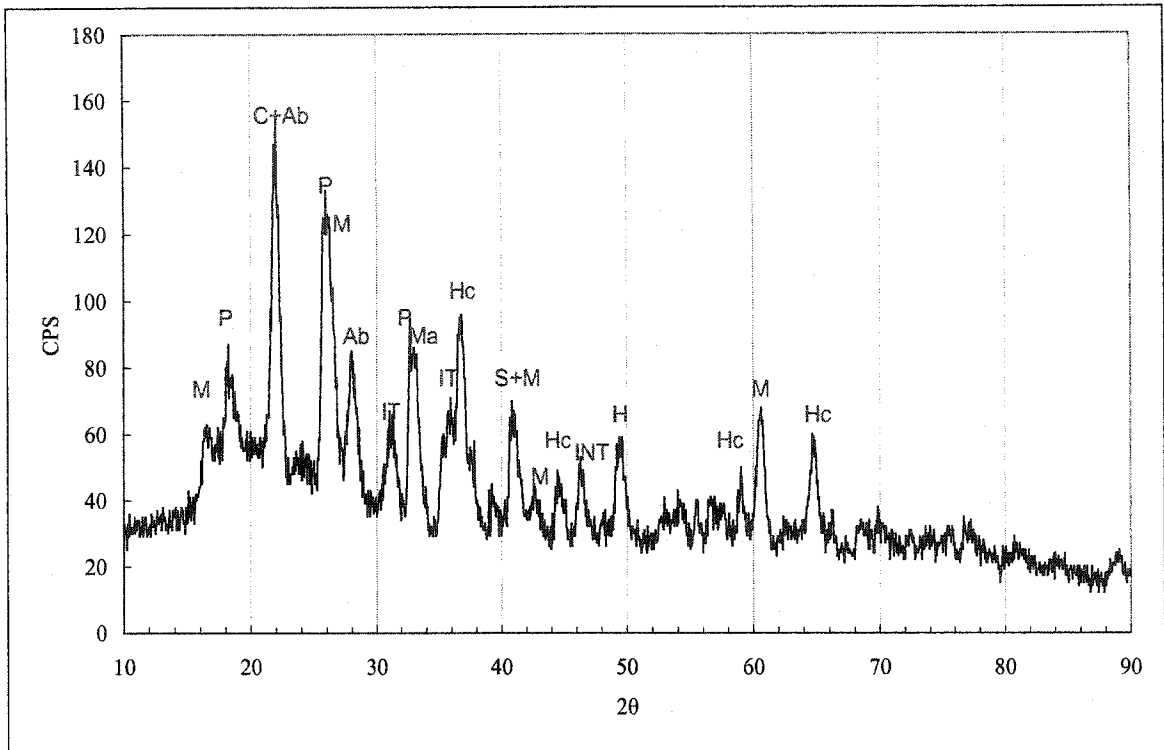
(A 1.4) XRD Raw Pattern of Suncor Ash at 600°C



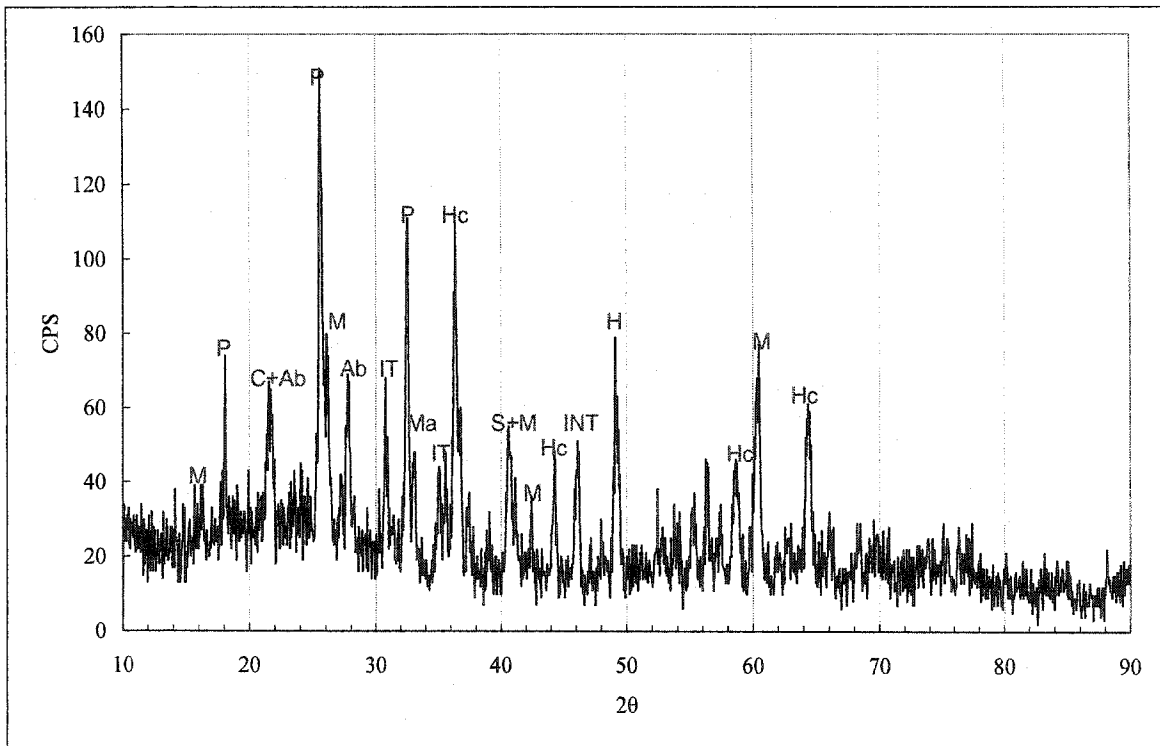
(A 1.5) XRD Raw Pattern of Suncor Ash at 700°C



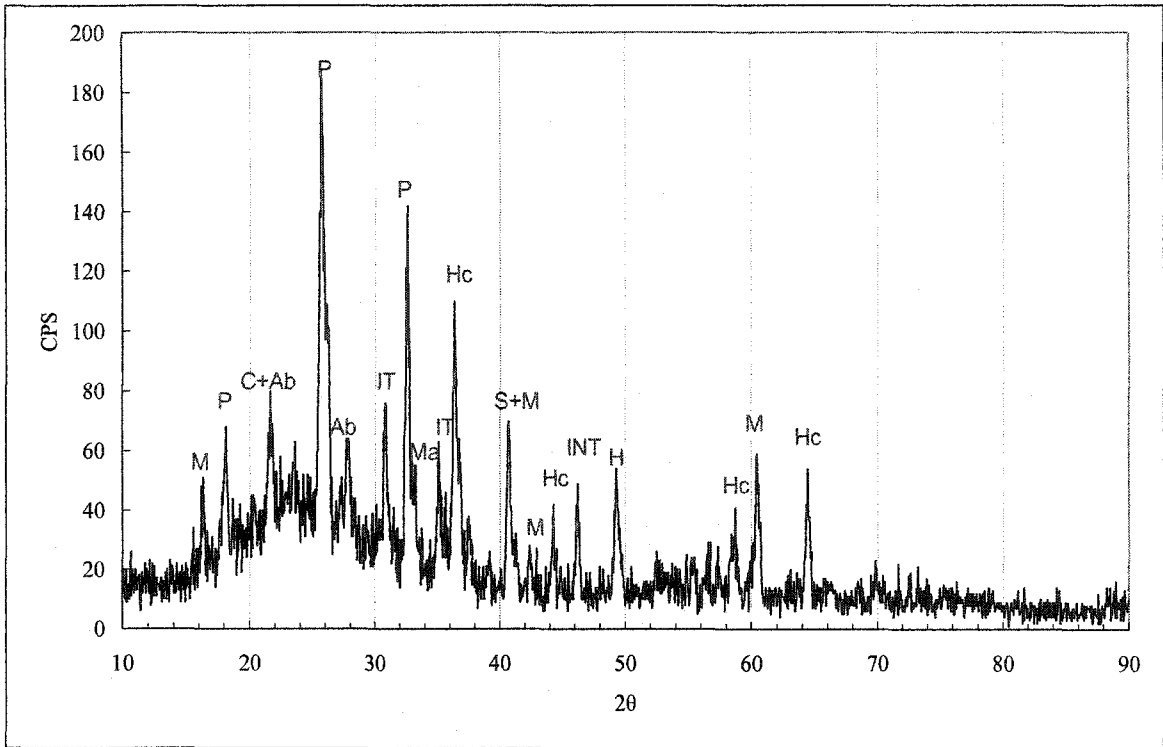
(A 1.6) XRD Raw Pattern of Suncor Ash at 800°C



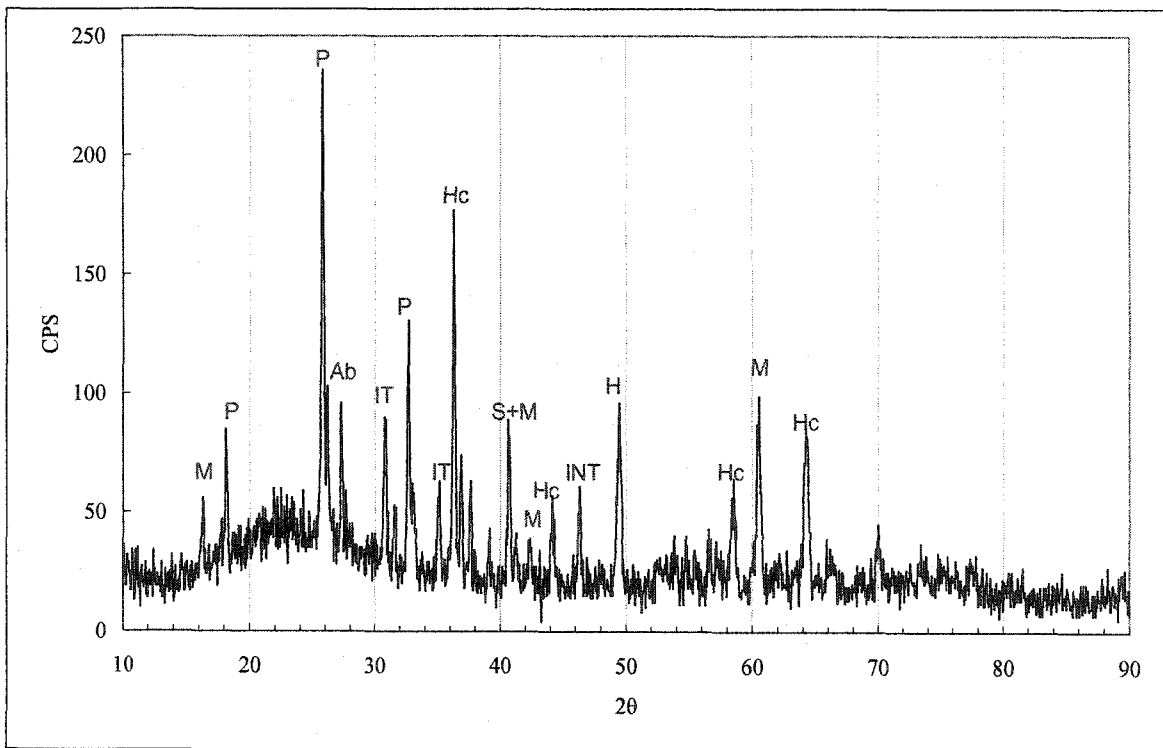
(A 1.7) XRD Raw Pattern of Suncor Ash at 900°C



(A 1.8) XRD Raw Pattern of Suncor Ash at 1000°C

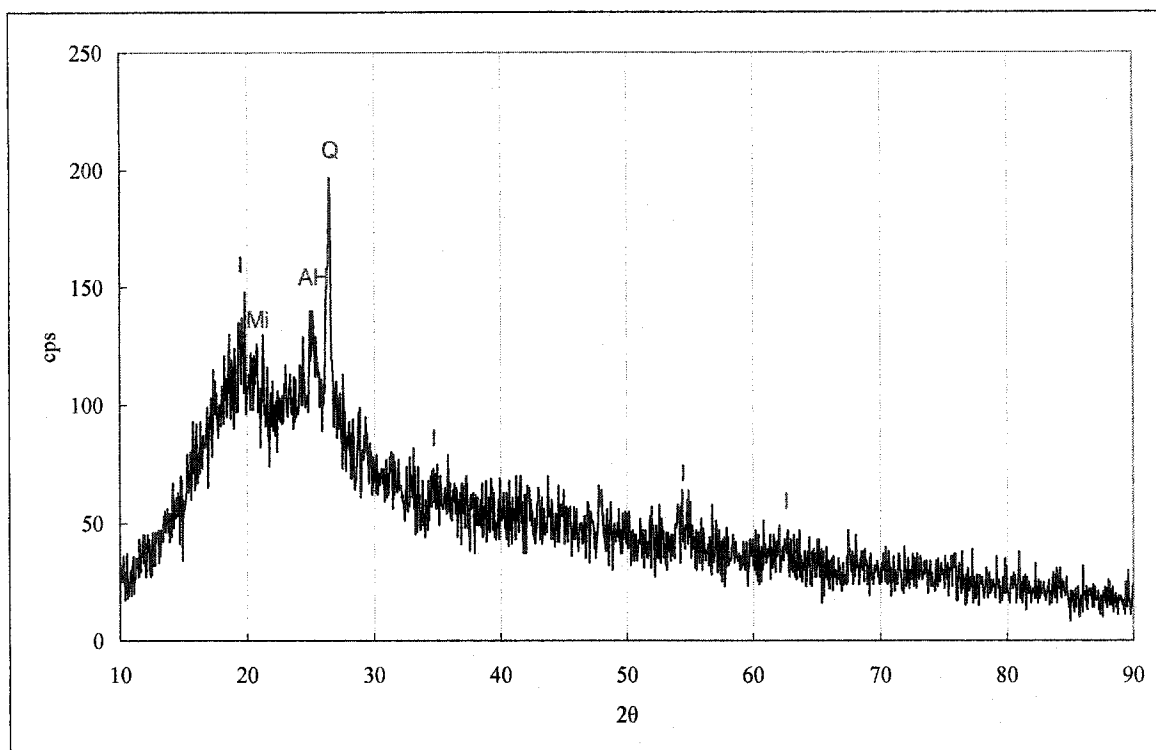


(A 1.9) XRD Raw Pattern of Suncor Ash at 1100°C

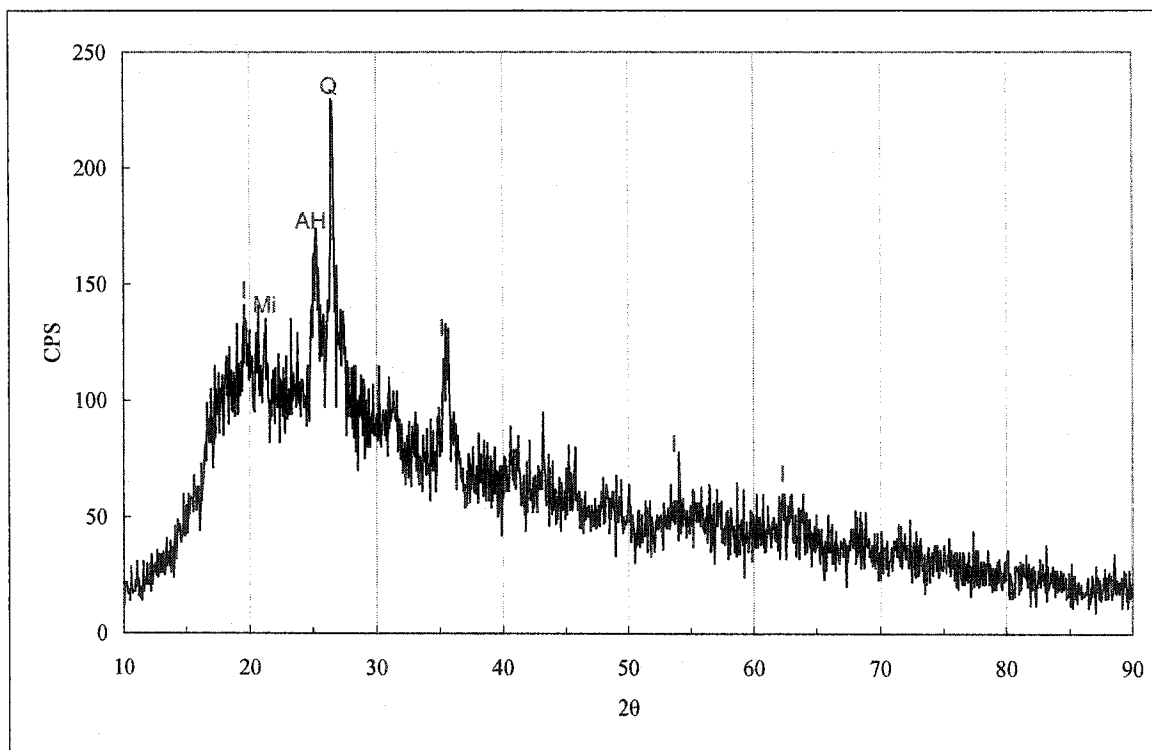


(A 1.10) XRD Raw Pattern of Suncor Ash at 1200°C

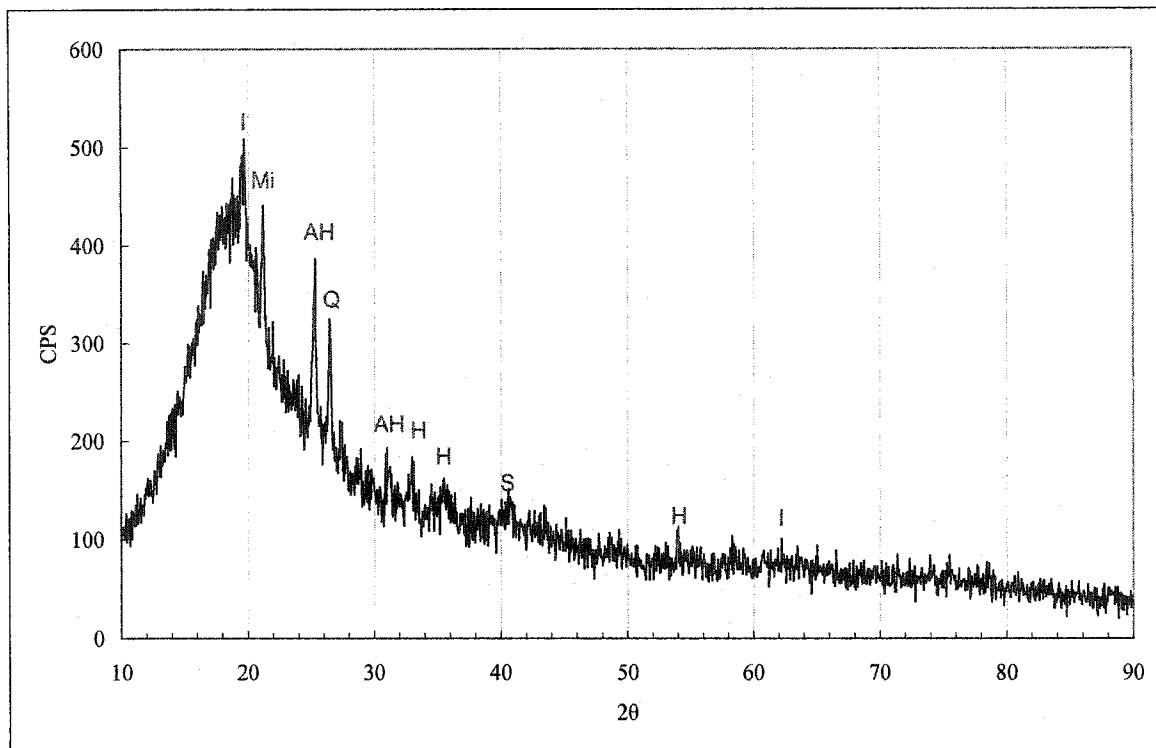
2. XRD Raw Patterns and Mineral Phases Identified in Syncrude Ash



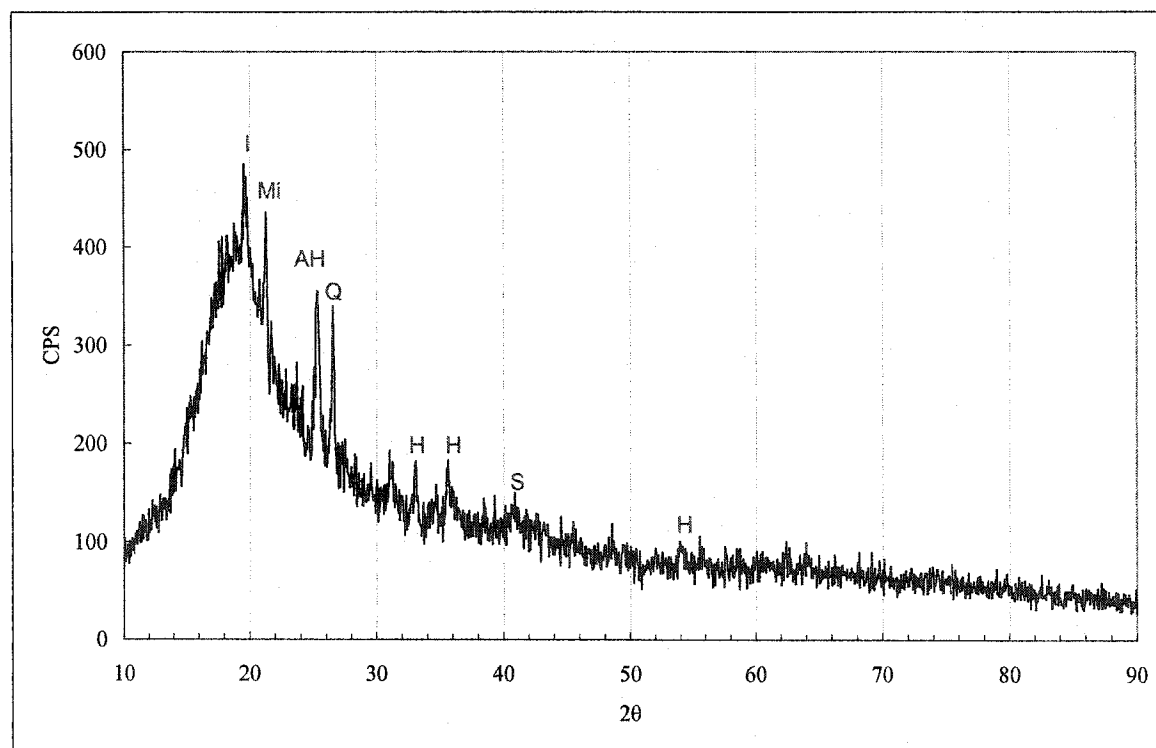
(A 2.1) XRD Raw Pattern of Syncrude Ash at LTA Temperature (600°C)



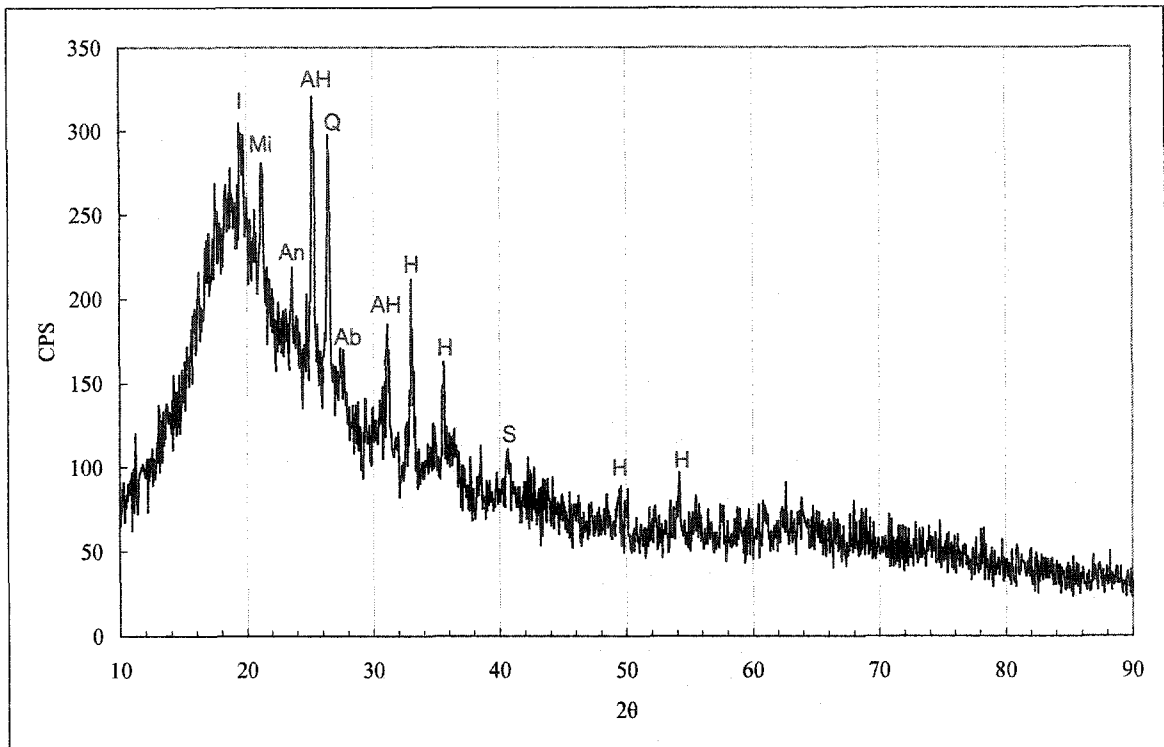
(A 2.2) XRD Raw Pattern of Syncrude Ash at 400°C



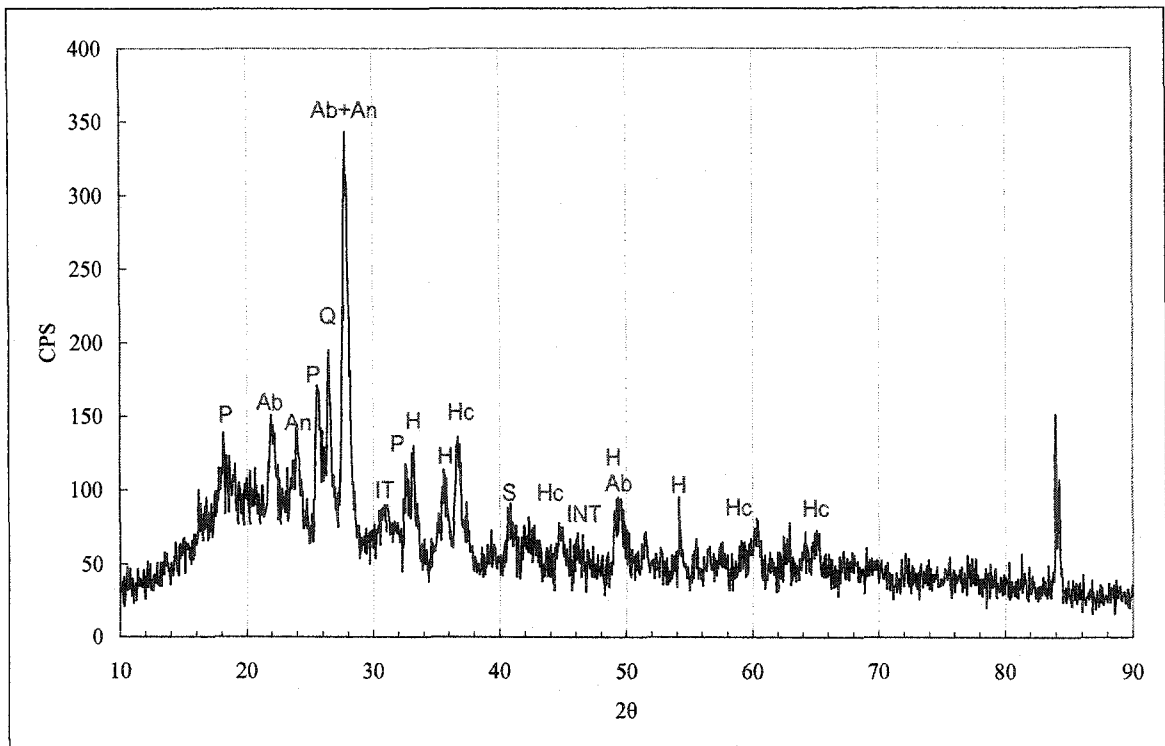
(A 2.3) XRD Raw Pattern of Syncrude Ash at 500°C



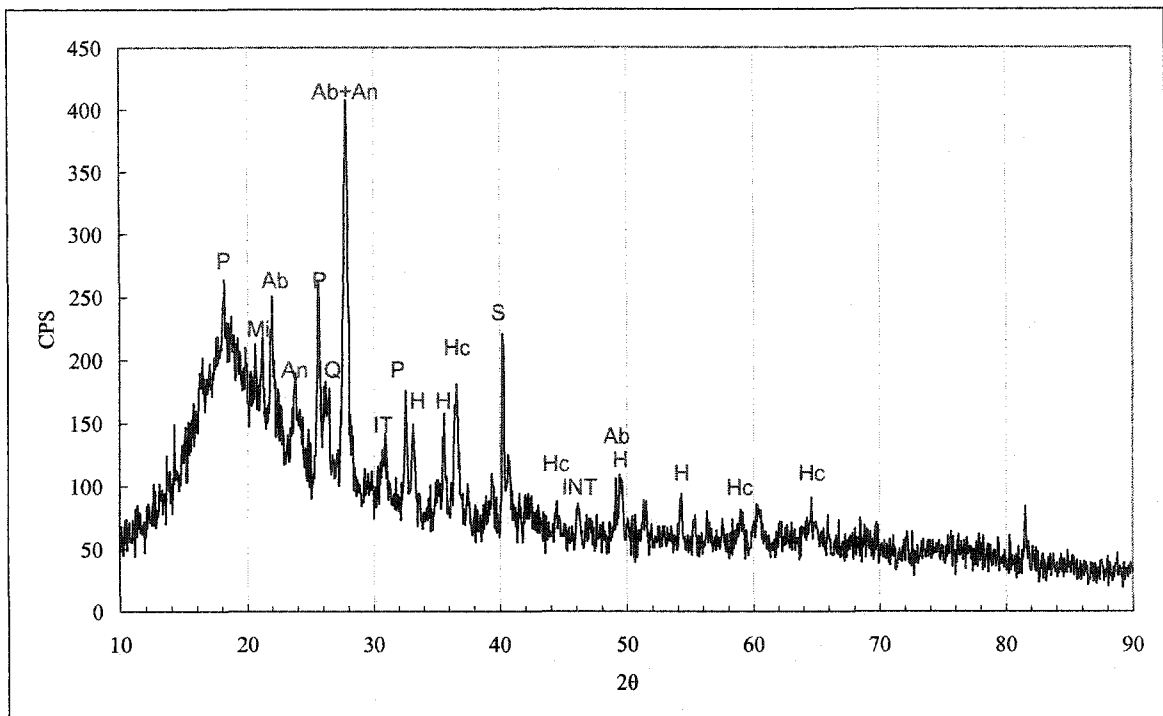
(A 2.4) XRD Raw Pattern of Syncrude Ash at 600°C



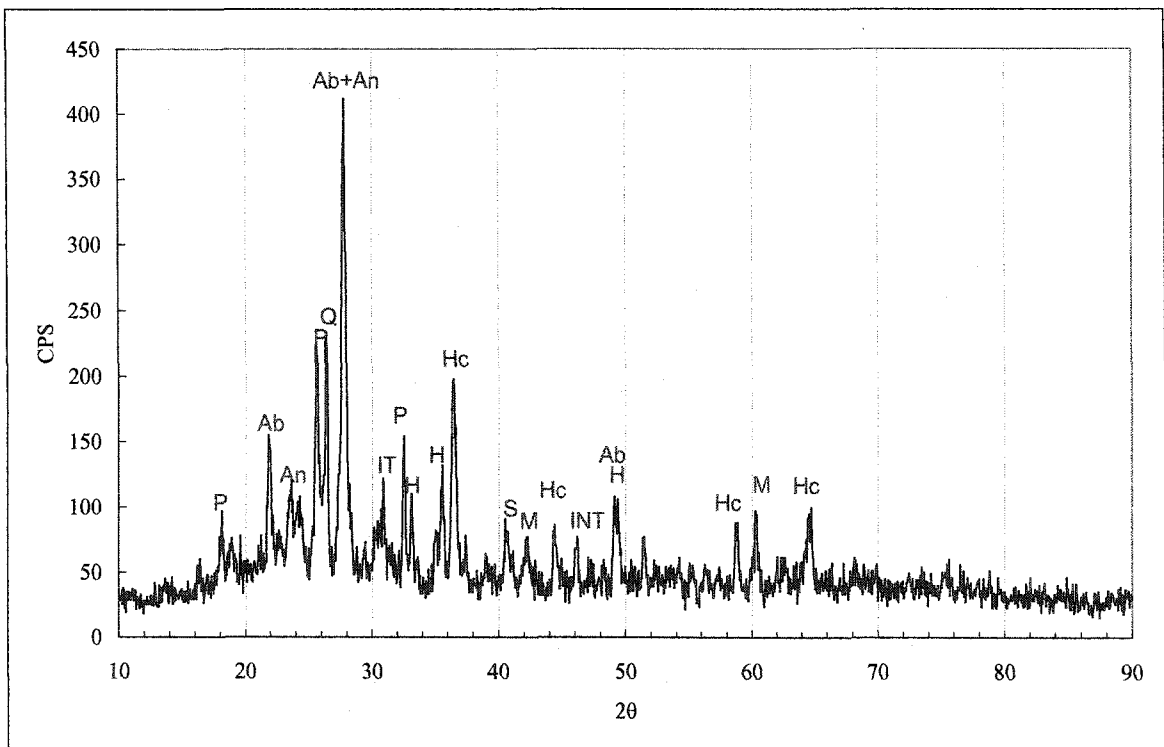
(A 2.5) XRD Raw Pattern of Syncrude Ash at 700°C



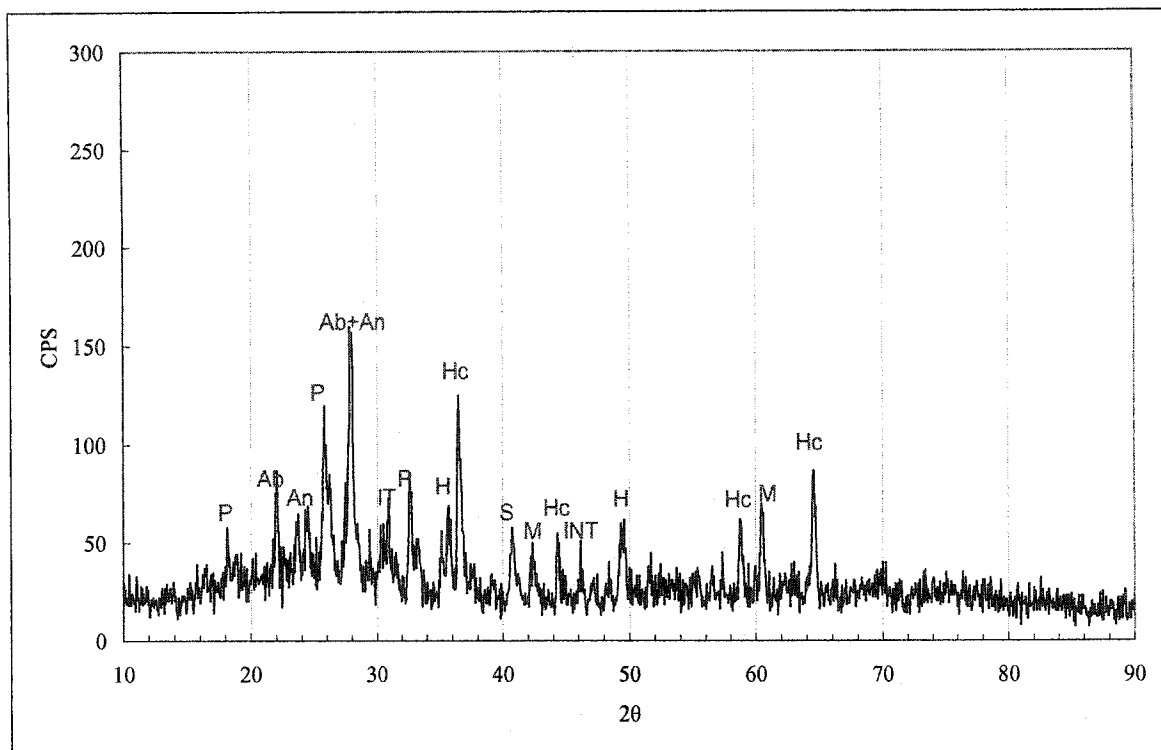
(A 2.6) XRD Raw Pattern of Syncrude Ash at 800°C



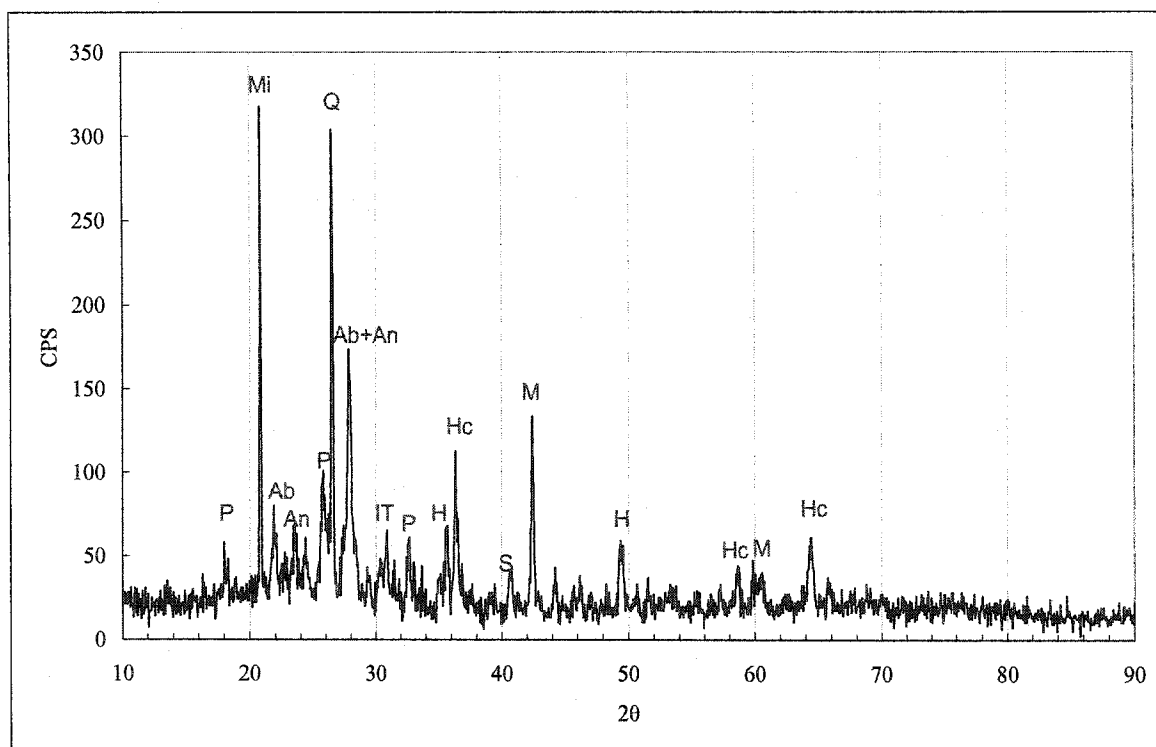
(A 2.7) XRD Raw Pattern of Syncrude Ash at 900°C



(A 2.8) XRD Raw Pattern of Syncrude Ash at 1000°C



(A 2.9) XRD Raw Pattern of Syncrude Ash at 1100°C



(A 2.10) XRD Raw Pattern of Syncrude Ash at 1200°C